# CALCINATION AND CHARACTERIZATION OF CLAYS OBTAINED FROM CEMENT PLANTS OF TURKIYE

A THESIS SUBMITTED TO
THE GRADUATE SCHOOL OF NATURAL AND APPLIED SCIENCES
OF
MIDDLE EAST TECHNICAL UNIVERSITY

BY

OĞUL CAN YEŞİLYURT

IN PARTIAL FULFILLMENT OF THE REQUIREMENTS
FOR
THE DEGREE OF MASTER OF SCIENCE
IN
CIVIL ENGINEERING

JANUARY 2023

Approval of the thesis:

**CALCINATION AND CHARACTERIZATION OF CLAYS OBTAINED FROM CEMENT PLANTS OF TURKIYE**

submitted by **OĞUL CAN YEŞİLYURT** in partial fulfillment of the requirements for the degree of **Master of Science** i**n Civil Engineering, Middle East Technical University** by,

Prof. Dr. Halil Kalıpçılar
Dean, Graduate School of **Natural and Applied Sciences** _____

Prof. Dr. Erdem Canbay
Head of the Department, **Civil Engineering** _____

Prof. Dr. İsmail Özgür Yaman
Supervisor, **Civil Engineering Dept., METU** _____

**Examining Committee Members:**

Prof. Dr. Erdal Çokça
Civil Engineering Dept., METU _____

Prof. Dr. İsmail Özgür Yaman
Civil Engineering Dept., METU _____

Prof. Dr. Sinan Turhan Erdoğan
Civil Engineering Dept., METU _____

Assoc. Prof. Dr. Çağla Meral Akgül
Civil Engineering Dept., METU _____

Prof. Dr. Burak Uzal
Civil Engineering Dept., Abdullah Gul Uni. _____

Date: 16.01.2022

**I hereby declare that all information in this document has been obtained and presented in accordance with academic rules and ethical conduct. I also declare that, as required by these rules and conduct, I have fully cited and referenced all material and results that are not original to this work.**

Name Last name : Oğul Can Yeşilyurt

Signature :

# ABSTRACT

## CALCINATION AND CHARACTERIZATION OF CLAYS OBTAINED FROM CEMENT PLANTS OF TURKIYE

Yeşilyurt, Oğul Can
Master of Science, Civil Engineering
Supervisor : Prof. Dr. İsmail Özgür Yaman

January 2023, 134 pages

With the increasing concern regarding global warming, alternative methods to improve the sustainability of cement manufacturing gained attraction. Partial cement substitution with supplementary cementitious materials (SCM) carries a huge potential to improve sustainability or even performance when optimized properly. The commonity of the clay deposits provides a huge advantage to the clays as SCM, but due to vast differences in composition and behavior, proper characterization of the clays is required. In this study, 8 clays that are obtained from various cement factories in Türkiye are calcined at 600 °C and 800 °C and characterized with various physical, thermal, and mineralogical experiments. Compressive strength, flexural strength, and Strength Activity Index (SAI) of all raw and calcined clay incorporating blends are tested for early, standard, and late ages. The relationships between the clay compositions and post-calcination behavior, along with several other factors, are discussed. It is observed that the calcite presence in the clay composition played a crucial role in the strength development. With 600 °C calcination 3 clays, with 800 °C calcination 5 clays, all of which incorporate >10% calcite, were able to satisfy the 75% SAI threshold stated in ASTM C-618 Standard.

Keywords: Characterization of Clays, Calcined Clay, Strength Activity Index, Clay Composition

# ÖZ

## TÜRKİYE ÇİMENTO FABRİKALARINDAN ELDE EDİLEN KİLLERİN KALSİNASYONU VE KARAKTERİZASYONU

Yeşilyurt, Oğul Can
Yüksek Lisans, İnşaat Mühendisliği
Tez Yöneticisi: Prof. Dr. İsmail Özgür Yaman

Ocak 2023, 134 sayfa

Küresel ısınmaya yönelik artan endişe ile birlikte çimento üretiminin sürdürülebilirliğini artıracak alternatif yöntemler giderek önem kazanmaktadır. Çimento İkame Malzemeleri (ÇİM) ile kısmi çimento ikamesi, uygun şekilde optimize edildiğinde sürdürülebilirliği ve hatta performansı iyileştirmek için büyük bir potansiyel taşımaktadır. Kil yataklarının yaygınlığı kile ÇİM olarak büyük bir avantaj sağlamaktadır, ancak her kilin bileşim ve performansında görülen büyük farklılıklar uygun karakterizasyon gerektirmektedir. Bu çalışmada Türkiye'deki çeşitli çimento fabrikalarından temin edilen 8 adet kil 600 °C ve 800 °C'de kalsine edilerek çeşitli fiziksel, termal ve mineralojik deneylerle karakterize edilmiştir. Tüm karışımların basınç ve eğilme dayanımı ile Dayanım Aktivite İndeksi (DAİ) erken, standart ve geç yaş için test edilmiştir. Kil bileşimleri ve deney sonuçları ilişkisi, bazı diğer faktörlerle birlikte tartışılmıştır. Kil bileşimindeki kalsitin dayanım gelişiminde önemli rol oynadığı görülmüştür. 600 °C kalsinasyon ile 3, 800 °C kalsinasyon ile 5 kil, ASTM C-618 Standartında belirtilen %75 DAİ gereksinimini karşılayabilmiştir. Bu killerin hepsi kompozisyonunda %10'dan fazla kalsit içermektedir.

Anahtar Kelimeler: Killerin Karakterizasyonu, Kalsine Kil, Dayanım Aktivite İndeksi, Kil Bileşimi

To my family,

To the bright future

## ACKNOWLEDGMENTS

Firstly, I would like to thank my supervisor and mentor Prof. Dr. İsmail Özgür Yaman for his great guidance, positive attitude, and endless support. His guidance allowed me to improve myself in more ways than I can express my gratitude.

Secondly, I would like to thank my Thesis Committee members, Prof. Dr. Erdal Çokça, Prof. Dr. Sinan Turhan Erdoğan, Assoc. Prof. Dr. Çağla Meral Akgül, and, Prof. Dr. Burak Uzal for all the invaluable information they taught me and their precious time.

Next, I would like to thank the Turkish Cement Manufacturers Association (TCMA) for providing me with the materials and technical support.

I also would like to thank Meltem Tangüler Bayramtan for being an amazing mentor. Her advice and support allowed me to overcome the difficulties easier.

I definitely will miss the companionship of Ömer Faruk Kalkan in the laboratory, and I would like to thank him for his great friendship.

Furthermore, I would like to thank all the researchers and staff of the METU Materials of Construction Laboratory for their assistance during my experiments.

Lastly, I would like to thank my parents Gülay and Nadir Yeşilyurt, my sister Ece Cansın Yeşilyurt, my uncle Hasan Yeşilyurt and all other relatives for believing in me.

## TABLE OF CONTENTS

## LIST OF TABLES

TABLES

## LIST OF FIGURES

FIGURES

## LIST OF ABBREVIATIONS

| | |
|---|---|
| SCM: | Supplementary Cementitious Materials |
| TCMA: | Turkish Cement Manufacturers Association |
| EN: | European Norms |
| ASTM: | American Society for Testing Materials |
| ACI: | American Concrete Institute |
| SAI: | Strength Activity Index |
| TGA: | Thermogravimetric Analysis |
| DTA: | Differential Thermal Analysis |
| XRD: | X-Ray Diffraction |
| XRF: | X-Ray Fluorescence |
| PSD: | Particle Size Distribution |
| OPC: | Ordinary Portland Cement |
| LC3: | Limestone Calcined Clay Cement |
| ASR: | Alkali-silica Reaction |
| NMR: | Nuclear Magnetic Resonance |

# CHAPTER 1

# INTRODUCTION

## 1.1 General

Due to the climate change caused by greenhouse gas emissions, sustainability has become an important focus and several countries agreed to reduce their $CO_2$ emissions (Ledley et al., 1999; United Nations, 2015). Concrete is the second most widely used substance after water (Scrivener, John, and Gartner 2018; Monteiro, Miller, and Horvath 2017), and its main binder Portland cement's annual production is expected to reach 5 billion tons by 2030 (Müller & Harnisch, 2008). Therefore, being under close scrutiny the cement industry has taken endeavors to improve the sustainability of cement production. High fuel consumption for over 1450 °C temperatures and released $CO_2$ during clinker manufacturing are major reasons for cement emissions (Bedard & Sordyl, 2007; Feiz et al., 2015; Kosmatka et al., 2002; Miller, 2018; van Oss & Padovani, 2003). Approximately 0.94 tons of $CO_2$ is released for 1-ton clinker production, 0.55 tons of which are released from the decomposition of limestone (Gartner, 2004; Pacheco Torgal et al., 2012). The usage of supplementary cementitious materials (SCM) not only reduces the $CO_2$ emissions from clinker production by partially replacing the cement but may even improve the mechanical properties of the blend and enhance service life (Duchesne, 2021; Prakasan et al., 2020). As Figure 1.1 shows cement is the most demanding component of concrete, in terms of cost and energy. The clinker burden can be reduced by partial replacement of cement with SCM (Ahmaruzzaman, 2010). Since most SCM are industrial by-products or naturally found, their need for treatment is minimal; thus, they can be used with cement to reduce overall environmental burden (Celik et al., 2015; Kajaste & Hurme, 2016; Miller, 2018).

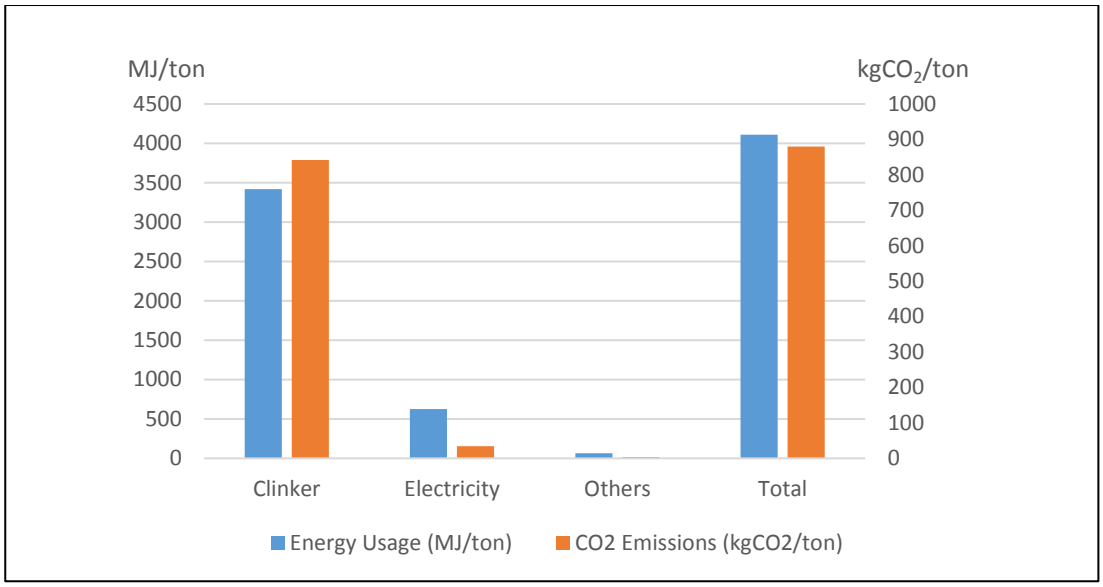


Figure 1.1. Simulated energy usage and $CO_2$ emissions of cement manufacture in the United States (Prakasan et al., 2020).

## 1.2 Objectives and Scope

This thesis is conducted on the raw clay materials that are provided by the Turkish Cement Manufacturers Association (TCMA, also known as TÜRKÇİMENTO) from various cement plants across Türkiye (formerly denoted as Turkey). The objectives of this study are to provide a basis for future studies including calcined clays of Türkiye, such as limestone calcined-clay cement (LC3) technology, by characterizing the Turkish clays with a frame based on the composition and performance relationship. The scope of this thesis includes the determination of the post-calcination strength of the clays according to the Strength Activity Index (SAI), applying analytical analysis methods, such as Differential Thermal Analysis (DTA), Thermal Gravimetric Analysis (TGA) and X-Ray Diffraction (XRD), physical methods, such as Particle Size Distribution (PSD) or Flow Table Test, to determine the compositions and taking an endeavor to unravel a correlation between the raw clay composition and post-calcination strength, while briefly considering other parameters such as fineness, water demand or limestone presence. The limits of the

thesis scope are as follows: A constant grinding time is adopted regarding the literature and particle size distribution tests. The clay samples are calcined at 600 °C and 800 °C temperatures, which are determined with the TGA/DTA and compared with their raw state. The samples are tested for their pozzolanicity at 7, 28, and 90-days to observe early, standard, and later age strength development. Both EN and ASTM Standards are adopted and modified for the study's needs.

In the second chapter of this thesis, an in-depth literature review regarding the supplementary cementitious materials (SCMs), most common SCMs, potential advantages of calcined clays over other SCM, hydration mechanisms of calcined clays, studies about the clay calcination parameters, effects of calcined clay usage on cement/concrete performance, and importance of clay characterization as highlighted in the literature, is conducted.

In the third chapter of this thesis, Experimental Program, materials used and their properties, experiment procedures, and results of some of the physical, chemical, and mineralogical tests are presented.

In the fourth chapter, Results and Discussion, critical findings and results are presented. Based on the evidence, scenarios regarding the correlation between the SAI results and other parameters are discussed. Also, based on the experiment results, several arguments that can benefit further studies are presented.

In the fifth chapter, Conclusion and Recommendations, the study and the notable discoveries are summarized, and key findings and recommendations for future studies are presented.

# CHAPTER 2

# LITERATURE REVIEW

## 2.1 Supplementary Cementitious Materials

Supplementary cementitious materials (SCMs) define the materials that can be used in corporation with the cement to improve the blend's properties (Panesar, 2019; Snellings et al., 2012). SCMs are either pozzolanic or self-cementitious materials: Pozzolanic materials consist of siliceous or siliceous and aluminous compounds, carry little to no cementitious properties by themselves but form pozzolanic reactions to contribute to the cement matrix strength with the presence of a hydrant -most commonly water- and $Ca(OH)_2$ or $Ca^{+2}$. Self-cementitious materials incorporate lime and do not require additional external lime to form pozzolanic reactions; thus, only require water (ASTM C-618, 2002; Dodson, 2013; Malhotra & Mehta, 2004; Snellings et al., 2012). While used as a cement substitute, pozzolanic SCM, such as Class F fly ash, silica fume, or ground granulated blast furnace slag, has arguable advantages over self-cementitious SCM, such as Class C fly ash or lime, due to a few factors: (i) cement already includes the lime which the pozzolanic reactions can consume, so no additional lime is needed (ii) replacing a self-cementing material with another self-cementing material is less convenient than using a pozzolanic SCM, (iii) pozzolanic SCM are generally more available than self-cementing SCM.

### 2.1.1 Hydration Mechanisms of Supplementary Cementitious Materials

During a pozzolan-lime reaction, silicates and aluminates of the pozzolanic material react with the lime in the water presence. The fundamental pozzolanic reactions are given in Equations [1] to [3], where C is CaO, S is $SiO_2$, A is $Al_2O_3$, and H is $H_2O$.

Dissolved silicates sourced from the pozzolan react with the water and lime to form C-S-H (tobermorite) phase (Snellings et al., 2012). Since C-S-H formation is a process where short monomer and dimer silicates convert to a longer polymer, it grants additional strength to the matrix (Brough et al., 1995). In a typical pozzolanic reaction, aluminates can either form calcium-aluminate-hydrates ($C_4AH_{13\text{-}19}$ C-A-H,) or partially incorporate into the C-S-H gel (I. G. Richardson, 2008; Taylor, 1997). During cement hydration, four main phases contribute to the strength gain: Alite ($C_3S$), belite ($C_2S$), aluminate ($C_3A$), and ferrite ($C_4AF$). While calcium silicates ($C_3S$ and $C_2S$) react with water to form C-S-H gel (Roller & Ervin Jr, 1940), reaction products of calcium aluminates depend on the sulfate content: When there are no sulfates and not enough $Ca(OH)_2$, which is most common when a calcined clay, such as metakaolin, is used as only SCM, $C_2ASH_8$ (strätlingite, C-A-S-H), $C_4AHx$ (hydrogarnet) or $C_3AH_6$ (calcium-aluminate-hydrate) is formed, depending on the temperature (Ambroise et al., 1994; Ogawa et al., 1980; Serry et al., 1984). Hydrogarnet is usually observed when the internal temperature is above 40 °C (de Silva & Glasser, 1992), or when it is stabilized with sulfates or carbonates (Pöllmann, 2006). When sulfates are provided to the system by gypsum addition or usage of SCM such as fly ash or GGBFS, $Ca(OH)_2$ will initially form C-A-$\bar{S}$-H ($C_6A\bar{S}_3H_6$, ettringite), where $\bar{S}$ is a hyphenation of $SO_3$, or $C_4A\bar{S}H_{12}$ (monosulfoaluminate), or both (Snellings et al., 2012; Taylor, 1997).

$$C_2S + 2H \rightarrow C_3S_2H_3\ (C-S-H) + CH \quad [1]$$

$$C_3S + 3H \rightarrow C_3S_2H_3\ (C-S-H) + 3CH \quad [2]$$

$$C_3A + 6H \rightarrow C_3AH_6\ (C-A-H\ ) \quad [3]$$

Ettringite (C-A-$\bar{S}$-H) formation is generally desired in a cementitious system since it prevents flash setting by increasing the setting time. In a traditional cement system, ettringite is converted to the monosulfoaluminate ($SO_3$-AFm) (Berman & Newman, 1963), after sulfate content drops below 3% (de Silva & Glasser, 1992). When adequate limestone is incorporated into the system, along with the sulfate, meta-stable hemicarboaluminate forms (Lothenbach et al., 2011) instead of monosulfoaluminate due to the increased concentration of initial carbonates. After around 1-year, the hemicarboaluminate phase converts to the monocarboaluminate ($CO_3$-AFm), which is a very stable product (François et al., 1998). Equations [4-7] show the ettringite stabilization process by the carboaluminate phase conversion reactions:

$$3C\bar{S}H_2 + C_3A + 26H \rightarrow C_6A\bar{S_3}H_{32} \quad [4]$$

$$C_6A\bar{S_3}H_{32} + 2C_3A + 4H \rightarrow 3C_4A\bar{S}H_{12} \quad [5]$$

$$3C_4A\bar{S}H_{12} + 2C\bar{C} + 18H \rightarrow C_6A\bar{S_3}H_{32} + 2C_4A\bar{C}H_{11} \quad [6]$$

$$C_3A + C\bar{C} + 11H \rightarrow C_4A\bar{C}H_{11} \quad [7]$$

While forming phases greatly vary, many studies (Atkins et al., 1992; Fujii & Kondo, 1981; Lothenbach et al., 2011; Roller & Ervin Jr, 1940; Walker et al., 2007) are conducted to layout the mechanisms behind, and a ternary diagram (Figure 2.1) that shows the relation between the main binding products and amount of $SiO_2$, CaO, and $Al_2O_3$ are created. Regardless of their performance, all relevant pozzolanic SCM obey the ternary diagram rules. For example, when the Ca/Si ratio is over ≈1.5, C-S-

H will co-exist with the portlandite (C-H). If the Ca/Si is lower than ≈0.7, C-S-H will co-exist with silica gel ($SiO_2$) (Lothenbach et al., 2011; Lothenbach & Nonat, 2015). Generally, C-S-H gel is one of the most important phases in a typical cement mixture because it covers more than half of the paste and contributes to the strength most (Bullard et al., 2011). Note that, while Figure 2.1 does not include sulfate, the diagram topology remains the same with sulfate presence, only changing ettringite and monosulfoaluminate being more stable (Snellings et al., 2012). Due to the high Ca content, a typical OPC blend usually has a high Ca/Si ratio (1.2-2.1) where C-S-H gel dominates (I. G. Richardson, 1999). The inclusion of SCM into the blends almost always reduces the Ca/Si ratio and increases the Al/Ca ratio, by bringing high amounts of Si or Al or both, which increases the C-A-S-H formation (I. G. Richardson, 1999, 2008; I. G. Richardson & Groves, 1997). Furthermore, while Ca/Si ratio in C-S-H gel decreases with pozzolan addition, overall C-S-H formation is increased, which greatly benefits the strength development (Massazza, 1993). To summarize, the literature showed that in a SCM incorporated cement system, silicates join the formation of tobermorite (C-S-H) and strätlingite ($C_2ASH_8$) phases, aluminates join the formation of calcium-aluminate-hydrate (C-A-H) and strätlingite ($C_2ASH_8$) phases, and sulfates join the ettringite (C-A-$\bar{S}$-H) and AFm conversions (monosulfoaluminate). Since the cement is quite rich in $Ca(OH)_2$, the addition of a SCM with high silicates and/or aluminates content, such as calcined clays, will form additional C-S-H, C-A-S-H (strätlingite) and C-A-H until one of the constituents is depleted. Also, due to the consumption of $Ca(OH)_2$, SCM incorporating systems usually have lower pH than cement-only systems. Strength and durability gain is tied to the formation of additional binding phases which enhance the gel-packing of the matrix and improve pore refinement and the filler effect of the SCM not only improves solid/water ratio but also provides the new nucleus for C-S-H gels to grow from; thus, also contribute to the strength (Bahhou et al., 2021; Dhandapani et al., 2018; Juenger et al., 2019). Note that, mentioned reaction products are of ambient temperature and the phase assembly also changes and the reactions occur faster with elevated temperatures (Shi & Day, 1993), which are not within the scope of this

study. Snellings et al. (2012) state that due to the difficulties caused by the greatly varying nature of the actual reactions, studies generally focus on empirical determination of the SCM performance, which further supports the importance of the characterization of SCMs.

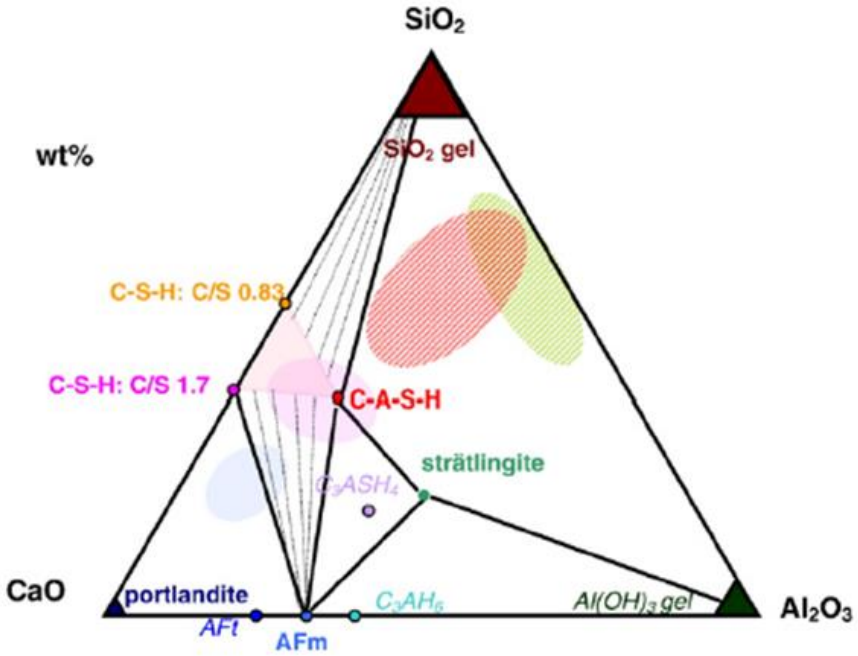


Figure 2.1. Ternary phase formation diagram with respect to Cao, $SiO_2$, and $Al_2O_3$ ratios (Lothenbach et al., 2011).

### 2.1.2 Usage of Notable Supplementary Cementitious Materials

Even though understanding SCM hydration mechanisms is relatively recent, SCM usage goes back. Since the Neolithic Era, the mixing of lime, gypsum, clay, or mud to form plaster was known (David Kingery et al., 1988; Gourdin & Kingery, 1975). Especially, lime usage was more common, as such, floors and coatings made out of lime plasters that include natural pozzolans are observed in ancient sites such as Asikli Höyük, Çatalhöyük, Tell Ramad, and Hathor Temple in Egypt (Chiotis et al., 2001; Mellaart, 1967; Todd, 1968). Shaw (2009) states that Minoans mixed lime, finely ground ceramics, and natural pozzolans originated from Crete Island, near the

city of Knossos, to produce water-resistant pastes. It is presumed that pozzolanic volcanic ash sourced from Santorini Island, also known as Santorin-earth, was later utilized in the mixtures (Kitsopoulos & Dunham, 1996). During a long period of time, this technology spread to the Roman Empire where the mixture is improved by using nearby volcanic tuff and pumice sources, such as Pozzulini where the "pozzolana" term originates from (Drdácký et al., 2013; Shaw, 2009). Some buildings, such as Pantheon or Ponte di Augusto (Figure 2.2), made with pozzolan-lime mortars still withstand due to the exceptional durability combined with the mixing and proportioning methodology developed by the Romans (Drdácký et al., 2013; Malinowski & Garfinkel, 1991). With the Industrial Revolution, increased demand for construction hastened cement development, which resulted in modern-day cement (Guillerme, 1986). However, developing technologies and industries also presented new supplementary cementitious materials which can provide new potential solutions for more eco-friendly cement-based materials (Scrivener et al., 2018). Currently, the most widely used and studied SCMs are fly ash (FA), ground granulated blast furnace slag (GGBFS), silica fume (SF), natural pozzolans, and calcined clays (WBCSD, 2014).

Figure 2.2. Restorated Ponte di Augusto (Drdácký et al., 2013).

#### 2.1.2.1 Fly Ash

Fly ash is the residual ash that is a by-product of pulverized coal combustion, which is collected with an electrostatic precipitator due to environmental regulations (Meyer, 2009; Shirkhanloo et al., 2021). It consists of silicon dioxide, calcium, aluminum, iron, and trace amounts of impurities, such as potassium, magnesium, sulfur, etc. (American Coal Ash Association, 2003). While there is also Municipal Solid Waste Incineration (MSWI) bottom ash, which is also a type of fly ash, it is usually not considered in the SCM studies due to the very high concentrations of hazardous heavy metals (Gartner & Hirao, 2015; Loginova et al., 2019; van Gerven et al., 2005). Joshi & Lohita (1997) states that approximately 80% of all industrially produced ash is fly ash, which is around 500 Mt (million tons). Produced fly ash is the most commonly used in concrete production but its utilization greatly varies between the regions, average fly ash utilization is only 16% of the total ash produced, which corresponds to 80 Mt (Ahmaruzzaman, 2010; Joshi & Lohita, 1997). A significant portion, for example, a quarter of the produced fly ash (approximately 32.5 Mt) in India, is used for the construction and cement industry (Bhattacharjee & Kandpal, 2002). According to the American Society for Testing and Materials (ASTM C-618, 2002), fly ash is divided into two classes: Class C and Class F. Class C fly ash is produced from the combustion of low-grade (lignite and sub-bituminous) coal, includes more calcium (>20% CaO) and fewer silicates than the Class F fly ash, which is produced from the high grade (bituminous and anthracite) coal combustion and includes high silicate content (Akbar, 2013; ASTM C-618, 2002; Shirkhanloo et al., 2021; Wardhono, 2018). Combustion of sub-bituminous, bituminous, and lignite is much more common compared to anthracite, which makes anthracite coal FA relatively rare (Ahmaruzzaman, 2010). In the study of Snellings (2016), the annual estimated volume of Class C FA is 100-200 Mt and Class F FA is 600-900 Mt. While both classes have pozzolanic properties, Class C fly ash also has self-cementing properties, which means it does not need a lime-including agent, such as cement, to be used as a stabilizer; thus, it is arguably more suitable to use Class F fly ash in

combination with the cement. Class C is self-cementitious (does not require lime) because according to the standard (ASTM C-618, 2002), it includes high lime and only 50-70% $SiO_2$ + $Al_2O_3$ + $Fe_2O_3$ content, which is at least 70% for the Class F; thus, Class C incorporation may not reduce the heat of hydration as much as Class F (Shirkhanloo et al., 2021). FA incorporation in cementitious mixtures is known to improve durability, reduce cost, provide higher late-age strengths, reduce the rate of heat, and improve workability (Assi et al., 2018; Ishak & Hashim, 2015; Meyer, 2009; Padhye & Deo, 2016; Rao & Babu, 2017; Thomas, 2007). Gupta & Sharma (2003) mentioned that the fly ash cost is virtually zero at the coal plant and without heavy transportation, laying and rolling costs FA can greatly reduce the economic burden of a cementitious blend. Several studies (Giaccio & Malhotra, 1988; Malhotra, 1990; Naik et al., 1991) analyzed the high cement replacement with Class F FA and proved that the FA-blends showed excellent strength and durability properties. Ravina & Mehta (1986) and Siddique (2004) showed that the Class F FA can be used up to 50% as a cement replacement. Pei-Wei et al. (2007) investigated the FA incorporation for dam construction, where the rate of heat reduction is important, and showed that 50% FA incorporation performs better than OPC-concrete dams. Several studies (Atiş et al., 2004; Yamei et al., 1997) proved that even non-standardized FA can be used to achieve satisfactory performance. These improvements are not only caused by the pozzolanic reactions, but also by the ball-bearing filler effect of the spherical shape of the FA particles, and 30% FA replacement of the binder is considered to improve strength and durability without compromising any other properties that come with higher replacement rates (Gutteridge & Dalziel, 1990; Snellings, 2016). However, FA also carries several disadvantages that cause concern regarding its usage as a SCM in the future: FA with desired quality is only available in relatively small regions and regional distribution may create additional transportation costs (Ahmaruzzaman, 2010; Lovecchio et al., 2020). Besides, the content of the FA is dependent on the origin matter and the required carbon, lime, and magnesium oxide limitations are not always possible to satisfy (Snellings, 2016). Ahmaruzzaman (2010) states that fly ash potentially

contains highly toxic elements, which not only carry potential harm to the environment but may also cause fly ash disposal to greatly increase in costs or even become illegal, in the future. This statement is supported by Snellings (2016), which also remarks on the possible indirect limitation to FA reserves due to environmental concerns. If coal power usage becomes wider in the future, FA disposal and transportation costs will increase; and if coal power usage is reduced in the future due to environmental concerns, FA production will be reduced (Ahmaruzzaman, 2010; Joshi & Lohita, 1997). Also, Scrivener & Kirkpatrick (2008) foresee a reduction in fly ash and GGBFS due to future technological advancements that provide better efficiency and fewer by-products. All in all, the literature shows that FA viability greatly depends on future advancements, and other alternative SCM which does not share the mentioned FA disadvantages can be invaluable for the forthcoming cement technologies.

#### 2.1.2.2 Ground Granulated Blast Furnace Slag

According to the ASTM C-125 (2003) definition, blast furnace slag (BFS) as a non-metallic molten blast furnace product that is produced with iron, consists of silicates and aluminosilicates of calcium and may include manganese, sulfur, or some oxides (Akbar, 2013). The majority of the BFS composition is $SiO_2$, $Al_2O_3$, CaO, and MgO (Xing et al., 2020). Blast furnace slag, or slag, in short, is a by-product product that is formed during the treating of iron oxide ore with coke and limestone at 1500 °C to produce pig iron (Yuksel, 2018). There are also other slag types, such as steel slag and copper slag, but studies suggest that more research is required for their usage as a SCM (Akbar, 2013; Scrivener et al., 2018; Snellings, 2016). Due to having lower density molten slag accumulates above the molten iron layer, where it can then be harvested. The chemistry and properties, thus, the naming of the BFS changes depending on its cooling rate and methods: When molten slag is left to slowly cool with the ambient temperature, it is denoted as air-cooled blast furnace slag (ABFS or ACBFS). Due to slow cooling, ABFS minerals turn into the crystalline form which

does not carry any pozzolanic properties but since ABFS becomes denser, it can be used as aggregate (Akbar, 2013; Federal Highway Administration, n.d.; Mostafa et al., 2001). When a molten slag is treated with a pelletizer which uses a mixture of water and air for cooling, it expands. This expanded material has huge pockets of air inside which makes it lightweight and a great insulator. Expanded blast furnace slag can be used for lightweight concrete applications as an aggregate. When molten slag is rapidly cooled via water jets, it gains a glassy texture which provides it cementitious properties due to the granulation of the glassy particles that form sand-like particles, caused by the rapid cooling process, new amorphous material is denoted as granulated blast furnace slag (GBFS). Since GBFS consists of coarse particles, it requires very fine grounding to elevate its cementitious properties, after which it is denoted as ground-granulated blast furnace slag (GGBFS) (Akbar, 2013; Pal et al., 2003; Yuksel, 2018). While GGBFS's importance as a SCM is recognized (Bougara et al., 2010), and various methods to correlate its reactivity and chemical content are explored (Behim et al., 2013; Yi et al., 2016), several studies (Behim et al., 2013; Chen & Brouwers, 2006; Swamy, 1993) reported that the GGBFS reactions are not fully understood due to too many factors affect the reactivity. For example, Pal et al. (2003) found no correlation between glassy mineral content and reactivity. Nonetheless, it is safe to say that the GGBFS addition obeys the rules of the previously mentioned ternary diagram by providing additional silicates, aluminates, and lime that forms new binding phases, such as C-S-H and C-A-H, and improve the overall performance. Several studies (Akbar, 2013; Hogan et al., 1981; Suresh & Nagaraju, 2015) showed that when GGBFS is incorporated (up to 50%), early-age strength development is slower than of control but after between 7-28 days, strength values are known to catch up and slightly surpass the control's strength at late ages. While up to 70% replacement is common (Scrivener et al., 2018), high GGBFS replacement rates reduce the strength, compared to a 100% cement blend (Zhang et al., 1999). With the GGBFS presence: (i) excess water that increases the capillary pores is reduced (Singh & Siddique, 2016) (ii) additional binding phases are formed (Suresh & Nagaraju, 2015), and (iii) cement matrix got denser due to the GGBFS

particles (Cheng et al., 2005); all of which impair the penetration of chemical agents and improve the durability. Slag addition is also known to improve workability (D. N. Richardson, 2006). Similar to the FA, GGBFS has several obstacles which significantly reduce its future potential as a SCM: Scrivener et al. (2018) estimate annual global available slag as 330Mt, which is already arguably limited, and states that it is diminishing. The study also states that most slag production occurs in industrially developed countries while most demand for cement and SCM incorporation is in developing countries. The study also mentions that almost all of the suitable BFS are already used as SCM, which indicates that there is not much room for improvement in terms of greenhouse gas reductions (Snellings, 2016; WBCSD, 2014). Furthermore, Scrivener et al. (2018) argue that, unlike air-cooled BFS, granulated BFS needs granulation equipment and facilities, which may be costly, and affect the cost reduction of the SCMs. The disadvantages of GGBFS motivate the research involving other SCMs with more potential.

#### 2.1.2.3 Silica Fume

Silica fume (SF), also referred to as microsilica, is an amorphous pozzolanic powder that consists of 85-98% SiO2, at the very least (ASTM C1240, 2005; Chung, 2002; de Belie et al., 2018). It is a by-product of high-temperature silicon or ferrosilicon alloy production in electric arc furnaces (de Belie et al., 2018). During this process oxygen from quartz is removed and as a result, silicon monoxide vaporizes at the furnace top, where is forms silicon dioxide (SF), which is later extracted via filters (Chung, 2002; de Belie et al., 2018). In 1951-1952 Norway, SF was first utilized in concrete but despite good results, the new technology was abandoned due to the lack of massive industrial capacity to produce meaningful volumes of SF, until Norway put new environmental laws two decades later and motivated the research about SF utilization. While the chemical composition of SF remains mostly the same regardless of the production, four different SF forms significantly affect the featured blend due to particle sizes and shapes: Undensified SF have a quite low bulk density

of 200-300 kg/m$^3$, which makes it unsuitable for many concrete applications. If SF is treated to improve its bulk density by the agglomeration of ultrafine particles, it is named densified SF, which can be utilized in a range of construction areas. SF can be pelletized, in a process similar to the FA, to be used as a landfill. Lastly, SF can be mixed with water to form a dense slurry that is suitable to be used with concrete but this process is more sophisticated that the other three (de Belie et al., 2018). American Concrete Institute (ACI) released an in-depth guide for SF usage in concrete (Aldred et al., 2006) and SF specifications are established in ASTM C-1240 and EN 13263-1 standards. Similar to other pozzolanic materials, silica fume reacts with the lime, which occurs very rapidly due to the high surface area of SF particles, when incorporated in a cement mixture (ASTM C1202, 2012; Kishar et al., 2010; Mitchell et al., 1998). SF incorporation improves the properties of the cementitious system by enhancing strength and durability, increasing the concrete volume per kg cement and reducing the costs, and compensating for the delay caused by other SCM incorporations, such as FA (de Belie et al., 2018; Detwiler & Mehta, 1989; Diamond, 1986; Lewis, 2018; Sellevold & Radjy, 1983). Unlike other SCMs, the strength enchantment can be observed as early as within 24 hours (Hjorth et al., 1988; Sabir et al., 2001) and this effect is also observed at later ages, as some studies proved: Kumar & Roy (1984) showed that 10% silica fume improved strength by 30-50% at 28 days. In a cementitious system matrix, the weakest spot is generally the transition region between the aggregate and cement, the interfacial transition zone (ITZ) (Ollivier et al., 1995). Due to its very fine and highly reactive particles, SF fills the ITZ and creates a homogeneous zone between the aggregate and binder, which immensely improve the strength (Bentur et al., 1987; Claisse, 1988; Regourd, 1984). Due to this effect, SF is often used in high-strength (+80 MPa) and very-high-strength concrete (+120 MPa) (de Belie et al., 2018). While SF provides many benefits, its stockpiles are quite low to be impactful (1-2.5 Mt/year) (Juenger et al., 2019; Scrivener et al., 2018), it causes a reduction in consistency and workability (Collins & Sanjayan, 1999; El-Didamony et al., 1999; Punkki et al., 1996; Thomas et al., 1999), and with the modern arc furnaces producing fewer by-products, its

supplies may reduce in the future. Thus, currently, SF is a material with limited availability that is used for sophisticated applications, such as high-strength concrete, and their potential is arguably minimal compared to other widely-found SCMs, such as calcined clays.

#### 2.1.2.4 Natural Pozzolans and Calcined Clays

Massazza (1976) initially defined natural pozzolans as pozzolanic materials which only require grinding to react with lime, which leaves calcined clays out of the classification due to the required calcination process. On the other hand, Mehta (1987) categorized natural pozzolans into four categories: volcanic tuff, raw or calcined opaline silica, unaltered volcanic glass, and shale or calcined clay. ASTM C-618 refers to various materials which require calcination to achieve satisfactory cementitious properties, such as clays or shales, as "calcined natural pozzolans" and places them under Class N for further standardization. For the sake of consistency, the ASTM C-618 approach is adopted in this study.

## 2.2 Clays and Clay Minerals

### 2.2.1 Clays

The term "Clay" has different meanings which often creates confusion; thus, many endeavors have been taken to clear its definition (Grim, 1952, 1953; Guggenheim & Martin, 1995; Hillier, 1978; Murray, 1999; Wentworth, 1922). Bergaya & Lagaly (2006) state that various disciplines have various definitions for "clay", "clays" and "clay minerals" and it is not possible to find a definition that satisfies all parties. Grim (1953) states that the accurate description of clay as a rock term is difficult. As Murray (2000) explains, clay is most commonly used to define a natural, earthy soil that is composed of fine particles, simply, a soil type. However, this definition may also include shales or argillites. Another definition for clays, which is common

among mineralogists, is used for fine particles that are smaller than 4 microns, as a size term (Mukherjee, 2013; Weaver, 1989; Wentworth, 1922). However, Bergaya & Lagaly (2006) state that there is no generally accepted upper limit and some sciences use 1 micron as the definition cap. Besides, not all materials that are fine enough do not carry the other clay properties, which makes the definition unapplicable in most cases (Mukherjee, 2013). Additionally, Velde (2013) argues that the clay definition associated with particle size was due to a lack of a better understanding of crystal structures. Clay Minerals Society (CMS) and Association Internationale pour l'Etude des Argiles (AIPEA) organized Joint Nomenclature Committees (JNC) which tried to clarify clay definition and defined clay as a fine-grained natural material which is generally plastic at appropriate water content and harden when dried or fired (Guggenheim & Martin, 1995). While this definition is vague, it also includes shales and argillites and excludes several non-plastic clays (Bergaya & Lagaly, 2006). Also, the plasticity requirement at appropriate water content does not apply to some clay, such as flint clay or Fuller's earth, and due to the same reason, Mukherjee (2013) suggests that the term should not be used to define post-diagenesis rocks, such as pelitic rocks or claystone; and suggest the usage of "argilloid" as a more inclusive term. There are also specific market names for clays as follows: ball clay, bentonite, bleaching earth, China clay, Fuller's earth, primary and secondary kaolin, nanoclay, etc. (Bergaya & Lagaly, 2006). The "clay mineral" definition is separated from the "clay" term by Guggenheim & Martin (1995) and it is recommended to refer to phyllosilicate minerals that are commonly found in clays, such as kaolinite, smectite, illite, chloride, and palygorskite and sepiolite, as "clay minerals" (Murray, 2000). Clay minerals must be natural, and impart plasticity but do not have to be phyllosilicate by definition (Mukherjee, 2013). Mukherjee (2013) also argues that if a natural, plasticity-providing but non-phyllosilicate mineral is discovered in the future, it should also be defined as clay. All in all, this study experimented on clayey soils that are used in cement plants in Türkiye, harvested from natural clay deposits, and provided by the Turkish Cement Manufacturers' Association (TCMA); these materials will be simply referred to as

“clays”. Phyllosilicate minerals that are commonly found within the clays, such as kaolinite, montmorillonite, illite, etc., will be referred to as “clay minerals”.

### 2.2.2 Clay Minerals

Clay is a raw and abundant material with properties that heavily depend on the amount of clay minerals, non-clay minerals, impurities, fineness, etc. (Grim, 1953). The most commonly found clay deposits are shown in Figure 2.3. Clays are utilized in many industries, including agriculture, paper, ceramic, construction, mining, drilling, etc. (Murray & Staff, 2000). Mukherjee (2013) explains clay constituents as (i) associated phases, (ii) associated minerals, and (iii) clay minerals. Associated phases are impurities, such as organic materials or some amorphous phases. Associated minerals are present in clay soil in most cases but do not contribute to plasticity, for example, quartz, iron oxides, aluminum oxides, hematite, magnetite, etc. Clay minerals are minerals that give clay its plasticity, and hardening with drying or firing properties. Note that, some studies categorize the clay minerals differently; for example, JNC (Guggenheim & Martin, 1995) defines chloride as a clay mineral by stating that all phyllosilicates should be considered as clay minerals, Mukherjee (2013) challenges this by remarking on the lack of plasticity effect chloride provides and suggesting that it should be referred to as an associated mineral. In this study, JNC’s definition is adopted as it is more commonly adopted in the literature, and further supported by Dixon & Schulze (2002).

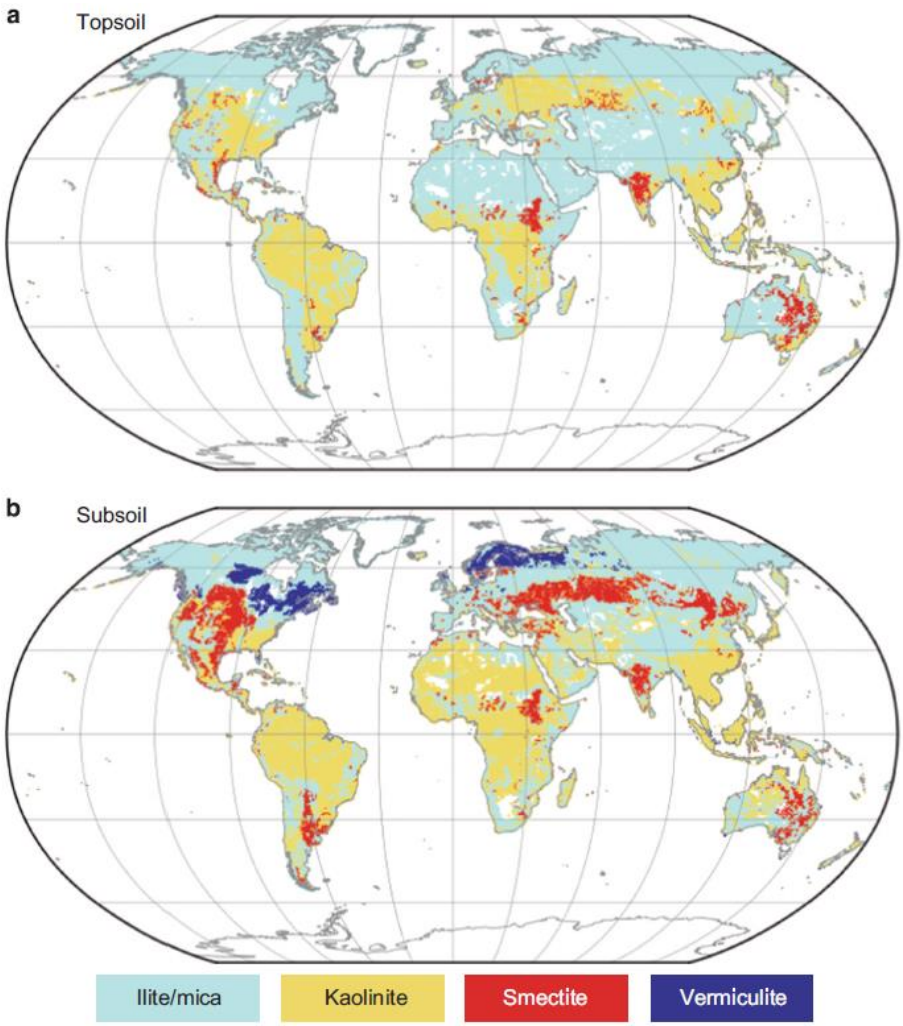


Figure 2.3. Worldwide distribution of most common clay deposits on (a) topsoil and (b) subsoil (Ito & Wagai, 2017).

Clay minerals belong to the silicate mineral class, which means that their main unit cell is four $O^{-2}$ ions, surrounding a $Si^{+4}$ ion in a tetrahedron form ($SiO_4^{-4}$) due to the rules of orbital bonding geometry (Guggenheim & Martin, 1995; Mukherjee, 2013). A subclass of clay minerals is phyllosilicates, which define the sheet-like shape formed by the linked $SiO_4^{-4}$ tetrahedra. These sheet-like structures are formed by oxygen ion interlinking of two $SiO_4^{-4}$ tetrahedra and their width is approximately 20 times its thickness (Velde, 2013); thus, these structures are often approached as 2D. It is important to highlight that $Mg^{+2}$ may substitute the $Si^{+4}$ ions, which give the tetrahedra sheet a net negative charge. This is called isomorphic substitution and

combined with the unshared oxygen on the edges, various net negative charges govern the layer mechanisms of clay minerals (Wang et al., 2017). In a clay mineral, $SiO_4^{-4}$ tetrahedron never occurs alone and always with another crucial polyhedron, octahedra, which is formed by six oxygen surrounding a cation (Velde, 2013). The central cation is $Al^{+3}$ in most cases but it can be replaced by $Mg^{+2}$ or $Fe^{+2}$ due to the isomorphic substitution. The aluminum octahedron is also named gibbsite. In clay minerals, tetrahedral and octahedral layers are linked through shared oxygens and clay mineralogists use a combination of these tetrahedral/octahedral sheets to categorize clay minerals (Brigatti et al., 2006; Velde, 2013; Yariv, 1992): If a clay is consisting of tetrahedral-octahedral layers (a single tetrahedral layer linked with a single octahedral layer, where dash represents the linkage), it is categorized as 1:1 layer clay mineral. Kaolinite, halloysite, dickite, and nacrite are members of the 1:1 layer group, also known as kaolin minerals (Grim, 1953). A tetrahedra-octahedra-tetrahedra structure is categorized as a 2:1 layer structure. Smectite minerals (montmorillonite, nontronite, vermiculite, saponite, hectorite and sauconite) and illite are the members of the 2:1 layer group (Grim, 1953; Grim et al., 1937). A complex tetrahedra-tetrahedra-octahedra structure which includes a brucite-like octahedra interlayer is categorized as a 2:1:1 layer structure. Chlorite minerals are members of the 2:1:1 group, also known as the regular mixed-layer group (Gieseking, 2012). If various layers of a clay mineral are substituted with another clay mineral structure and discontinuities occur, these clays are categorized as mixed-layer clays (Velde, 2013). Members of this mixed layer group are denoted by the layer constitutes, such as kaolinite-smectite, illite-smectite, smectite-chlorite, etc. There is also sepiolite - palygorskite structures, which have a needle-like or chain-like shape rather than a sheet but behave similarly to the smectites. Members of this group are palygorskite and sepiolite, as the name suggests, and they have a very high surface area (Hillier, 1978; Murray, 2000; Velde, 2013). Stacking of these specified layer combinations -sheets- on top of each other forms the clay mineral. A schematic representation of clay mineral layers is given in Figure 2.4.

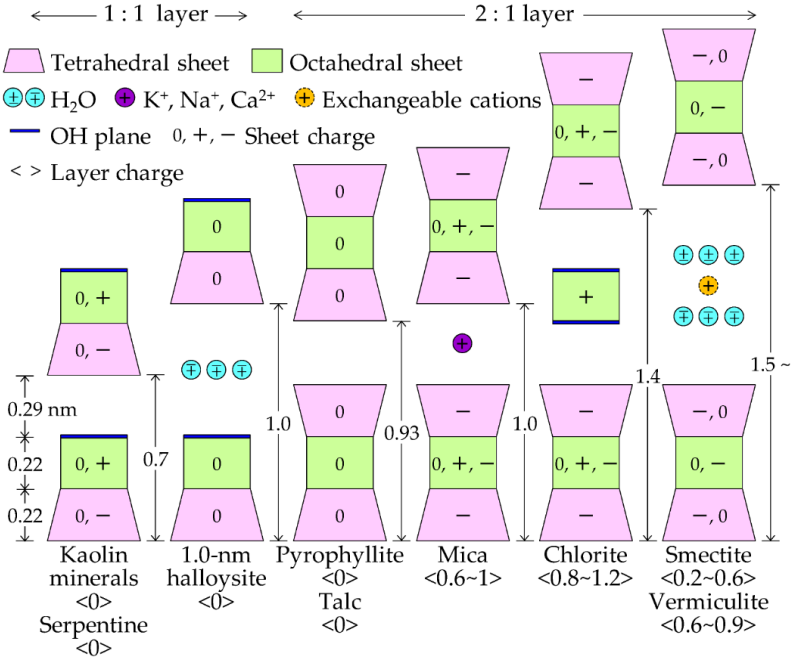


Figure 2.4. Schematic representation of clay mineral layers (Kohno, 2020).

The net negative charge of clay minerals caused by the isomorphic substitution and border oxygens might allow for an interlayer between tetrahedral and octahedral layers to satisfy electrochemical rules. Apart from the layer structure, interlayer presence is also used to categorize the clay minerals as it drastically changes the behavior of a clay mineral, most notably the swelling. The 1:1 layer group, kaolin group, has strong hydrogen bonds between the sheets. Due to the strong hydrogen bonds, water cannot form an interlayer and the clay does not swell. The most notable member of this group is the kaolinite mineral (Grim, 1953; Murray, 2000; Ross & Kerr, 1930). The 2:1 layer group often has $Al^{+3}$ cations substitute the $Si^{+4}$, which disrupts the charge balance and creates a positive charge deficiency. In this state, the bonds between the sheets are Van der Waals bonds, which are weak, and allow water in between; thus, causing swelling. The smectite group, most notably montmorillonite, is an example of this structure. However, when $Al^{+3}$ substitution is more than what is typical in a montmorillonite structure, a cation interlayer may form between the sheets to balance positive charge deficiency (Wang et al., 2017). This cation layer can consist of $K^{+}$, $Ca^{+2}$, $Mg^{+2,}$ or $Na^{+}$, and depending on the cation, a

different clay mineral is formed. Illite, which includes a $K^+$ interlayer is the most notable member of this group. Due to the cation interlayer, bonds between the sheets are stronger than those of Val der Waals but weaker than hydrogen bonds, so, the swelling of illite is more than kaolinite but less than montmorillonite. There are numerous other clay minerals to discuss but only five clay minerals, kaolinite, montmorillonite, illite, nontronite, and clinochlore that had any significant quantity in Rietveld Analysis results of this study will further be explained. Nontronite is formed by the $Fe^{+2}$ substitution of $Al^{+3}$, it behaves quite similarly to montmorillonite. Consequently, the main focus of this study was on the most notable clay minerals, kaolinite, montmorillonite (smectite group), illite, and clinochlore, similar to several other studies (I. W. M. Brown et al., 1987; Fernandez et al., 2011; He, Osbaeck, et al., 1995; Jaskulski et al., 2020).

#### 2.2.2.1 Kaolinite

Kaolinite is a 1:1 layer clay mineral that consists of water, aluminates, and silicates (Grim, 1953; Ross & Kerr, 1930). Apart from being a clay mineral group name, the *Kaolin* term is also used for rocks that consist of kaolinite minerals. Kaolin also called China clay, has white-ivory color and is commonly used in paper, paint, rubber, and ceramic industries (Murray, 1991; Wesley, 2014). Note that, there is no unification regarding what is called kaolin clay, as the term is used for high-grade kaolinite deposits from as low as 10% (low-grade) kaolinite contents (Murray, 2000). Most industries require high-grade kaolin clays for applications and any impurities which change the kaolin color may render the material unusable in color-sensitive industries like paper, paint, or ceramic, but these kaolin clays can be used as a SCM in the cement manufacturing industry, where the color is less critical (Murray, 2000; Wesley, 2014). Two color-sensitive industries, paper, and ceramic, are the biggest kaolin consumers. Murray (2000) states that the total annual global kaolin manufacture is $4 \times 10^7$ tonnes and the largest producers are England and the United

States. Besides, there are other notable kaolin deposits in China (Wilson, 2004), Brazil (Wilson et al., 2006), and Ukraine (Perederij, 2001).

#### 2.2.2.2 Montmorillonite

Montmorillonite is a 2:1 smectite group clay mineral, which have Na-montmorillonite ($Na^{+}$ substitutes $Al^{+3}$), and Ca-montmorillonite ($Ca^{+2}$ substitutes $Al^{+3}$), variations. Since other smectite group minerals, nontronite ($Fe^{+2}$ substitutes $Al^{+3}$), saponite ($Zn^{+2}$ substitutes $Al^{+3}$), and hectorite ($Mg^{+2}$ substitutes $Al^{+3}$), have similar behavior with the arguably most significant member of the smectite group, montmorillonite, "smectite" and "montmorillonite" terms are sometimes used interchangeably (Murray, 2000). Mukherjee (2013) and Wright (1968) suggested the usage of bentonite to define montmorillonite, which is another common montmorillonite term. The most important property of smectites is their swelling capacity. As defined by Douglas et al. (1980), "swelling" is the ability to keep cation structure with the presence of polar molecules, such as water. As the swelling property depends on the bond strength between the clay layers, only smectites and vermiculates show this property (Meunier, 2005). Swelling is completely reversible and causes volume changes, which may lead to catastrophic construction failures if ignored. There are many montmorillonite deposits all around the world including the United States, Wyoming (Knechtel & Patterson, 1962), Germany, Bavaria (Fahn, 1965), India, Dhani (Siddiquie and Bahl 1965), and Greece (Grim & Guven, 2011). According to Murray (2000), global annual bentonite production is $11.5 \times 10^{6}$ tons.

#### 2.2.2.3 Illite

Illite term is both the name of a mineral group and the clay mineral. Illites are similar to micas (Grim et al., 1937) and they are almost always mixed with other clays, non-clays, or shales (Murray, 2000). Their deposits can be found virtually anywhere in the world (Murray, 2000), and are one of the most abundant sedimentary rock

minerals (Mukherjee, 2013) but they are generally exclusively mined for structural applications, such as bricks, tiles, terra cotta, rather than more sophisticated applications, because of the difficulties to determine their physical properties due to impurities. Murray (2000) estimates that annual illite production is over 1 x $10^8$ tons.

#### 2.2.2.4 Clinochlore

To understand the effects of clinochlore decomposition on a calcite-calcined clay blend, it is important to understand chlorite formation: Cai & Inoue (2019) explain that chlorites are formed when antigorite $(Mg, Fe^{2+})_3Si_2O_5(OH)_4$ is stabilized with high amounts of $Al^{+3}$ under high pressure and with the presence of water. Clinochlore ($Mg_5Al_2Si_3O_{10}[OH]_8$) is the most common member of the chloride group which is rich in $Al^{+3}$ (Carrillo García et al., 2021). Also, Steudel et al. (2016) studied the various chlorites, including clinochlore, and showed that carbonates decompose at between 400-800 °C. Additionally, another study (Carrillo García et al., 2021) showed clinochlore decomposition at 425-800 °C, where secondary decomposition starts at 675 °C. Furthermore, chlorites decompose into forsterite, pyrope, spinel, and water between 750-900 °C (Staudigel & Schreyer, 1977). While there is arguably not enough research about the exact mechanisms behind the effects of the decomposed clinochlore, it is logical to assume that the conversion of Al-rich clinochlore into other phases introduces more exposed aluminates into the system, which can participate in the formation of binding phases.

### 2.2.3 Advantages of Clays as a Supplementary Cementitious Material Source

While other SCM sources have the risk to be reduced, the potential clay amount the Earth has is virtually limitless. As Eberl (1984) and Tardy et al. (1973) explained, clays are continuously formed in nature by weathering and transformation cycles and there are more than enough clay deposits to meet the needs, on the condition that the

technology is developed enough to utilize most of them. Besides, none of the clay is dangerous to human health, unlike some SCM, such as FA (Murray, 2000). Currently, many industries require clays with certain specifications and quality, such as proper color, and there is a high demand for high-grade / almost-pure clay deposits. However, the cement industry is more robust and can incorporate these previously underutilized sources to improve the cost-efficiency and eco-friendliness of the cement. Many studies (Antoni, 2013; Bratoev et al., 2018; Canut et al., 2020; Díaz et al., 2018; Hollanders et al., 2016; Jaskulski et al., 2020; Krishnan et al., 2018, 2020; Lemma et al., 2015; Nguyen et al., 2020; Rakhimova & Rakhimov, 2020; Sabir et al., 2001; Scrivener et al., 2018; Tironi et al., 2013; Trümer & Ludwig, 2018) are conducted on how to utilize clays and proper calcination process is discovered to improve the reactivity of some clays.

## 2.3 Activation of Clays by Heat Treatment

By default, cement includes a high amount of portlandite, some of which remain unreacted and provide high pH to the system. Consequently, there is excess C in the system, and by incorporating a high-silicate (S) and/or high-aluminate (A) SCM, it is possible to form more binding phases (de Silva & Glasser, 1990; Dunster et al., 1993; Massazza, 1993; Turrizani, 1964). In addition to the extra binder phases, some SCM such as calcined clays, create a filler effect and more hydration nuclei, which further enhance the early strength (Wild et al., 1996). While raw clays include high amounts of silicates and aluminates, many phases that would contribute to pozzolanic reactions are trapped within the mineralogical structure of the clay; thus, these beneficial phases cannot be utilized to the fullest extent without calcination. Calcination is the heat treatment of raw clays, in order to improve their reactivity and it works by disrupting the clay structure and exposing the reactants, especially aluminates (Fernandez et al., 2011): When a clay is subjected to heat (Figure 2.5), clay get dehydrated and free water evaporates, initially (80 - 300 °C). Next, hydroxides decompose and chemically bound water evaporates (225-450 °C) (Garg

& Skibsted, 2016). After this phase, organic components combust and clay dehydroxylation occurs. Optimal dehydroxylation temperature depends on the clay type; for example, kaolinite requires a temperature range of 600-800 °C for complete dihydroxylation (Ambroise et al., 1985; Tironi et al., 2012), while montmorillonite requires 550-850 °C (Alujas & Fernando Martirena, 2015; Jaskulski et al., 2020) and illites 600-900 °C (Fernandez et al., 2011). If calcination temperature is increased beyond the dehydroxylation limit, such as more than 850 °C for kaolinite (Sperinck et al., 2011), new more stable crystalline phases may start to form and reduce clay reactivity (Hanein et al., 2022; Sabir et al., 2001). It is crucial to highlight that complete dihydroxylation is not mandatory to achieve desired strength results as even partial dihydroxylations at lower temperatures, combined with the other positive effects of calcined clays (filler effect, pore refinement, more nucleus for phase growth, etc.), can yield satisfactory results, as such, Boakye et al. (2021)'s study showed a great risk of strength compromise at temperatures above 900 °C and Alujas et al. (2015)'s study of the calcination temperature and reactivity relationship supports this by showing the reduced reactivity due to formed mullite and sintering effect above 900 °C. This causes great difficulties to determine optimal calcination temperatures for non-pure clays, as the temperature required to completely active a clay mineral may cause other clay minerals to "burn" (Sayanam et al., 1989). Apart from the mineralogical composition and calcination temperature; clay type (Fernandez et al., 2011) time (Ambroise et al., 1985), grinding method, and fineness (Mishra et al., 2019; Zunino et al., 2020), and kaolinite content (Krishnan et al., 2020) are other factors which affect the reactivity. For calcination, several studies (Canut et al., 2020; Nguyen et al., 2020; Pinho et al., 2020) suggest rotary kiln usage, however, Krishnan et al. (2018) also showed the effectiveness of static calcination.

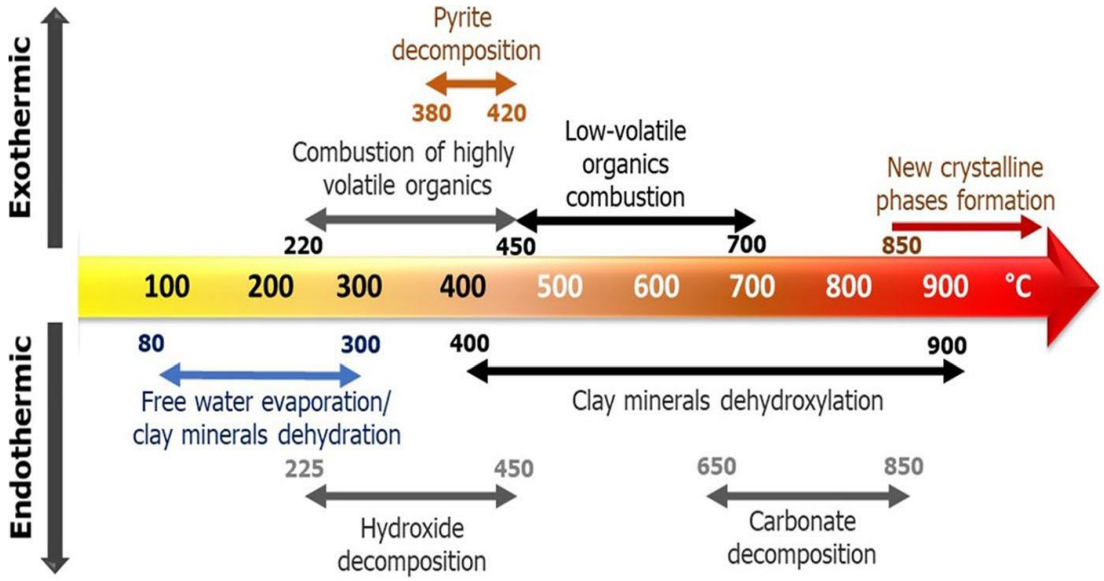


Figure 2.5. Typical changes that occur in a clay during calcination (Hanein et al., 2022).

As explained, clay minerals consist of silica-tetrahedra, aluminate-octahedra, and hydroxides that bind them. Inherently, silicate phases are resistant to heat and do not decompose as easily as hydroxides; thus, when heat is applied, aluminate phases get trapped within the silicate layers in illite and montmorillonite minerals, whereas much more aluminate exposition occurs when kaolinite is calcined (Fernandez et al., 2011). This main mechanism not only determines the required calcination temperature for the activation, but also the reactivity of the calcined clay (Fernandez et al., 2011). As seen in Figure 2.6, kaolinite has the easiest and most exposition when OH groups are removed, which makes it the most reactive calcined clay, followed by montmorillonite and illite (Ambroise et al., 1985). Fernandez et al. (2011) studied the post-calcination reactivity of montmorillonites and illites, and reported them as having lower reactivity than calcined kaolinite. Due to this, calcined kaolinite, also known as *metakaolin* is the most widely used and studied calcined clay (Badogiannis et al., 2005; Rakhimova & Rakhimov, 2020). In short, a partially retained silicate structure makes calcined montmorillonite and illite less reactive than metakaolin, due to the reduced exposed aluminate amount.

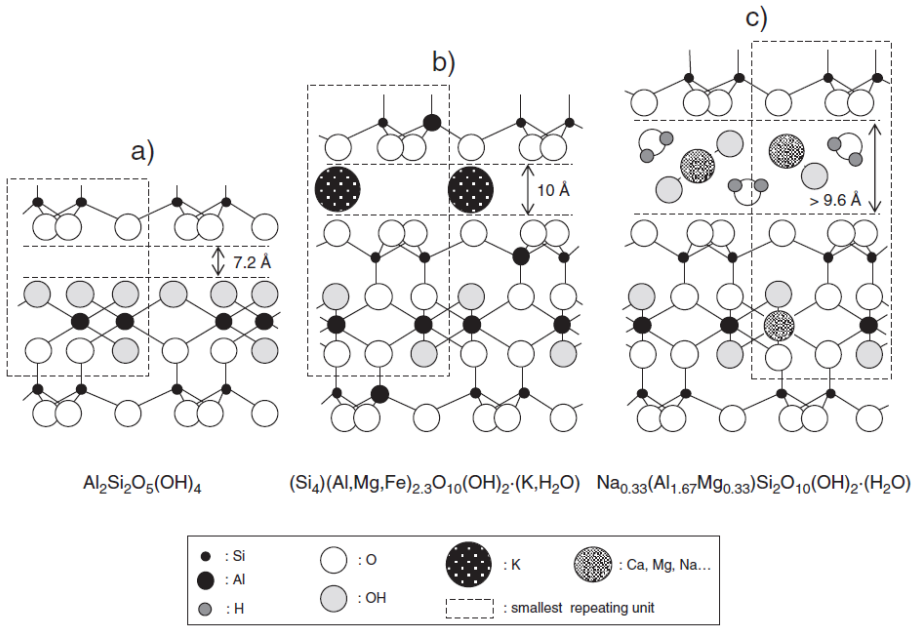


Figure 2.6. Ideal representative mineral structure of a) kaolinite, b) montmorillonite, and c) illite (Fernandez et al., 2011).

The earliest extensive studies about metakaolin characterization date back to 1959 (Brindley & Nakahira, 1959b, 1959c, 1959a). Further, (He et al., 1995) discovered the potential reactivity increase of metakaolin by calcination. Ambroise et al. (1985) and Walters & Jones (1991) studied the purity-reactivity relationship of metakaolin and found that higher-grade calcined clays display better reactivity. However, Krishnan et al. (2020) state that in terms of compressive strength, there is a neglectable benefit to using calcined clays with more than 60% kaolinite. Poon et al. (2006)'s study proved that metakaolin is more reactive than FA or even silica fume. Qian & Li (2001) incorporated 15% metakaolin into the concrete and observed a nearly 50% compressive strength increase. Wild et al. (1996) reported a 35% compressive strength increase with 25% metakaolin incorporation. Alujas et al. (2015) proved that calcined kaolin with 40% kaolinite content can replace OPC without any comprise to the compressive strength. Rakhimova & Rakhimov (2020) states that even less than 10% metakaolin incorporation may greatly increase flexural strength. Garg & Skibsted (2014, 2015) studied the montmorillonite calcination and

proved that montmorillonite is one of the most active clays in its raw state and can exhibit pozzolanic activity when calcined, up until 1100 °C. Illite shows no reactivity in the raw state (Jaskulski et al., 2020) but the studies (He et al., 1995; Lemma et al., 2015) showed a moderate pozzolanic reactivity gain with the calcination process. Note that, due to their relatively small particle size, illite is known to contribute to the strength by better densification of the matrix, and showing similar strength results of the OPC control, according to Marchetti et al. (2020). Bratoev et al. (2018) showed that in clays with multiple dominant clay minerals, only kaolinite and montmorillonite contents mattered, as the impact of chloride and illite minerals was neglectable, however, Marchetti et al. (2020) proved that calcined illite-chlorite shales can surpass OPC blends in terms of strength due to dilution effect, which indicates that SCM potentials of the less studied materials, such as clinochlore, should also be explored.

The grade of a calcined clay defines its reactive clay mineral content. A high kaolinite content almost guarantees high reactivity, as stated by Rakhimova & Rakhimov (2020). For example, a high-grade metakaolin should include high percentages of kaolinite mineral, but there are no definite percentage values for the grade; thus, the term is used liberally. Sabir et al. (2001) define high-grade metakaolin as clays with more than 90% kaolinite content. According to Trümer & Ludwig (2018), at least 40% kaolinite content is required to achieve the same strength values as an OPC blend. While it is possible to find high-purity kaolin deposits, high-grade metakaolin demand is high due to its usage in paper, paint, ceramic, construction, etc. industries. As sources (Murray, 2000; Wesley, 2014) remark, high-grade metakaolin is high in demand due to its color, reactivity, and predictability as the paper industry uses most of the high-grade metakaolin. Murray (2000) and Wesley (2014) also argue that the cement industry still is not one of the major users of this desired material. Due to this, the price of metakaolin is 2-3 times the cost of OPC (Scrivener et al., 2018), which motivated the construction material researches to utilize low-grade metakaolin, use other clays for calcination such as montmorillonite, or use calcined clays in ternary blends to further improve

substitution rate with minimal compromise to the strength and durability. Several studies (Amin et al., 2016; Fernandez et al., 2011; Hollanders et al., 2016) proved that satisfactory results can be obtained even with low to mid-grade kaolin clays.

One of the crucial factors to understand why low-grade calcined clay utilization or ternary blends work is the bottleneck effect that occurs within the blended cement matrix: A reaction, such as the pozzolanic reaction, continues as long as there exist enough reactants and proper conditions. In a traditional cement matrix, there exists unreacted Portlandite (C-H), which increases the pH of the solution but is also proven to reduce durability (Žemlička et al., 2015). These C-H phases can react with the aluminum oxides (A) and silicon oxides (S) sourced from calcined clay in a binary blend; however, due to high A and S amounts of calcined clays, Portlandite may deplete at high substitution ratios, which not only reduce pH and stop C-S-H and C-A-S-H formation but also reduce the stability of existing binding phases (Avet et al., 2019; Avet & Scrivener, 2020; Sabir et al., 2001). To overcome this problem, numerous studies about limestone incorporation to develop an optimized ternary blend are conducted: Kostuch et al. (2000) proved that only 20% calcined kaolin incorporation was enough to remove all C-H in the concrete in 28-days. Oriol & Pera (1995)'s study on cement pastes also showed depletion of all Portlandite with 30-40% metakaolin substitution in 28-days. In a ternary blend, limestone provides additional calcium phases for aluminate and silicate phases of calcined clay to react. This simple design approach allows for greatly increased binding phases, which allows for the utilization of lower-grade calcined clays or much higher substitution rates (Antoni et al., 2012). One of the most promising trends of these ternary blends is Limestone Calcined-Clay Cement (LC3), which has a traditional composition of 50% cement clinker, 30% calcined clay, 15% limestone, and 5% gypsum **(**Figure 2.7).

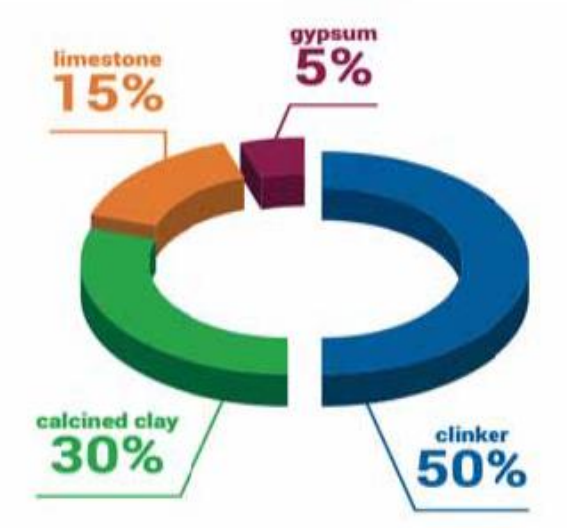


Figure 2.7. Suggested LC3 composition. Source: https://lc3.ch/

Several studies (Alujas et al., 2015; Fernandez et al., 2011; Scrivener et al., 2018) proved that a traditional LC3 blend with 40% kaolinite content calcined clay, is enough to show comparable strength results with OPC at 7-days. Krishnan et al. (2019) compared various blends and showed that the LC3 blend has the same strength values as OPC at 28 and 56 days but no notable strength gain was observed at 90 days. Antoni et al. (2012) compared 11 different blends with OPC and reported that 15% metakaolin incorporation improved strength at all ages; 30%, 45%, and 60% had higher strengths after 7-days; and even 60% substitution had a Strength Activity Index (SAI) value of 93% at 28-days. Apart from the physical property improvements, calcined clay incorporation also reduces $CO_2$ emissions (Antoni et al., 2012; Güneyisi et al., 2005) and improves durability. Studies (Antoni, 2013; Samson et al., 2003) about chloride attack show that LC3 is superior to OPC in terms of chloride ingression, as such, LC3's diffusion coefficient was only 10% of the OPC's. Nguyen & Castel (2020) studied the corrosion resistance of LC3 with 20% calcined clay and reported that while reduced pH makes the blend more susceptible to reinforcement corrosion, improved refinement greatly reduces the permeability; thus, balancing the reduced pH effect. Several studies (Scrivener et al., 2018; Shah & Bishnoi, 2018) the carbonation resistance of ternary blends, and it is stated that

while reduced Portlandite content reduces the $CO_2$ binding capacity of the blend, this problem is also balanced by the lower permeability caused by the pore refinement. Chappex & Scrivener (2012) investigated SCM usage against alkali-silica reaction (ASR), and it is proven that high alumina – high silica incorporating SCM, such as calcined clays, is one of the best methods to prevent ASR since reactive alumina in calcined clay adsorbs the reactive silica and prevents its dissolution. The same study (Chappex & Scrivener, 2012) also shows that 15% metakaolin reduces the matrix alkali concentrations by a factor of 3. In addition, Gettu et al. (2019) reported that calcination energy is 40% less than the energy required for cement manufacture.

## 2.4 Calcination Temperature for Optimum Reactivity

In order to achieve optimum calcined clay reactivity, calcination temperatures require to be high enough to disrupt the mineral structure by completely removing water and hydroxides but low enough so that reduced reactivity caused by crystallization or formation of unwanted phases, such as mullite, is avoided. Furthermore, it is important to consider that there are two calcination temperature ranges, theoretical and optimal, for clay minerals: Theoretical calcination temperatures define the temperature limit of a clay mineral to decompose (Hanein et al., 2022). Optimal temperature is where the clay mineral structure is the most disrupted, thus, exhibits the highest reactivity after calcination. For example, calcination of kaolinite technically occurs within the 500-650 °C (Gasparini et al., 2013; Ortega et al., 2010) but Fernandez et al. (2011)'s study with $^{27}Al$ NMR (Nuclear Magnetic Resonance) shows a great increase in structural disorder between 600-800 °C in the mineral structure. In other words, while kaolinite mineral technically decomposes at lower temperatures, 600-800 °C is considered as optimum calcination temperature due to the increased amount of exposed aluminates. Montmorillonite minerals have a wider calcination temperature range of 550-850 °C (Alujas & Fernando Martirena, 2015; Jaskulski et al., 2020). Illite minerals include the most silicate in their mineralogical structure, thus, their optimum calcination

temperature is 600-900 °C, while their theoretical calcination temperature is 450-700 °C according to some studies (Irassar et al., 2019; Msinjili et al., 2019) and 350-800 °C according to another (Avet et al., 2016). Additionally, above 850-950 °C, specific surface, thus, the reactivity of the clay reduces because of the newly formed crystal minerals (Figure 2.8).

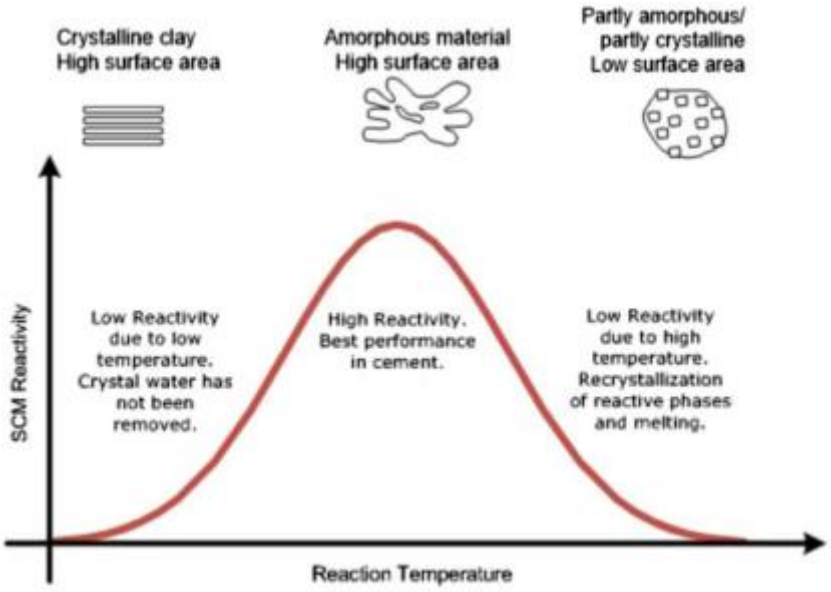


Figure 2.8. Representative SCM reactivity versus temperature graph of a clay calcination process (Hanein et al., 2022).

Another crucial aspect to consider when selecting the calcination temperature is the decarbonization of the calcites which occurs at ~700-750 °C (Dathe et al., 2021). While industrially pure limestone decarbonates at 900 °C (Hanein et al., 2021), several studies proved that decarbonization is possible at lower temperatures: Hanein et al. (2021) showed the decarbonization of the limestone is even possible at atmospheric temperatures. The lower temperature decarbonization of calcite is caused by the increasing $CO_2$ pressure, which increases the solubility of the calcite. Dathe et al. (2021) inspected the effects of lime decomposition on calcined clay reactivity and showed that the calcite decomposes into insoluble Ca-rich amorphous phases: During the calcination of clay, calcite ($CaCO_3$) releases the $CO_2$ and

decomposes into calcium oxide (CaO, quicklime) which may react with the $CO_2$ to re-crystallized into the calcite or convert to other phases. However, in the study (Dathe et al., 2021), the previous amount of calcite is not detectable with XRD post-calcination, which shows that calcite is not re-crystallized. Furthermore, at calcination temperature above 902 °C, the formation of Gehlenite ($Ca_2Al\ [AlSiO_7]$), an Al-including phase, is observed which shows that the CaO favors the reaction with the exposed aluminates of the disrupted clay mineral structure over the re-crystallization. Thus, when hydrated, the matrix system has more carbonates that can be used to form main binding phases, most notably calcium-silicate-hydrate (C-S-H) gel and calcium-(alumino)silicate-hydrate (C-A-S-H) gel. The significance of this mechanism is huge because of the previously explained bottleneck effect where C-A-S-H formation is limited by the carbonate amount. Besides, due to the potentially increased Portlandite, the pH of the system increases, which further positively benefits the reactivity speed (Shi & Day, 2000).

Based on the literature data on clay calcination, calcite decomposition, and TGA/DTA analyses conducted for the thesis, two calcination temperatures, 600 °C, and 800 °C are selected for this study, so the differences between optimal and theoretical calcination, calcite decarbonization, decomposition process of mixed clays, etc. could be observed.

## 2.5 Importance of Clay Characterization in Literature

While the literature revolving around calcined clays and their usage has been greatly developed in recent years, due to the utilization of X-Ray Diffraction (XRD) (G. Brown, 1982), Scanning Electron Microscopy (Morgan & Gilman, 2003), thermal analyses (Smothers & Chiang, 1966), and other modern methods on clay minerals; details of these advancements are still recent and more comprehensive studies about clay calcination is required, as many studies (Jaskulski et al., 2020; Mukherjee, 2013; Murray, 2000) imply. As Jaskulski et al. (2020) state, studies about clay in the civil engineering discipline are very vast, and Scrivener et al. (2018) state that extensive

local research about the calcined clays is required so that the blend designs and formulas can properly be optimized. Besides, almost all clay, calcined clay, and the blend properties depend on countless factors, ranging from composition, fineness, temperature, etc., which makes the characterization crucial. Previously, there are many different methods to characterize calcined clays were suggested: Díaz et al. (2018) introduced an assessment depending on the clay composition; Juenger & Siddique (2015) and Tironi et al. (2013) suggested various methods for determining the pozzolanic activity; Kim & Olek (2012) suggested a thermal analysis; and Odler & Skalny (1973) suggested strength methods. However, as several studies (Donatello et al., 2010; Frías et al., 2005; McCarter & Tran, 1996; Payá et al., 2001) prove, Strength Activity Index (SAI), where 20% of the cement is replaced with the test material, is one of the better methods to highlight correlations. Characterization studies containing both accurate mineralogical and empirical analyses, which include identification and quantitation data, would prove invaluable for the optimal usage of local clays as a SCM, from an engineering point of view (Murray, 2000).

# CHAPTER 3

# EXPERIMENTAL PROGRAM

## 3.1 Materials

### 3.1.1 Clays

In this study, 8 different clays that originate from various cement factories in different locations in Türkiye are provided by the TCMA. The assigned names and typical view, thus color, of those clays are shown in Figure 3.1. The XRD analyses of clays at raw state are also provided by TCMA and are given in Figure 3.2.


Figure 3.1. Raw clays with their assigned names.

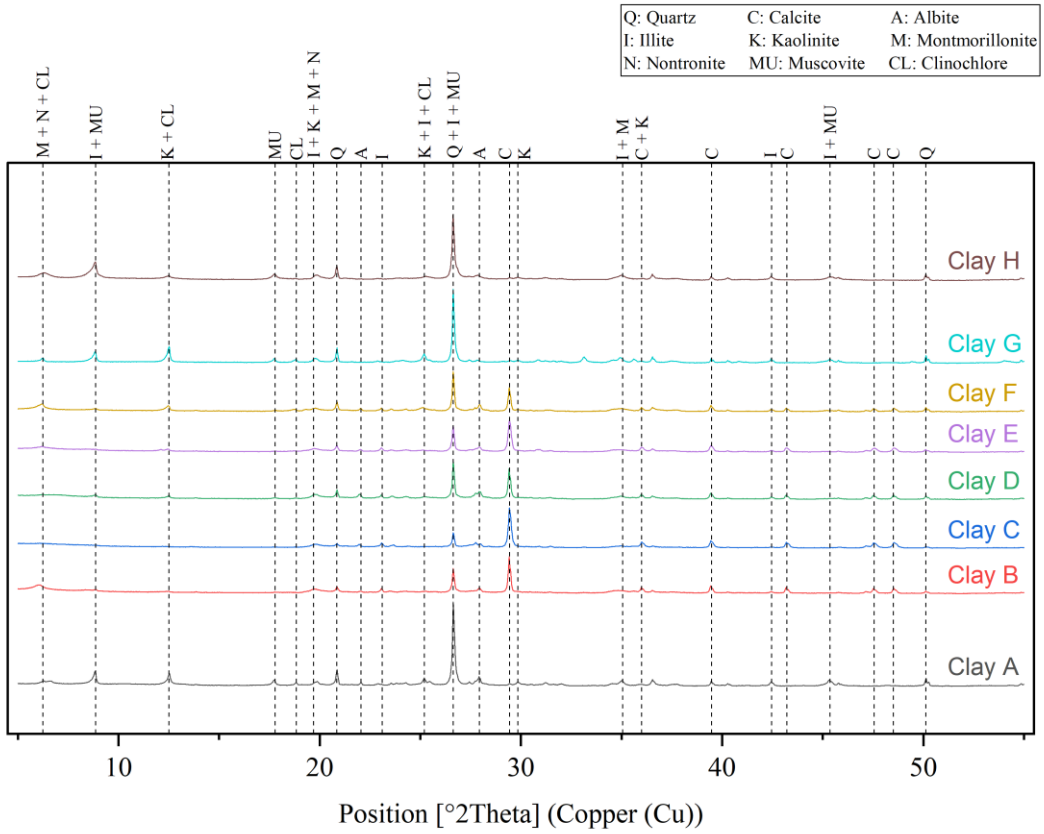


Figure 3.2. XRD analyses of non-calcined clays as performed by TCMA.

### 3.1.2 Portland Cement

For all blends of this study, CEM I 42.5 R Portland cement is used (Figure 3.3). The cement had a density of 3.11 g/cm$^3$. X-Ray Fluorescence (XRF) and X-Ray Diffraction (XRD) analysis results are given in Table 3.1 and Figure 3.4, respectively. Chemical analysis results are provided by TCMA. XRD analysis is conducted with Olympus BTX III Benchtop XRD Analyzer. X'Pert Highscore Plus software was used to process the XRD data.

Figure 3.3. CEM I 42.5 R Portland Cement.

Table 3.1 Chemical Analysis Results of Cement.

| Name of the Experiment | *Measurement Results (%)* | *Measurement Uncertainty (%)* | *Test Method* |
|---|---|---|---|
| Loss on Ignition | 6.82 | 0.08 | EN 196-2 |
| $SiO_2$ | 18.32 | - | EN 196-2 |
| $Al_2O_3$ | 4.48 | - | EN 196-2 |
| $Fe_2O_3$ | 2.84 | - | EN 196-2 |
| CaO | 61.30 | - | EN 196-2 |
| MgO | 1.59 | - | EN 196-2 |
| $SO_3$ | 2.78 | 0.13 | KKL.TA.12 |
| $Na_2O$ | 0.28 | - | EN 196-2 |
| $K_2O$ | 0.81 | - | EN 196-2 |
| $Na_2O$ Equivalent Total Alkali | 0.81 | - | Calculation |
| $Cl^-$ | 0.0425 | 0.0094 | EN 196-2 |

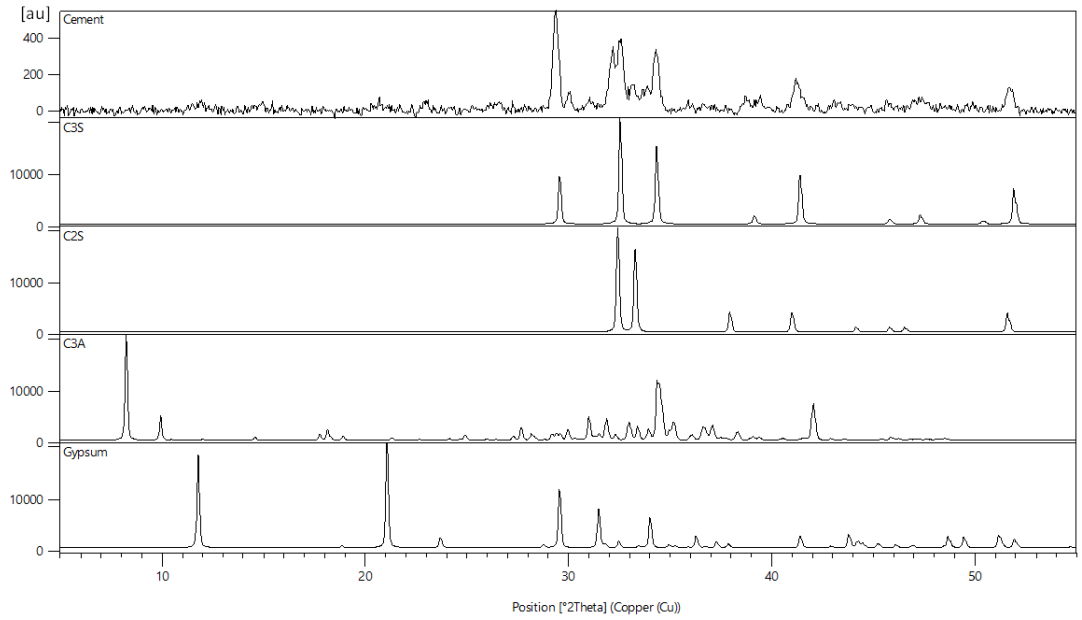


Figure 3.4. X-Ray Diffraction Analysis of Cement.

### 3.1.3 Water

In this study, Middle East Technical University tap water was used as a hydrant**.** All samples are cured in lime-water solution in a moist room following the related standard (ASTM C109, 2008).

### 3.1.4 Sand

As an aggregate for the mortar samples, available crushed limestone sand that is sourced from TAMTAŞ Construction Materials Co. was used (Figure 3.5). A sieve analysis is conducted to determine its gradation (Table 3.2), according to the ASTM C-136. Retained sand of each sieve is shown in Figure 3.6**.**

Figure 3.5. Crushed sand used during the experiments

Table 3.2 Sieve Analysis results of the sand used.

| *Sieve Number* | *Diameter (mm)* | *Soil Retained (g)* | *% Passing* |
|---|---|---|---|
| 3/8 in | 9.50 | 0.00 | 100.00 |
| No. 4 | 4.76 | 11.74 | 98.82 |
| No. 8 | 2.38 | 275.57 | 71.12 |
| No. 16 | 1.19 | 265.25 | 44.47 |
| No. 30 | 0.59 | 233.83 | 20.97 |
| No. 50 | 0.297 | 79.74 | 12.96 |
| No. 100 | 0.149 | 61.85 | 6.75 |
| Pan (Total) | - | 67.12 | - |

Figure 3.6. Sand retained on sieves during the Sieve Analysis.

## 3.2 Sample Preparation Procedures for Clays

To ensure consistency throughout the results, utmost care is given to apply the same preparation procedures for each sample. The procedures were as follows: Initial sieving and crushing, quartering, drying, grinding, sieving, calcination, and packaging. Next, packaged samples are further prepared according to the procedure of the corresponding future experiment. The following sections provide the details of the sample preparation techniques.

### 3.2.1 Initial Sieving and Crushing

Each clay sample arrived in two approximately 20kg bags (Figure 3.7) and in order to both separate the aggregates that are too large to be crushed and to see if there exists any organic material or impurities, such as leaves or pieces of rope, the whole bag is sieved throughout a 2cm sieve. Any impurities are removed after a visual inspection. As the quartering standard (ASTM C702/C702M-18, 2018) states, the maximum aggregate size should be around 50% of the splitter chutes; thus, crushing is required. Note that, the inclusion of particles larger than 2cm has a few benefits: Clay particles that coat the large aggregates get released, as hinted by Muñoz et al.

(2010); it slightly increases the overall bulk of the material, and the sample represents clay soil more accurately. With the inclusion of large particles for further procedures, grinding time becomes important in order to avoid excess grinding of the gravel. The selection of grinding time is detailed in the grinding section. Next, retained material is crushed through a mechanical crusher (Figure 3.8), then quartered through the mechanical splitter (Figure 3.9).

Figure 3.7. Clay samples have arrived in bags and stored in material storage.

Figure 3.8. Mechanical crusher used for the crushing procedures.

### 3.2.2 Quartering

Quartering is a sampling process that is used to select a small portion of a material that best represents the bulk of the material. Note that, since only a small portion of the sample material is used in the experiments, fluctuations occur within the results. To minimize the fluctuations and homogenize the material, the quartering procedure is performed according to standards (ASTM C702/C702M-18, 2018). Manual quartering or a mechanical splitter can be used. For the sake of convenience, a mechanical splitter (Figure 3.9) is used in this study. The required amount of material is separated and packaged for further procedures.

Figure 3.9. Mechanical splitter used for the quartering procedures.

### 3.2.3 Drying

Quartered material is spread out into trays and left in the 120 °C oven for at least 24 hours before grinding (Figure 3.10). This allowed the sample to lose its physically bounded water and dry, which eliminated any risk of the sample sticking to the grinder.

Figure 3.10. Clay samples are dried in the 120 °C oven before the grinding.

### 3.2.4 Grinding and Sieving

Dried samples are ground in a rotary ball mill grinder (Figure 3.11) for a constant time of 60 minutes which is decided after several iterations, as it provided the adequate fineness of more than 80% of the material passing through the 75-micron (No. 200) sieve. The usage of a constant grinding time is adopted from the following studies: (Pérez et al., 2018; Souza & Dal Molin, 2005; Vizcaino Andres et al., 2015). Besides, this duration allowed adsorbed clay soil on the coarse aggregates to be separated, in accordance with the literature (Katsioti et al., 2009; Muñoz et al., 2010).

Figure 3.11. Rotary ball mill grinder equipment that is used in the study.

After 60 minutes, the ground material is removed from the grinder and passed through the No. 200 (75-micron) sieve. No. 200 sieve is selected for its convenience and it allows future comparison with other fineness standards, such as ASTM C-117-17 (2018), and is convenient. The dry sieve method is adopted as many of the clay samples included smectite group clay minerals which swell with water presence, thus making wet sieving, not a viable option (Norrish, 1954). Adequate amounts of sieved raw and calcined material are separated for the following experiments, especially Strength Activity Index (SAI).

### 3.2.5 Calcination

Adequate calcination temperature for the study is selected by three factors: According to the studies (Ambroise et al., 1985, 1986, 1992) 600-800 °C calcination is required for complete activation of kaolinite minerals that are the most important, in terms of providing reactivity to the calcined material; thus, 600-800 °C degree is suggested by the literature. Secondly, thermogravimetric analysis (TGA) is conducted on the tested clay samples and their calcination temperature range is selected accordingly. It is crucial to note that, other clay minerals which require much higher temperature ranges for complete dihydroxylation, such as montmorillonite, can still be partially calcined and gain reactivity. This approach is arguably better as calcination above 900 °C is advised against, as some studies (Alujas et al., 2015; Boakye et al., 2021; Sayanam et al., 1989) highlight the decrease in reactivity. Calcination temperature selection is detailed in Section 2.4. Calcination Temperature for Optimum Reactivity.

For the calcination, Protherm MoS Series Chamber Furnace is used (Figure 3.12). The materials are placed in the oven in heat-resistant crucibles. The samples are heated to the target calcination temperature with a rate of heat of 5 °C/min. Next, the samples are kept at the target calcination temperature for 60 minutes to allow

complete calcination. The calcined samples are left to cool in the oven. Cooled samples are removed and packaged to prevent any dust or impurities.

Figure 3.12. Protherm MoS Series Chamber Furnace used for the clay calcinations.

Color change of the clays with the calcination is discussed by Hanein et al. (2022) and it is explained by the oxidation or reduction of iron-oxide in the clay composition (Figure 3.13). This phenomenon is detected during the study (Figure 3.14).


Figure 3.13. Color change of raw clay with the calcination under a) oxidizing b) reducing conditions (Hanein et al., 2022).

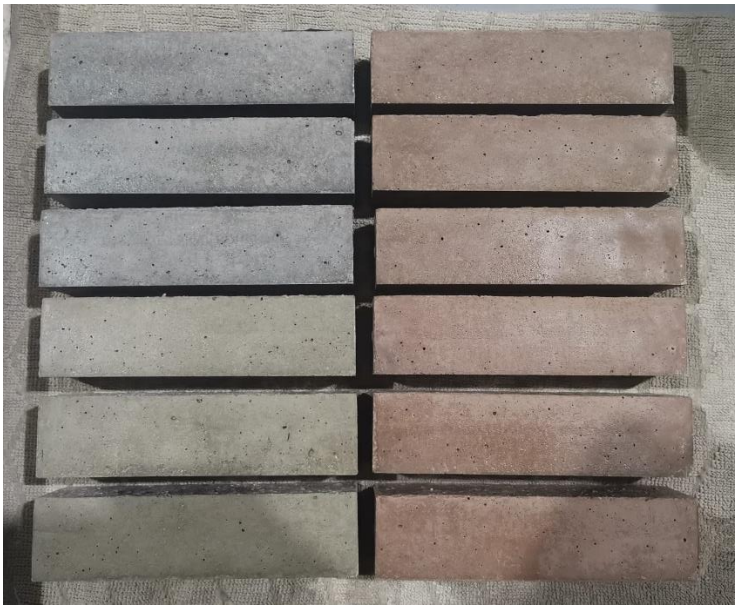

Figure 3.14. Color changes of various clay samples after the calcination.

## 3.3 Experimental Procedures

### 3.3.1 X-Ray Diffraction (XRD) and Rietveld Analyses

To identify the distribution of the minerals in the clay samples, most importantly the reactive clay minerals, the XRD method is benefitted. XRD analyses of raw clays are provided by the TCMA with the Rigaku Ultima IV/PC apparatus. XRD analyses of calcined clays and the cement were conducted with Olympus BTX III Benchtop XRD Analyzer (Figure 3.15). XRD data was processed with X'Pert Highscore Plus software. Rigaku PDXL was used for the Rietveld Analyses. ICDD PDF4 and COD databases were used.


Figure 3.15. Olympus BTX III Benchtop XRD Analyzer used for the XRD analyses.

### 3.3.2 Thermal Gravimetric Analysis and Differential Thermal Analysis (TGA/DTA)

In order to determine the changes that occur in a clay sample during the calcination, TGA/DTA analyses are conducted at the METU Central Laboratory, Thermal Analysis Laboratory with TA Instruments SDT 650 Simultane DSC/TGA equipment. For the analysis parameters, 25-900 °C is selected as the temperature range and 10 °C/min is selected as the rate of heat. Normalized heat flow (W/g), weight (%), and derived weight (%/ °C) data were obtained. Calcination temperatures were selected according to the endothermic and exothermic peaks of the derived weight curve. Combining the obtained data with the literature allowed for the anticipation of weight changes, such as the removal of physically bonded water, or combustion of organic materials, due to the calcination process.

### 3.3.3 Particle Size Distribution

Particle Size Distribution (PSD) analyses were conducted to check the raw fineness of the clay minerals versus the post-calcination. PSD curves of raw clays are given in Figure 3.16 and 800 °C calcined clays are given in Figure 3.17. PSD analyses were conducted by TCMA via Mastersizer 2000 with Scirocco 2000 with Hopper apparatus.

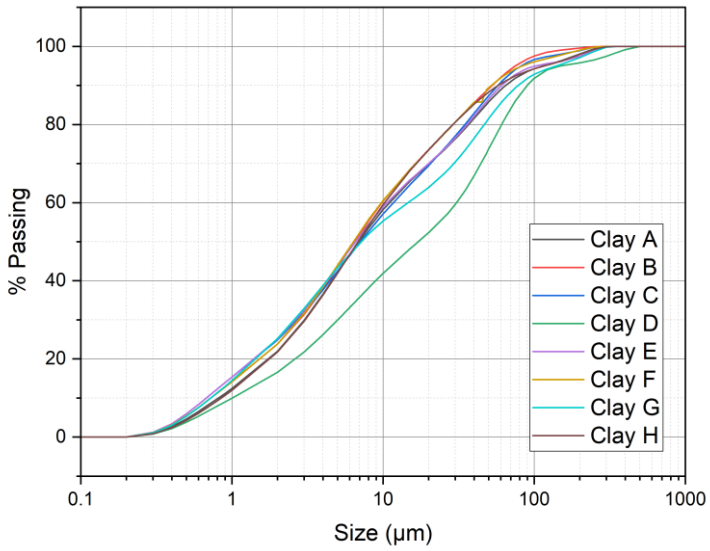


Figure 3.16. Particle Size Distribution Curves of the Raw (Non-calcined) Clays.

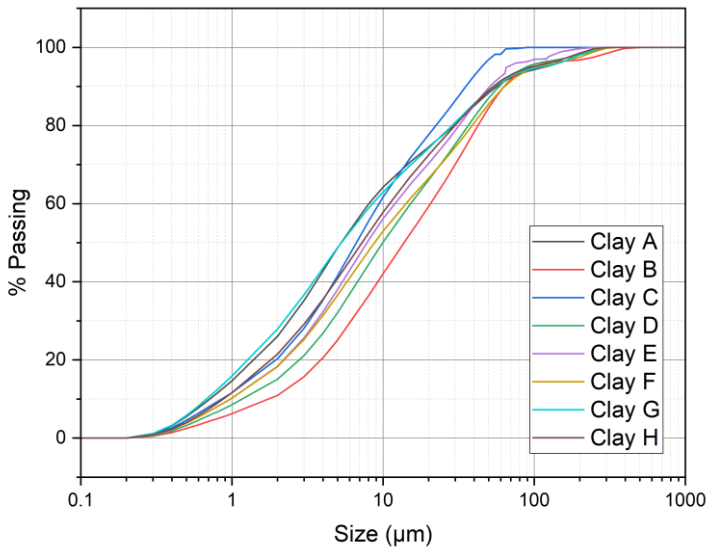


Figure 3.17. Particle Size Distribution Curves of the Clays Calcined at 800 °C.

### 3.3.4 Flow Table Tests

Constant flow is adopted for the samples prepared for the flexure and compressive strength tests. To determine the mixture flow, flow table tests are conducted (Figure 3.18). All test procedures are conducted according to ASTM C-230 and ASTM C-1437. The percentage water demand increases relative to the constant flow of the clay samples are given in Table 3.3**.**

Table 3.3 Water demand increase of clay samples for constant flow, relative to the control.

| | Water Demand Increase Relative to the Control for Constant Flow* | | |
|---|---|---|---|
| Clay Type | *No Calcination* | *Calcined at 600 °C* | *Calcined at 800 °C* |
| Clay A | +13.1% | +8.1% | +8.7% |
| Clay B | +38.2% | +10.8% | +10.8% |
| Clay C | +21.7% | +10.2% | +10.8% |
| Clay D | +15.9% | +7.0% | +7.6% |
| Clay E | +21.0% | +9.6% | +11.5% |
| Clay F | +17.0% | +9.5% | +8.3% |
| Clay G | +10.8% | +12.0% | +9.5% |
| Clay H | +20.4% | +14.6% | +12.1% |

**Procedure specified for SAI in ASTM C311 is adopted.*

Figure 3.18. Flow Table Test.

### 3.3.5 Flexure and Compressive Strength

Ground and packaged samples are tested with a reference cement sample to determine their Strength Activity Index (SAI), according to the ASTM C311–16. As the standard explains, a reference mixture of 500g cement, 1375g sand, and adequate water are compared with the mixtures prepared with 100g clay, 400g cement, 1375g sand, and adequate water for the same flow (Figure 3.19). The mixture procedure was conducted according to the ASTM C305 with the tabletop mixer (Figure 3.20).

Figure 3.19. Prepared material and testing apparatus before the mixing procedure.

Figure 3.20. Tabletop mixer that is used to mix mortar samples.

Next, 40x40x160mm prism molds (EN 196-1, 2005; EN 12390-1, 2000) are filled to the half and compacted with a TONINDUSTRIE compaction table. EN molds are preferred over ASTM molds due to their allowance of flexure strength. Another compaction is applied after the other half is filled and the poured samples are left to set (Figure 3.21). After 24 hours, the samples are demolded and placed in limey water within a moisture room until the day of testing.

Figure 3.21. Typical view of molded samples.

Figure 3.22. Samples in the moist room.

Flexure and compressive strength tests are conducted with UTEST UTCM-3742.FPR Automatic Cement Flexure/Compression Testing Machine (Figure 3.23), and according to the ASTM C-308 and ASTM C-109, respectively. The coefficient of Variation (CoV) is calculated to ensure test consistency. The flexure and compressive strength results of each clay are compared with its reference sample to determine its strength percentage (Strength Activity Index). SAI calculation is given in Appendix A. ASTM C-618 states that either the 7-day or 28-day SAI requirement needs to be met to prove satisfactory reactivity of the sample; however, all 7-day, 28-day, and 90-day strengths are tested in this study to observe strength development over a wider range of ages, as natural pozzolana behavior, such as clay, is arguably more changeable compared to the cement. Demolded samples at pre- and post-flexure strength tests are shown in Figure 3.24.


Figure 3.23. UTEST UTCM-3742.FPR Automatic Cement Flexure/Compression Testing Machine.

Figure 3.24. Cured samples ready for flexure or compression strength tests.

# CHAPTER 4

# RESULTS AND DISCUSSION

In this section, experimental results are presented and discussed to characterize the clays before and after calcination. Relationship between the clay composition, mineralogical, thermal, physical tests, and the Strength Activity Index (SAI) results are analyzed for each clay. Next, patterns observed for the clays of the study are discussed. Possible mechanisms for the performance of calcined clays are inspected, with the aid of the related literature.

## 4.1 Characterization of Clays and Calcined Clays

### 4.1.1 Clay A

Rietveld Analysis (Table 4.1) shows that Clay A is an Illite/Kaolinite Clay with trace amounts of montmorillonite and clinochlore clay minerals. Clay A includes the second-highest kaolinite content with 27.7% after Clay F (28.3%). Furthermore, Clay A includes a considerable amount of illite with 15.7%. Montmorillonite (8%) and clinochlore (6.5%) content is arguably too low to have a noticeable strength contribution in SAI. The material has 11.1% albite which is as inert as the quartz mineral (23%) (Harada & Hagiwara, 1984). The clay also had a calcite amount of 5.9%.

Table 4.1 Rietveld Analysis of Clay A

| Crystal Name | *Amount (%)* |
|---|---|
| **Quartz** | **23.0** |
| Calcite | 5.9 |
| **Albite** | **11.1** |
| **Illite** | **15.7** |
| **Kaolinite** | **27.7** |
| Montmorillonite | 8.0 |
| Clinochlore | 6.5 |
| Alunite | <0.1 |

TGA/DTA analyses are conducted on Clay A to inspect the weight change with respect to the temperature and determine the calcination temperatures (Figure 4.1). Considering the changes in clays during the calcination process, a summary of which is provided in Figure 2.5, the TGA/DTA analysis results indicate that the evaporation of free water occurs between 60-100 ℃ and highly volatile organic materials combust between 100-200 ℃. Next, dehydration (release of chemically bonded water) occurs between 200-300 ℃. Between 300-450 ℃, hydroxides start to decompose. Between the 450-600 ℃ calcination of the kaolinite starts to occur. Between 600-850 ℃, illite decomposes, with a slight increase in weight loss at around ~750 ℃ likely due to the decarbonization of the calcite.

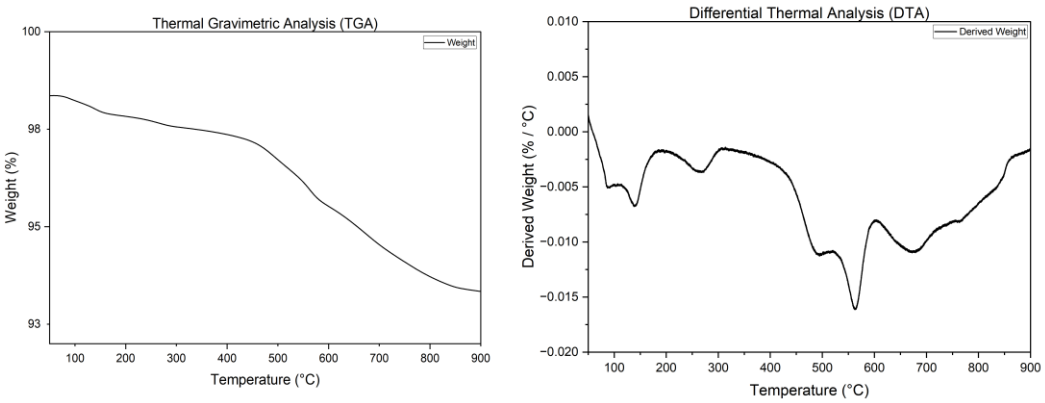


Figure 4.1. TGA/DTA Analyses of Clay A

Particle Size Distribution (PSD) analyses are conducted on Clay A to check the fineness of the material at various experiment steps (Figure 4.2). A slight increase in fineness was observed with the 800 °C calcination. This might be due to the thermal cracking, changes in the refraction which is used during the PSD testing, or the heterogeneous nature of the clay. Nonetheless, the fineness change of Clay A is arguably too small to have an impactful effect on the strength results.

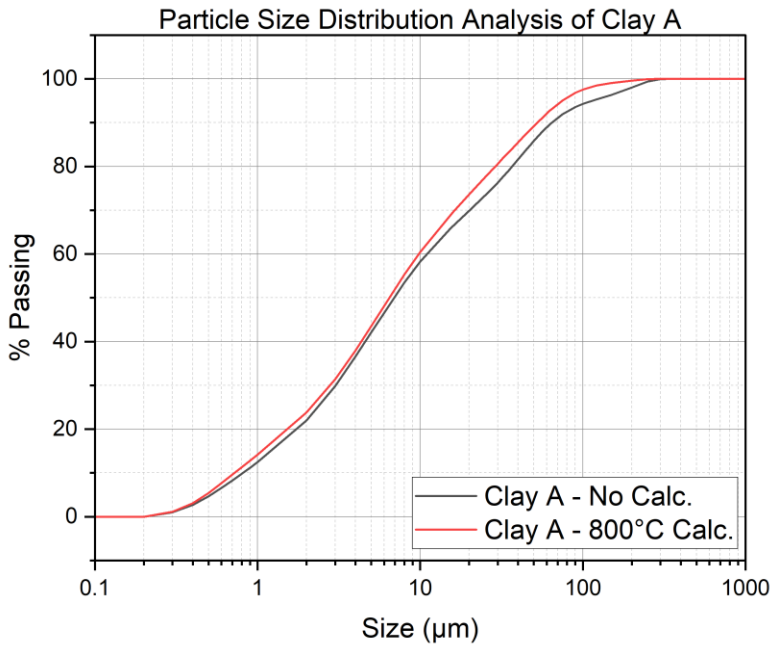


Figure 4.2. Particle Size Distribution (PSD) analysis of Clay A.

From the XRD analysis conducted on raw and calcined states of Clay A (Figure 4.3), it is clearly visible that the kaolinite peak at 2θ=12.3° disappeared after the calcination, which indicates the complete decomposition, thus, thermal activation of the kaolinite at both temperatures. Note that, while kaolinite can decompose at 550-600 °C, its optimum reactivity is achieved when the calcination temperature is between 600-800 °C, due to the additional disruption of the mineral structure (Fernandez et al., 2011). This is further detailed in section 2.4. Calcination Temperature for Optimum Reactivity. Additionally, the illite peak at 2θ=8.4° mostly disappeared at 600 °C and completely disappeared at 800 °C which indicates two things: Even though illite's decomposition temperature ranges at 600-850 °C, long calcination duration (60 mins.) at 600 °C allowed most of the illite to decompose. Secondly, a slight peak is still visible at 600 °C and it completely disappears at 800 °C which means that the remaining illite decomposed. XRD data shows that the calcination of Clay A was successful. Furthermore, inert material (quartz and albite peaks) remains the same, as expected. The decrease of sharpness of the albite peak at 2θ=29.1° is due to the disappearance of the overlapping illite peak. Formation of a new peak at 2θ=19.7° that corresponds to a silicious spinel, Potassium Aluminium Silicate ($Al_3KO_{11}Si_3$), is observed with the calcination.

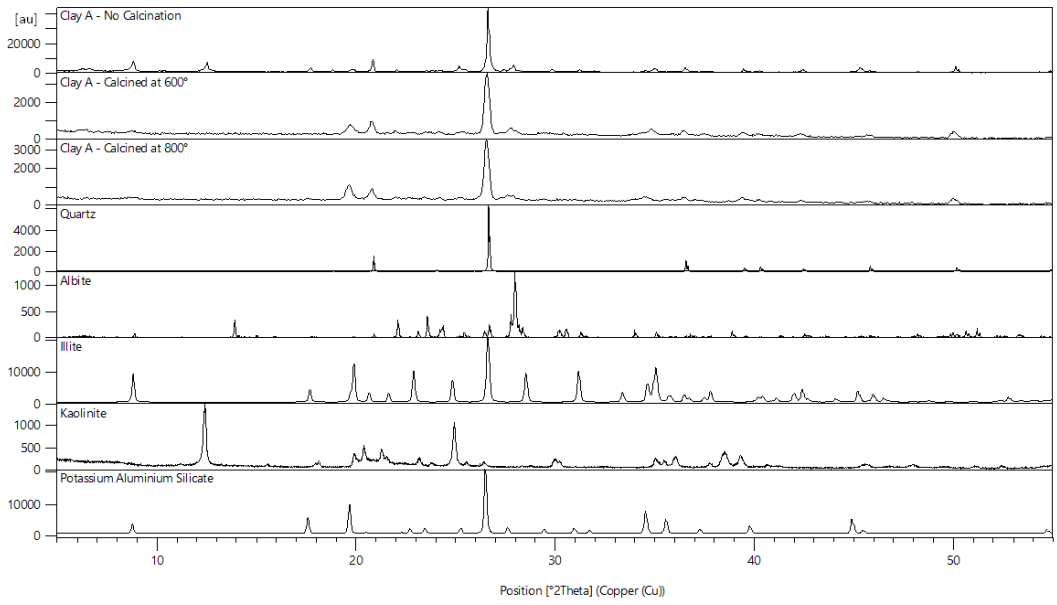


Figure 4.3. XRD patterns of raw and calcined Clay A.

Compressive strength, coefficient of variation (CoV), and Strength Activity Index (SAI) results of Clay A are given in Table 4.2. Without calcination, kaolinite or illite clays do not bear any reactivity and only act as an impurity, which explains the relatively lower (~60%) SAI results. Additionally, no increase in strength with the age is observed for the non-calcined state. With the calcination, kaolinite and illite clays decompose and gain reactivity but it is likely that due to the very limited calcite amount to provide the necessary CaO to the matrix, only a brief increase in strength is observed at 600 °C and 800 °C. Furthermore, SAI results at 7 and 28 days are similar for 600 °C and 800 °C because at 600 °C, kaolinite and most of the illite were decomposed and calcination of the remaining illite at 800 °C did not have much effect since illite has the lowest reactivity compared to the kaolinite or montmorillonite (Fernandez et al., 2011) because of the lower exposed aluminate supply of the calcined illite (Ambroise et al., 1985). It is likely that after the available CaO is depleted, the formation of binder phases came to a halt which explains the relatively lower SAI results at 90-days compared to the other clays. This points out that despite having successful calcination at various temperatures and enough kaolinite/illite content, an adequate calcite content is required for a clay to achieve satisfactory compressive strength results. Flexure strength results of Clay A are given in Appendix B.

Table 4.2 Compressive Strength Test, Coefficient of Variation, and Strength Activity Index results of Clay A

| Sample | *7-day* | | | *28-day* | | | *90-day* | | |
|---|---|---|---|---|---|---|---|---|---|
| | *MPa* | *CoV (%)* | *SAI (%)* | *MPa* | *CoV (%)* | *SAI (%)* | *MPa* | *CoV (%)* | *SAI (%)* |
| Not Calcined | 25.8 | 4.8 | 62.5 | 28.4 | 3.2 | 60.7 | 41.0 | 4.2 | 68.5 |
| Calcined at 600 °C | 29.7 | 2.6 | 72.1 | 32.2 | 1.3 | 68.8 | 38.8 | 5.0 | 77.9 |
| Calcined at 800 °C | 28.6 | 3.1 | 69.5 | 34.7 | 2.3 | 74.1 | 44.2 | 2.0 | 80.6 |

### 4.1.2 Clay B

Rietveld Analysis (Table 4.3) shows that Clay B is a Smectite Clay with nontronite being the major clay mineral. Nontronite occurs when $Fe^{+2}$ substitutes $Al^{+3}$ in montmorillonite mineral (Murray, 2000), as such, two clay minerals behave very similarly in most cases and have similar XRD results. Apart from the nontronite, Clay B has negligible amounts of illite and kaolinite as clay minerals. Clay B has a significant calcite presence of 29% and a moderate quartz presence of 17.2%.

Table 4.3 Rietveld Analysis of Clay B

| Crystal Name | *Amount (%)* |
|---|---|
| **Quartz** | **17.2** |
| **Calcite** | **29.0** |
| Albite | 7.8 |
| Illite | 0.8 |
| Kaolinite | 2.6 |
| Bentonite | 2.9 |
| **Nontronite** | **34.7** |
| Microcline | 5.0 |

TGA/DTA analysis results of Clay B indicate the evaporation of free water between 50-100 °C, combustion of volatile organic material between 120-160 °C, and dehydration (release of chemically bonded water) between 160-200 °C. The peak at ~500 °C is suspected to be the combustion of low-volatile organic compounds. Next, a significant peak is observed between 700-750 °C. This is likely due to the decarbonization of the calcite, overlapping with the montmorillonite decomposition that starts at ~575 °C.

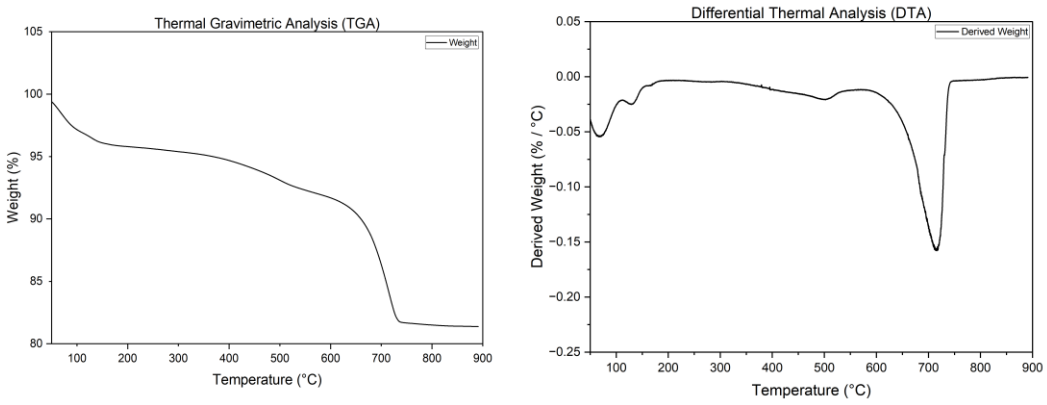


Figure 4.4. TGA/DTA Analyses of Clay B.

Particle Size Distribution (PSD) analysis results of pre and post-calcination Clay B are provided in Figure 4.5. While Clay B was slightly finer than the average at raw state, it became the least fine clay after the 800 °C calcination. Ferreiro et al. (2019) state the formation of spherical shapes during the conversion of clay minerals to amorphous phases, which may be the cause of the reduced fineness. Additionally, nontronite presence may have played a role as the montmorillonite minerals are proven to intensify the sintering effect within a calcined clay (Abdrakhimov et al., 1999). Nonetheless, despite the decreased fineness, the strength results of the Clay B calcined at 800 °C were satisfactory.

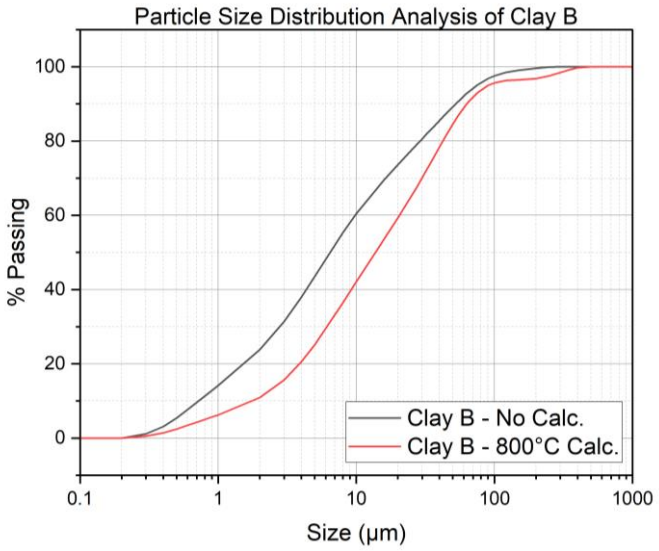


Figure 4.5. Particle Size Distribution (PSD) analysis of Clay B.

According to the XRD analysis of Clay B (Figure 4.6), the visible nontronite peak at 2θ=6.3° disappears after the calcination, which indicates the decomposition of the nontronite. While nontronite, same as the montmorillonite, has a decomposition temperature range of 550-850 °C, it is seen that 60-minute static calcination was arguably enough to decompose most of the clay mineral. Additionally, the calcite peak at 2θ=29.4° completely disappears at 800 °C. This is due to the calcite decarbonization at 700-750 °C, where calcite emits $CO_2$ and converts to amorphous phases. Additionally, the disappearance of calcite peaks at 2θ=36.7°, 2θ=39.4°, 2θ=43.2°, 2θ=47.5°, and 2θ=48.5° also indicates the decomposition, which is a trend in calcite containing clays of the thesis.

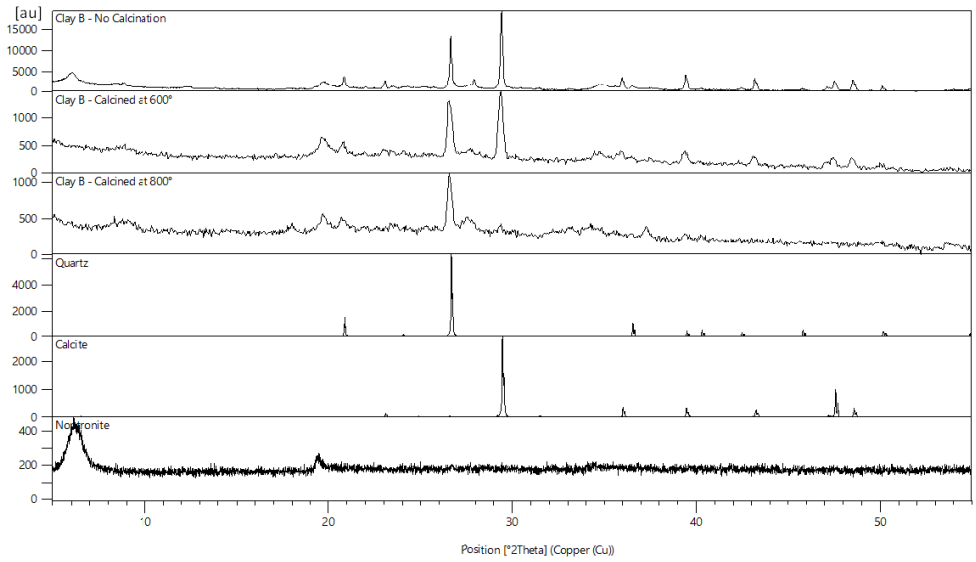


Figure 4.6. XRD patterns of raw and calcined Clay B.

Compressive strength and SAI results of Clay B are given in Table 4.4. As expected, non-calcined clay act as an impurity and greatly reduces the strength compared to the control. Based on the XRD data, calcination of nontronite for the 600 °C and 800 °C benefits the SAI greatly, even at 7-day. At 7-days, additional strength increases of 800 °C calcination are likely to be caused by the decomposition of the calcite, which increased the CaO content of the matrix solution. Note that, SAI results for

the 7 and 28 days at 600 °C are quite close, which indicates that the binder phase reactions occur at the same rate as the control sample. Furthermore, it is presumed that the increase from 44.5% to 71.4% and 43.4% to 70.4% is also positively affected by the physical effect, as calcite may have acted as a mineral admixture where more nucleus is available for the phase growth. Besides, decomposed calcite potentially increased the pH of the solution which may further hasten the reactions. The effect of formed additional binder phases with the reaction between the aluminates sourced from the decomposed nontronite and decarbonated calcites is more distinguished at 28-days, where the strength benefit of the clay calcination alone (600 °C) was weaker than when both clay and calcite is calcined (800 °C). This trend is also visible at 90-day, as 800 °C calcined Clay B reaches up to 91.1% in SAI. This scenario proves that while a strength increase can be obtained with the calcination of nontronite at 600 °C, an increased nontronite decomposition and calcite decarbonization at 800 °C is greatly beneficial for the formation of binder phases. In short, with 800 °C calcination, the material may have acted similarly to hydraulic lime, with the difference of the main reaction product assumed to be calcium-aluminum-silicate-hydrate (C-A-S-H) rather than dicalcium silicate ($2CaOSiO_2$). Another aspect to note is that Clay B has the lowest amount of combined quartz and albite and the lowest SAI at the non-calcined state, which may indicate the filler effect of the inert materials. Flexure strength results of Clay B are given in Appendix B.

Table 4.4 Compressive Strength Test, Coefficient of Variation, and Strength Activity Index results of Clay B

| | *7-day* | | | *28-day* | | | *90-day* | | |
|---|---|---|---|---|---|---|---|---|---|
| Sample | *MPa* | *CoV (%)* | *SAI (%)* | *MPa* | *CoV (%)* | *SAI (%)* | *MPa* | *CoV (%)* | *SAI (%)* |
| Not Calcined | 18.5 | 1.4 | 44.5 | 23.0 | 1.9 | 43.4 | 25.7 | 2.0 | 48.6 |
| Calcined at 600 °C | 29.7 | 2.0 | 71.4 | 37.4 | 2.7 | 70.4 | 40.5 | 2.9 | 76.5 |
| Calcined at 800 °C | 32.6 | 1.9 | 78.4 | 45.1 | 2.3 | 85.1 | 48.3 | 2.5 | 91.1 |

### 4.1.3 Clay C

Rietveld Analysis results (Table 4.5) show that Clay C falls under the Illite Clay Group with the highest illite percentage (17.1%). The material includes notable inert quartz (13.2%) and albite (20.2%), and negligible amounts of other clay minerals (kaolinite and montmorillonite-chlorite mixed structure). Out of the all clays of the study, Clay C has the highest calcite amount (43.8%).

Table 4.5 Rietveld Analysis of Clay C

| Crystal Name | *Amount (%)* |
|---|---|
| **Quartz** | **13.2** |
| **Calcite** | **43.8** |
| **Albite** | **20.2** |
| **Illite** | **17.1** |
| Kaolinite | 0.2 |
| Montmorillonite-chlorite | 1.0 |
| Sanidine | 4.6 |

Clay C's TGA/DTA results can be interpreted as follows: As expected, physically and chemically bonded water evaporates between 50-200 °C. Next, at around ~600 °C, the derived weight slope starts to increase significantly which corresponds to the illite decomposition, up until the massive endothermic peak at around ~700-750 °C caused by the decarbonization of the calcite. TGA/DTA results of Clay C are quite similar to Clay D and E.

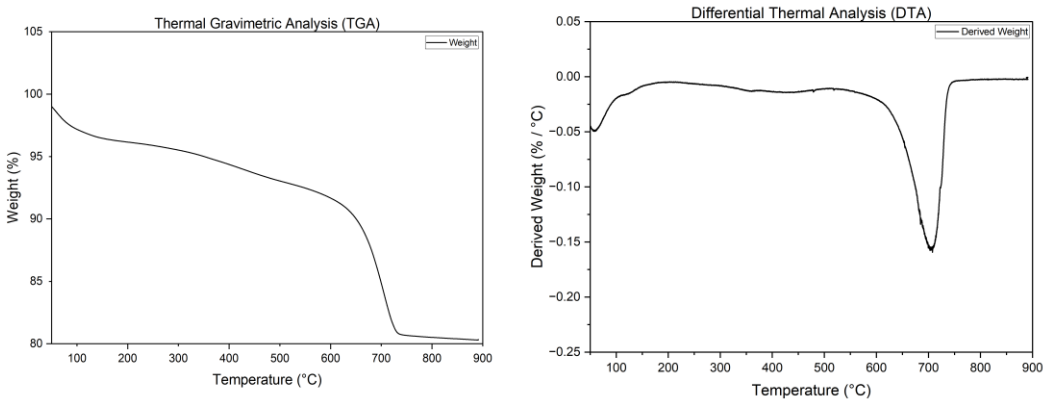


Figure 4.7. TGA/DTA Analyses of Clay C

According to the PSD analysis results of the Clay C (Figure 4.8), with 800 °C calcination, fineness decreases below 6 µm and increases above 6 µm. This trend is also observed in Clays D and E. The reason for this change may be the thermally-induced physical cracking of the particles coarser than 10 µm as Cwik et al., 2022's study shows the thermal decrepitation of limestone at 800 °C, and this mechanism might have been more effective in Clay C, which incorporates the highest calcite content.

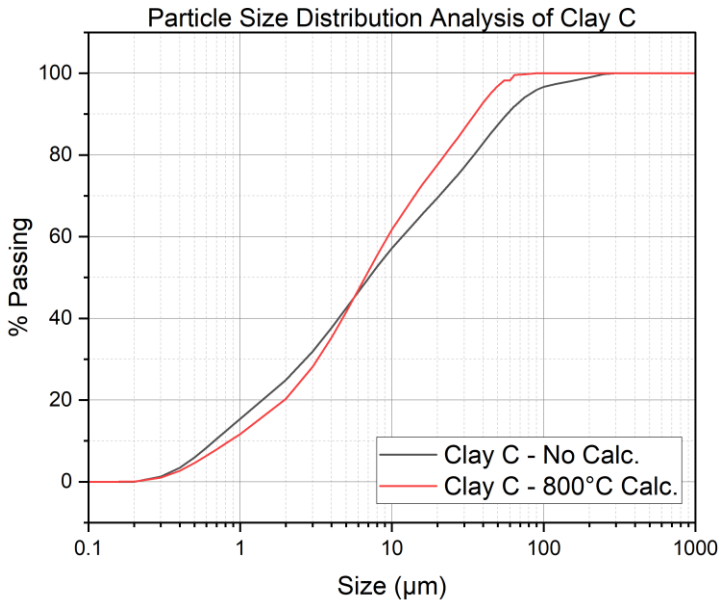


Figure 4.8. Particle Size Distribution (PSD) analysis of Clay C.

XRD analysis results of Clay C are shown in Figure 4.9. Compared to the other clay materials, Clay C includes the highest calcite and albite content, both of which have overlapping peaks with the illite. Furthermore, the very high calcite content and relatively lower clay mineral content of Clay C makes it harder to detect changes in other minerals, however, the disappearance of non-overlapping small illite peaks are observed at 2θ=23.0°, 2θ=31.2°, 2θ=34.9°, and 2θ=42.4°, after deeper inspection. While still small, some illite peaks, which completely disappear at 800 °C, were visible at 600 °C. This shows that illite was partially decomposed at 600 °C and decomposition increased with the calcination temperature increase. Most notably, decarbonization of the calcite from 600 °C to 800 °C is observed with the disappearance of the peak at 2θ=29.4°.

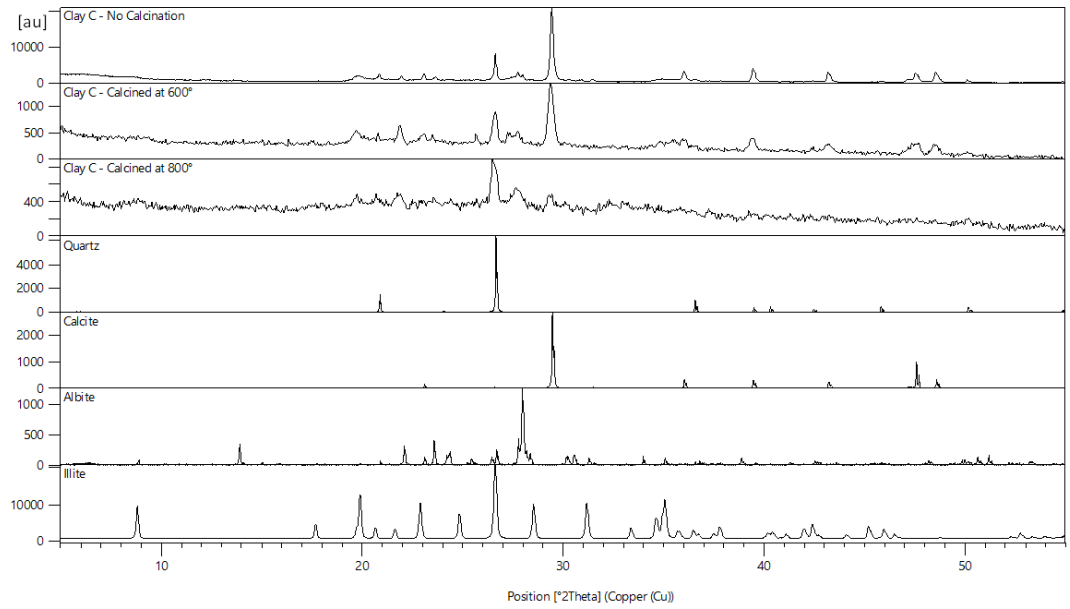


Figure 4.9. XRD patterns of raw and calcined Clay C.

Compressive strength and SAI results of Clay C are given in Table 4.6. As expected, at the non-calcined state Clay C acts as an impurity and reduces the strength by approximately 40% compared to the control. In the non-calcined state, mostly the

filler effect takes action which is not enough to compensate for the strength loss. After calcination, a significant SAI increase is observed at all ages. This is due to the decomposition of illite minerals which provide aluminates into the system. In the XRD analysis of Clay C (Figure 4.9), illite peaks were still visible at 600 °C, which indicates a partial decomposition. With 800 °C calcination, more illite decomposed, and more aluminates are exposed to the system. More importantly, based on the XRD data, it can be inferred that the decarbonization and quite possibly crystal-to-amorphous phase transformation of the calcite provided more free Ca-rich compounds into the matrix system, which became more effective at later ages, where SAI goes up to 101.9% at 90-days. Clay C exhibited the highest strength improvement with the calcination, likely due to the overcoming of the bottleneck effect by the highest calcite content of the clay. This is further explained in section 4.2.2 About the Strength Activity of Calcined Clays. While 800 °C calcined Clay C surpassing the control strength at 90-days is impressive, reaching the 90% SAI at 7-days is arguably more promising and further verifies the potential of calcined clays as SCMs. Flexure strength results of Clay C are given in Appendix B.

Table 4.6 Compressive Strength Test, Coefficient of Variation, and Strength Activity Index results of Clay C

| | *7-day* | | | *28-day* | | | *90-day* | | |
|---|---|---|---|---|---|---|---|---|---|
| Sample | *MPa* | *CoV (%)* | *SAI (%)* | *MPa* | *CoV (%)* | *SAI (%)* | *MPa* | *CoV (%)* | *SAI (%)* |
| Not Calcined | 24.8 | 1.5 | 61.9 | 33.0 | 2.1 | 63.8 | 39.8 | 1.3 | 68.4 |
| Calcined at 600 °C | 33.1 | 1.2 | 82.7 | 45.7 | 1.5 | 88.4 | 49.6 | 3.7 | 85.2 |
| Calcined at 800 °C | 36.0 | 1.4 | 90.0 | 50.4 | 1.6 | 97.5 | 59.4 | 2.0 | 101.9 |

### 4.1.4 Clay D

Rietveld Analysis (Table 4.7) shows that Clay D is a Smectite Clay, with a significant montmorillonite amount (%33.5). The material also includes kaolinite (11.7%) and illite (4.6%) clay minerals. Clay D has a similar amount of inert material (14.5% quartz and 13.1% albite) compared to the other clays and the third lowest calcite content (14.8%).

Table 4.7 Rietveld Analysis of Clay D

| Crystal Name | *Amount (%)* |
|---|---|
| **Quartz** | **14.5** |
| **Calcite** | **14.8** |
| **Albite** | **13.1** |
| Illite | 4.6 |
| **Kaolinite** | **11.7** |
| **Montmorillonite** | **33.5** |
| Anorthite | 6.7 |
| Muscovite | 1.1 |

TGA/DTA analysis of Clay D (Figure 4.10) yields similar results to Clay C and Clay E, where physically and chemically bonded water evaporates between 50-200 °C and calcite decomposes at around 700-750 °C. Since the dominant clay mineral, montmorillonite, has a wider calcination temperature, a small peak that indicates its decomposition can be observed at around 550 °C.

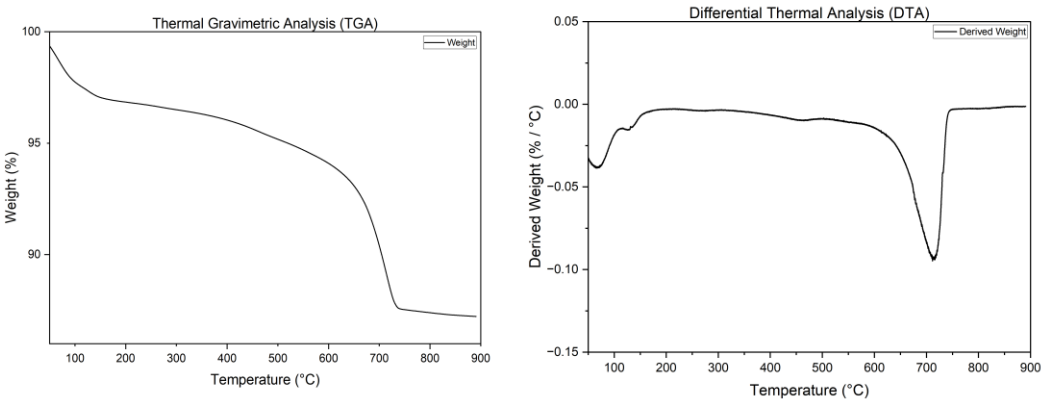


Figure 4.10. TGA/DTA Analyses of Clay D

Even though PSD analysis results of Clay D (Figure 4.11) show that the material is the coarsest among other clays of the study at both 800 °C calcined and raw state, according to the SAI performance given in Table 4.8, the material performed satisfactorily and passed the 75% compressive strength value of the control threshold given in ASTM C-618.

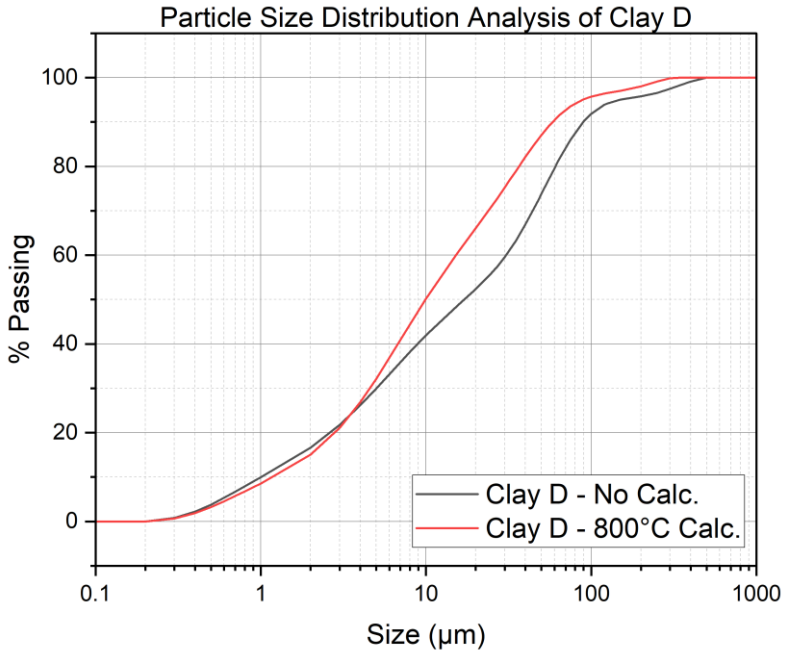


Figure 4.11. Particle Size Distribution (PSD) analysis of Clay D.

In the XRD analysis results of Clay D (Figure 4.12), a flattation of the peak, which increases from 600 °C to 800 °C, is observed at 2θ=6.4°. Additionally, the small montmorillonite peak at 2θ=34.9° completely disappears after the calcination. While the changes are only visible with a deeper inspection, increasing peak reduction at the montmorillonite peaks indicates at least a partial decomposition of the mineral. This theory is supported by the literature data where montmorillonite starts to decompose at 550° up until 850° (Alujas & Fernando Martirena, 2015; Jaskulski et al., 2020). More importantly, the reduction of calcite peak at 800 °C calcination indicates the decarbonization of the calcite mineral. Distinctly, the presence of a calcite peak at 2θ=29.4° is still observed which might indicate the non-decomposed calcite presence.

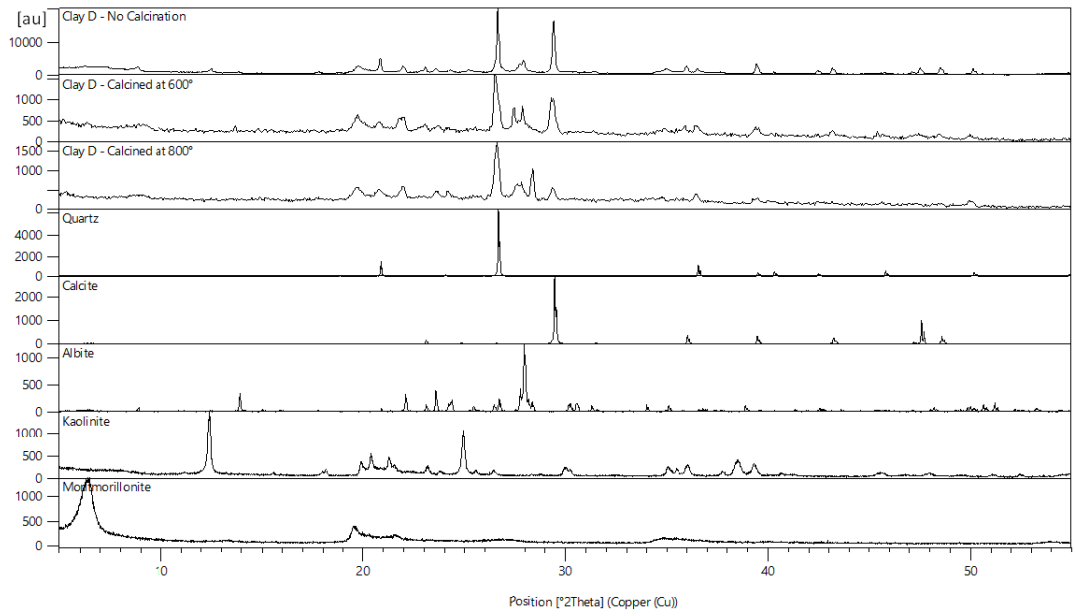


Figure 4.12. XRD patterns of raw and calcined Clay D.

Compressive strength and SAI results of Clay D are given in Table 4.8. Non-calcined Clay D shows similar SAI results with the other non-calcined clays. At 600 °C kaolinite completely decomposes, however, as Fernandez et al. (2011) proved, the

reactivity of kaolinite increases with the temperature increase up to 800 °C caused by the disruption of the mineral structure. This also reflects in the SAI results: Decomposed kaolinite and partially decomposed montmorillonite react with calcite to participate in the strength gain at 600 °C. This mechanism is improved at 800 °C to provide higher SAI results. In contrast to other clays of the study, Clay D shows higher strength results relative to its lower calcite content. This is likely due to the effect of 6.7% anorthite in the composition and underlaying mechanisms of anorthite presence are explained in section 4.2.2. About Strength Activity of Calcined Clays. Another thing to notice is that there is no SAI increase between 28 to 90 days. Since the SAI results at 7-day are lower than at 28-day, it is safe to say that decomposed minerals played a higher role after the early ages. Flexure strength results of Clay D are given in Appendix B.

Table 4.8 Compressive Strength Test, Coefficient of Variation, and Strength Activity Index results of Clay D

| | *7-day* | | | *28-day* | | | *90-day* | | |
|---|---|---|---|---|---|---|---|---|---|
| Sample | *MPa* | *CoV (%)* | *SAI (%)* | *MPa* | *CoV (%)* | *SAI (%)* | *MPa* | *CoV (%)* | *SAI (%)* |
| Not Calcined | 26.5 | 2.3 | 66.3 | 33.9 | 2.2 | 65.5 | 37.5 | 2.0 | 64.3 |
| Calcined at 600 °C | 31.2 | 2.8 | 77.8 | 44.6 | 4.2 | 86.2 | 50.0 | 2.2 | 85.8 |
| Calcined at 800 °C | 32.9 | 2.4 | 82.3 | 48.1 | 1.5 | 93.0 | 53.3 | 3.0 | 91.5 |

### 4.1.5 Clay E

Rietveld Analysis (Table 4.9) shows that Clay E falls under the Chlorite Group Clays with a clinochlore content of (21%). Calcined clinochlore is proven to show slow but decent pozzolanic activity (Irassar et al., 2019). Besides, the material includes illite (5%) and kaolinite (2.3%) minerals with negligible amounts. Clay E also consists of the second-highest calcite content of the study with 31%. The quartz amount (19.1%) is similar to the other clays of the thesis.

Table 4.9 Rietveld Analysis of Clay E

| Crystal Name | *Amount (%)* |
|---|---|
| **Quartz** | **19.1** |
| **Calcite** | **31.0** |
| Albite | 8.0 |
| Illite | 5.0 |
| Kaolinite | 2.3 |
| **Clinochlore** | **21.0** |
| Dolomite | 3.5 |
| Palygorskite | 10.0 |

Based on Clay E's TGA/DTA experiment results (Figure 4.13), the weight change between 50-100 °C indicates moisture evaporation. A slight weight loss at ~140 °C indicates the dehydration of the specimen. Between 400-800 °C dehydration and decarbonization of the clinochlore are expected. At around ~750 °C calcites decompose and clinochlore minerals are assumed to be converted into minerals forsterite, pyrope, and spinel by losing another water molecule. Decomposition of the Al-rich clinochlore potentially provided exposed aluminates to the system.

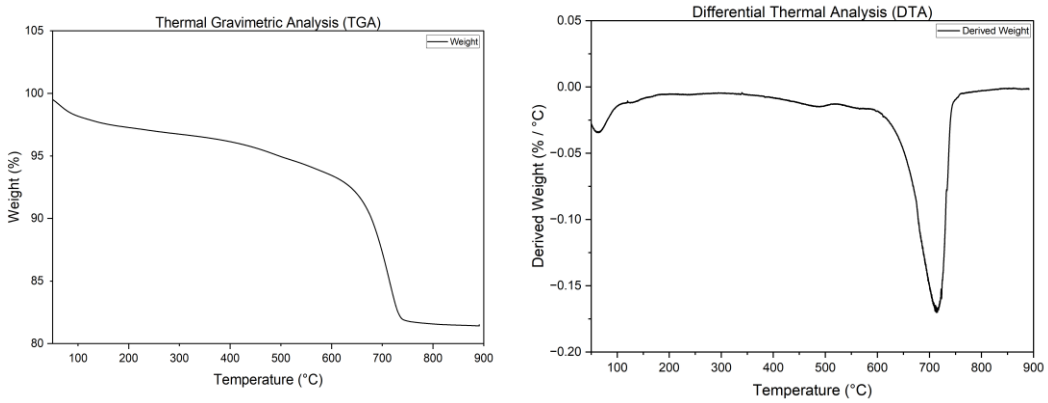


Figure 4.13. TGA/DTA Analyses of Clay E

Particle Size Distribution (PSD) results given in Figure 4.14, show nothing notable as the fineness results at raw and calcined state are quite close to each other. Yet, the fineness change is arguably not significant enough to make a considerable change in the strength results.

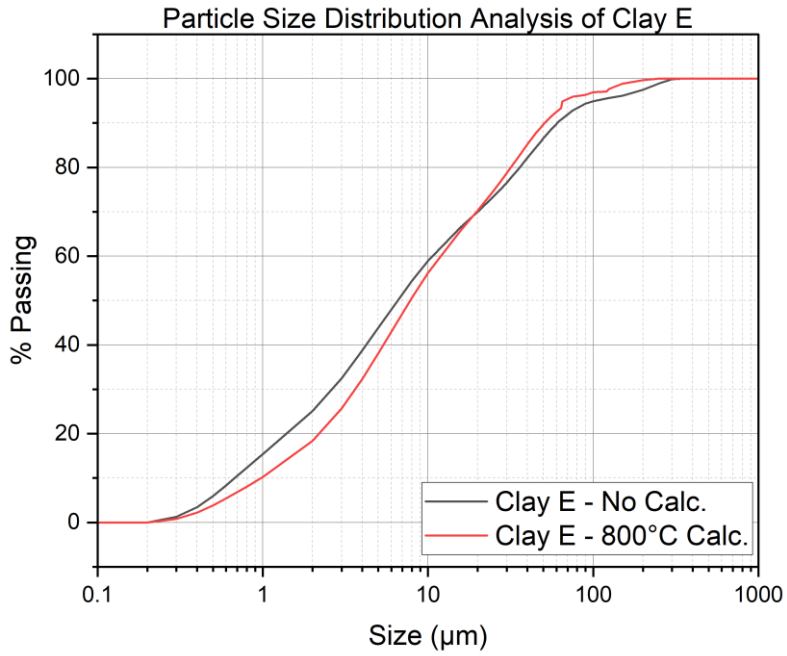


Figure 4.14. Particle Size Distribution (PSD) analysis of Clay E.

XRD analysis results of the Clay E prove the calcination of the clinochlore with the disappearance of the peaks at the 2θ=6.2° and 2θ=12.5°. Also, clinochlore peaks completely disappear at 600 °C which indicates a complete decomposition. Interestingly, 600 °C calcination caused a reduction of calcite peak at 2θ=29.4°, which means a calcite phase change into the amorphous state. Calcite decomposition that is observed in a lower temperature, 600 °C calcination, may be due to a flux effect, as the calcite can decarbonate even at atmospheric temperatures with the proper conditions (Guihua et al., 1998). Furthermore, a calcite peak (2θ=29.4°) larger than 600 °C is observed at 800 °C. This may simply be due to the heterogeneous nature of the material and sampling variance or a re-crystallization of the calcite. Similarly to the latter assumption, Rodriguez-Navarro et al. (2016) investigated the

amorphous calcium carbonate (ACC) and showed a conversion of ACC to metastable vaterite (and partially aragonite) which then precipitates into calcite crystals. In a re-crystallization case, the vaterite-calcite transformation mechanism might have caused the increase in the calcite peak at 800 °C calcination. Post-calcination, the material appears to include partially decomposed and partially precipitated calcite.

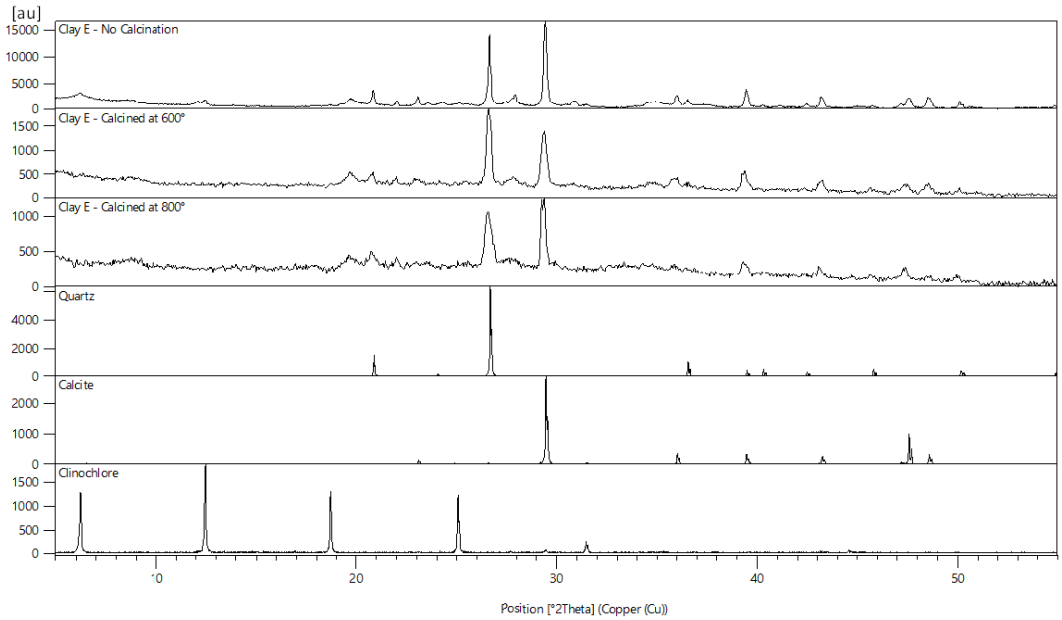


Figure 4.15. XRD patterns of raw and calcined Clay E.

According to the compressive strength and SAI results of Clay E given in Table 4.10, non-calcined Clay E performs the worst compared to the 600 °C and 800 °C calcination. At 7-days, strength development at 600 °C Clay E can be explained by decomposed clinochlore reacting with the CH in the system. For 800 °C at the same age, SAI increases as the mineral structures are more disrupted. Additionally, even though the calcite is not decomposed, it is dissolved during the mixing, thus participating in the strength development. At later ages, SAI values are quite close for both 600 °C and 800 °C calcination, which indicates that the strength development rate of the samples is similar to the control. Flexure strength results of Clay E are given in Appendix B.

Table 4.10 Compressive Strength Test, Coefficient of Variation, and Strength Activity Index results of Clay E

| Sample | *7-day* | | | *28-day* | | | *90-day* | | |
|---|---|---|---|---|---|---|---|---|---|
| | *MPa* | *CoV (%)* | *SAI (%)* | *MPa* | *CoV (%)* | *SAI (%)* | *MPa* | *CoV (%)* | *SAI (%)* |
| Not Calcined | 24.2 | 3.2 | 60.5 | 30.5 | 1.4 | 58.9 | 32.6 | 1.7 | 56.0 |
| Calcined at 600 °C | 29.2 | 3.1 | 73.0 | 35.6 | 1.1 | 68.9 | 41.9 | 2.1 | 71.9 |
| Calcined at 800 °C | 33.5 | 1.7 | 83.8 | 45.0 | 2.7 | 86.9 | 49.8 | 1.8 | 85.4 |

### 4.1.6 Clay F

Rietveld Analysis results (Table 4.11) show that Clay F is a Kaolinite/Montmorillonite Clay with a significant presence of kaolinite (28.3%) and montmorillonite (27.9%). Compared to the other clays of the study, Clay F includes the second highest amount of combined clay minerals. Clay F also includes a trace amount of illite (1.6%). It has a calcite amount of 12.9% with moderate inert material content (17% quartz and 9.9% albite).

Table 4.11 Rietveld Analysis of Clay F

| Crystal Name | *Amount (%)* |
|---|---|
| **Quartz** | **17.0** |
| **Calcite** | **12.9** |
| Albite | 9.9 |
| Illite | 1.6 |
| **Kaolinite** | **28.3** |
| **Montmorillonite** | **27.9** |
| Muscovite | 2.5 |

Evaporation of physically bonded water between 30-120 °C and combustion of highly volatile organic materials between 120-200 °C can be deduced in Clay F's TGA/DTA analysis results. Between 200-300 °C, chemically bonded water

evaporates. Between 500-550 °C, kaolinite decomposes, as its technical calcination temperature is 500-650 °C (Gasparini et al., 2013; Ortega et al., 2010). After 550 °C, the structure of decomposed kaolinite is further disrupted and calcination of the montmorillonite begins (up to 850 °C). Decarbonization of the calcite occurs between 700-750 °C.

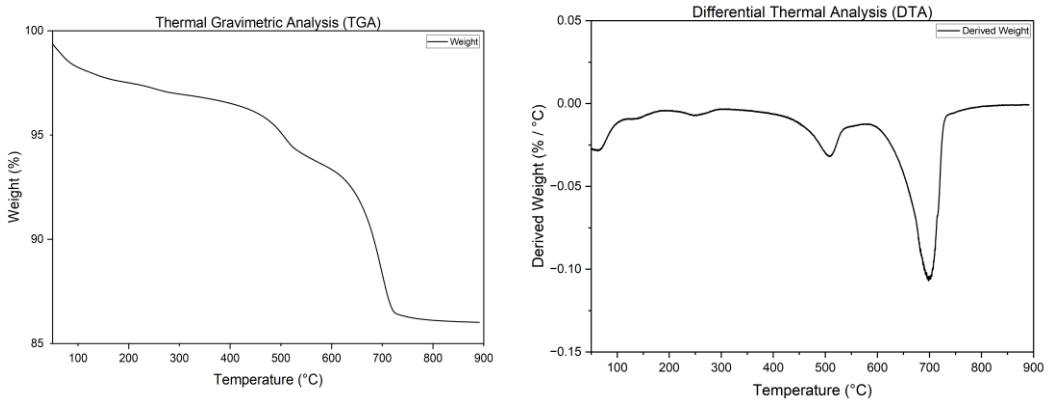


Figure 4.16. TGA/DTA Analyses of Clay F

Results of the PSD analysis of Clay F are given in Figure 4.17. After 800 °C calcination, a slight decrease of fineness is observed in Clay F. The mechanism behind the fineness decrease may be due to the clay particles forming spherical structures that slightly decrease the fineness as explained by Ferreiro et al., (2019), which is also suspected for Clay B's PSD results. Both materials include a significant amount of Montmorillonite Group minerals (nontronite and montmorillonite) and according to the study of Abdrakhimov et al. (1999), having ~30% montmorillonite clay in the composition increases the intensity of sintering of kaolinite clays. While both Clay B and Clay F show the same trend, the fineness decrease is more noticeable in Clay B which may be due to the 6.8% more Montmorillonite Group mineral, because of the explained effects. In addition, Matschei et al. (2007) explain that sintering of calcite can occur even at lower temperatures by the dissolution-recrystallization of the $CaCO_3$, which is called "cold sintering": At temperatures above 700-750 °C, where calcite starts to decarbonate, release $CO_2$ increase the

solution pressure which increases the solubility of $CaCO_3$. After the calcination, $CO_2$ release halts and pressure drops, which causes calcite to re-crystallize. This physical process, cold-sintering, might have been enhanced by the montmorillonite group mineral presence and slightly reduced the fineness of Clay F after the calcination. Nonetheless, the fineness decrease was arguably not significant enough to make a difference in strength results.

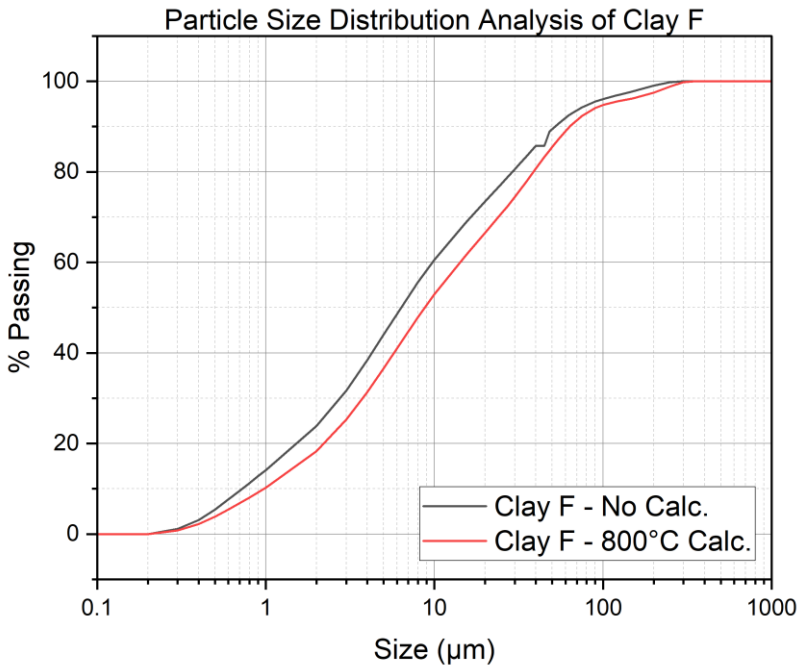


Figure 4.17. Particle Size Distribution (PSD) analysis of Clay F.

XRD analysis results of Clay F are given in Figure 4.18. Clear disappearance of peak at 2θ=6.2° indicates that montmorillonite is mostly decomposed at 600 °C and completely at 800 °C. Additionally, the disappearance of the peak at 2θ=12.5° shows that the kaolinite completely decomposed at 600 °C. Additionally, similar to the other calcite-containing clays (Clays A, B, C, D, and E), changes in calcite peaks at 2θ=29.4°, 2θ=36.2°, 2θ=39.4°, and 2θ=43.1° indicate the decarbonization of the mineral with the calcination.

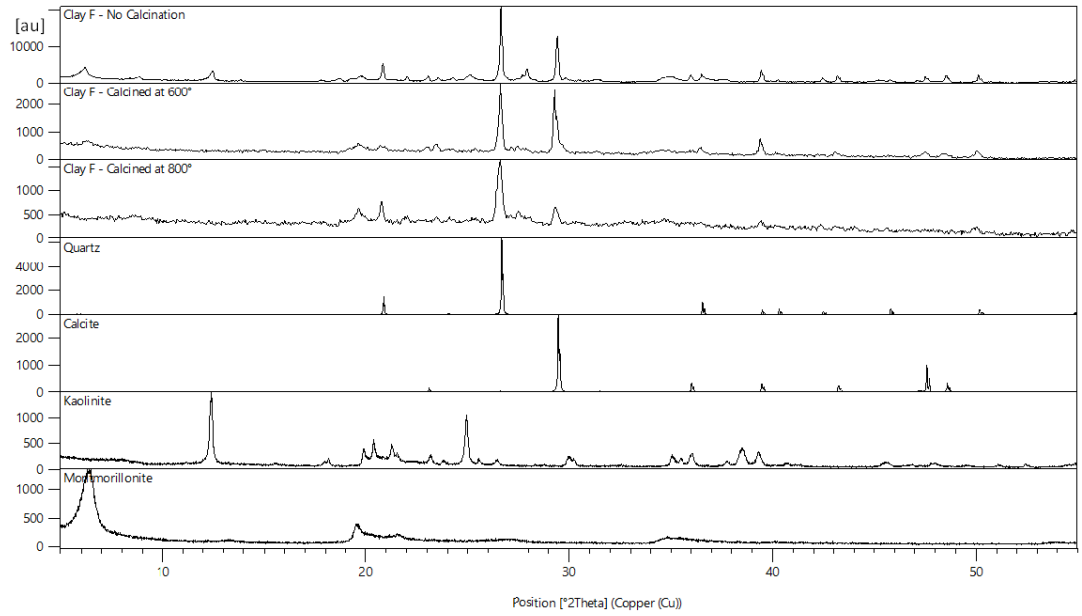


Figure 4.18. XRD patterns of raw and calcined Clay F.

Compressive strength and SAI results of Clay F are given in Table 4.12. Similar to other clays, non-calcined Clay F performs poorly in terms of strength. Calcined samples show an increase in strength, compared to the non-calcined, due to the calcined clays reacting with the calcites. 66.7% SAI at 28-day for 600 °C, which increases to 81.3% at 90-days indicates that the strength development at later ages, after 28-days, is more impactful for Clay F. This might be due to the relatively highest kaolinite content of the Clay F as by refining the pore structure the early kaolinite reactions may have surpassed the montmorillonite reactions, which came to an effect at later ages. At 800 °C, decarbonation of the calcite is assumed to improve the reactions between calcined clay aluminates and the calcium oxides, thus, resulting in a higher SAI. Flexure strength results of Clay F are given in Appendix B.

Table 4.12 Compressive Strength Test, Coefficient of Variation, and Strength Activity Index results of Clay F

| Sample | *7-day* | | | *28-day* | | | *90-day* | | |
|---|---|---|---|---|---|---|---|---|---|
| | *MPa* | *CoV (%)* | *SAI (%)* | *MPa* | *CoV (%)* | *SAI (%)* | *MPa* | *CoV (%)* | *SAI (%)* |
| Not Calcined | 24.7 | 1.0 | 59.3 | 31.6 | 1.2 | 59.5 | 34.6 | 3.0 | 65.2 |
| Calcined at 600 °C | 31.8 | 0.6 | 76.5 | 35.4 | 2.0 | 66.7 | 43.1 | 2.8 | 81.3 |
| Calcined at 800 °C | 34.1 | 2.0 | 82.0 | 42.9 | 1.1 | 80.9 | 45.7 | 1.9 | 86.3 |

### 4.1.7 Clay G

Rietveld Analysis (Table 4.13) shows that Clay G is an Illite/Kaolinite Clay with 16% illite and 14% kaolinite content. Compared to the other clays of the study, Clay G does not include any calcite. While the material has a higher quartz content (38%), it does not include any albite, thus, has a similar inert material content with the other clays. Muscovite is an aluminosilicate mineral that does not show any reactivity when calcined (Neisser-Deiters et al., 2019). Zhou et al. (2013) showed that muscovite presence can create a flux effect and reduce the temperature required for kaolinite dihydroxylation.

Table 4.13 Rietveld Analysis of Clay G

| Crystal Name | *Amount (%)* |
|---|---|
| **Quartz** | **38.0** |
| **Illite** | **16.0** |
| **Kaolinite** | **14.0** |
| Vermiculite | 6.0 |
| Dolomite | 7.0 |
| **Muscovite** | **13.0** |
| Hematite | 6.0 |

TGA/DTA analysis results of Clay G indicate that the evaporation of physically bonded water between 50-100 °C, removal of chemically bonded water between

200-300 °C and kaolinite dihydroxylation between 500-550 °C, occurred. Since this material does not include any calcite, the peak between 630-680 °C corresponds to the illite decomposition. Furthermore, Guggenheim et al. (1987) explain that the thermal decomposition of muscovite occurs in two-step: At 550 °C and 750 °C, which may have overlapped with the kaolinite dihydroxylation.

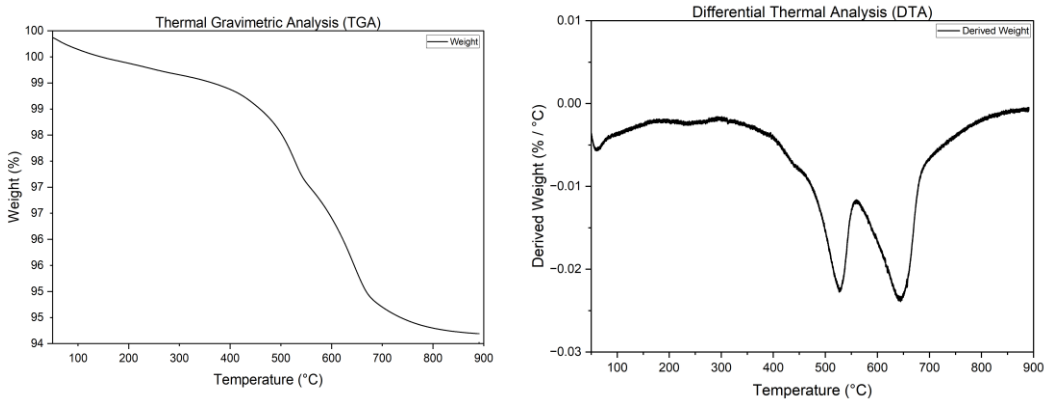


Figure 4.19. TGA/DTA Analyses of Clay G

Results of the Particle Size Distribution analysis of Clay G are given in Figure 4.20. There is a fineness increase in Clay G with the 800 °C calcination. This may be due to the thermally-induced physical cracking of the coarser particles residing within the natural clay. Still, the fineness change of the material was arguably not significant enough to have a great effect on the strength results.

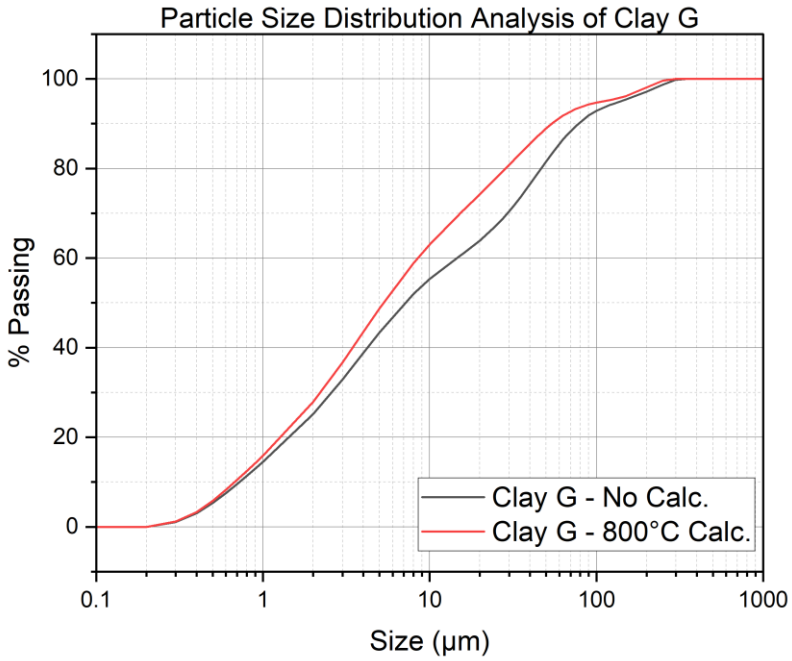


Figure 4.20. Particle Size Distribution (PSD) analysis of Clay G.

From the XRD analysis results of Clay G (Figure 4.21), peak changes at 2θ=8.8°, 2θ=17.7°, and 2θ=45.3° indicate the decomposition of the muscovite and illite, two similar minerals. Besides, the decomposition of kaolinite is clearly visible with the peak change at 2θ=12.5°. The results indicate that the decomposition of the majority of the clay minerals occurred at 600 °C, which is further improved at 800 °C. Since Clay G does not include any calcite, no calcite peaks are observed. Potassium Aluminium Silicate ($Al_3KO_{11}Si_3$) peak at 2θ=19.7° is observed after the calcination, which displays the formation of the phase.

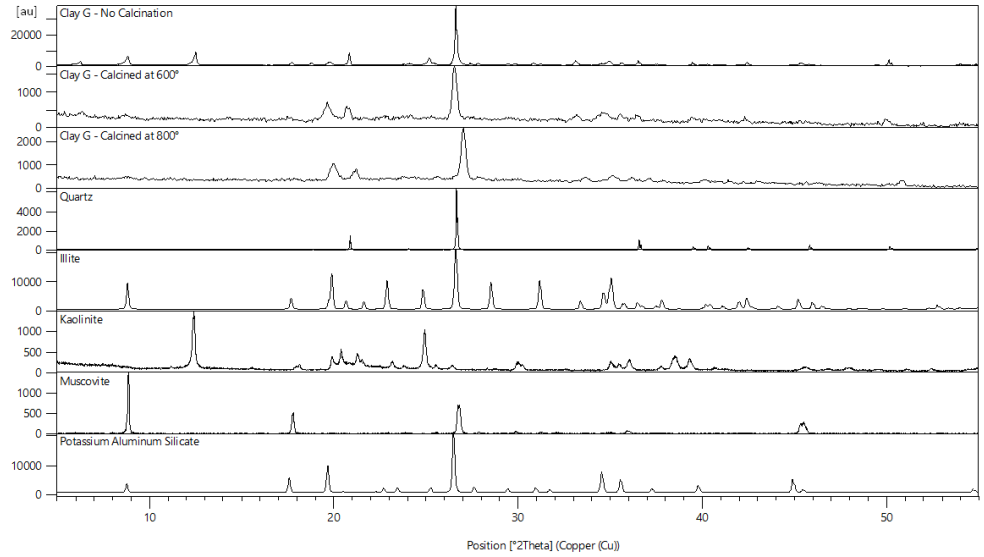


Figure 4.21. XRD patterns of raw and calcined Clay G.

Compressive strength and SAI results of the Clay G are given in Table 4.14. Despite high clay mineral content and successful calcination, strength increases at 600 °C and 800 °C calcination were minimal. This is due to the lack of calcite incorporated within the sample, as 7% SAI increase was likely due to the CH provided by the cement, and after CH depletion, no strength increase is observed. At 800 °C, the effects of enhanced decomposition caused by the increased temperature are visible but neglectable. The flexural strength results of Clay G are given in Appendix B.

Table 4.14 Compressive Strength Test, Coefficient of Variation, and Strength Activity Index results of Clay G

| | *7-day* | | | *28-day* | | | *90-day* | | |
|---|---|---|---|---|---|---|---|---|---|
| Sample | *MPa* | *CoV (%)* | *SAI (%)* | *MPa* | *CoV (%)* | *SAI (%)* | *MPa* | *CoV (%)* | *SAI (%)* |
| Not Calcined | 27.0 | 3.4 | 64.9 | 35.3 | 1.4 | 66.6 | 36.0 | 2.6 | 68.0 |
| Calcined at 600 °C | 30.0 | 1.5 | 71.9 | 36.3 | 1.3 | 68.5 | 37.3 | 2.1 | 70.5 |
| Calcined at 800 °C | 30.9 | 0.9 | 74.3 | 37.4 | 0.9 | 70.5 | 38.6 | 1.8 | 72.9 |

### 4.1.8 Clay H

Rietveld Analysis (Table 4.15) shows that Clay H is a Kaolinite Clay with 23% kaolinite minerals. Also, the material has the highest combined clay mineral amount with 16% montmorillonite, 16% clinochlore, and 8% illite. While Clay H has similar inert material content (29% quartz and 6% albite) to the other clay materials, it has negligible calcite (0.9%).

Table 4.15 Rietveld Analysis of Clay H

| Crystal Name | *Amount (%)* |
|---|---|
| **Quartz** | **29.0** |
| Calcite | 0.9 |
| Albite | 6.0 |
| Illite | 8.0 |
| **Kaolinite** | **23.0** |
| **Montmorillonite** | **16.0** |
| **Clinochlore** | **16.0** |

The following data can be inferred from Clay H's TGA/DTA analysis results: Between 50-100 °C physically bonded water evaporates. Between 100-150 °C highly volatile organic material combusts. Between 200-300 °C chemically bonded water evaporates. Between 400-500 °C clinochlore starts to decompose. Between 550-650 °C, kaolinite decomposes and montmorillonite starts to decompose. At 800 °C, complete calcination of kaolinite and partial calcination of montmorillonite and clinochlore is expected.

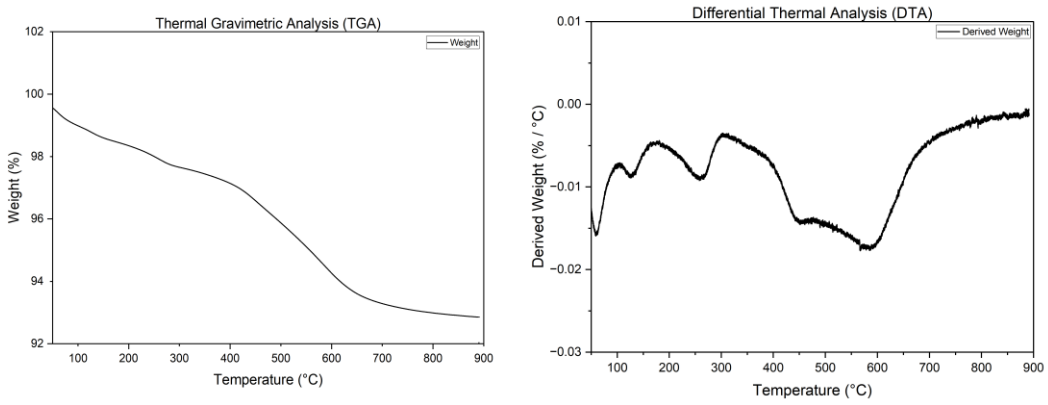


Figure 4.22. TGA/DTA Analyses of Clay H

Particle Size Distribution analysis results of Clay H are given in Figure 4.23. Interestingly, even though Clay H includes four clay minerals from various groups, illite, kaolinite, montmorillonite, and clinochlore, almost no change in the fineness is observed with the 800 °C calcination.

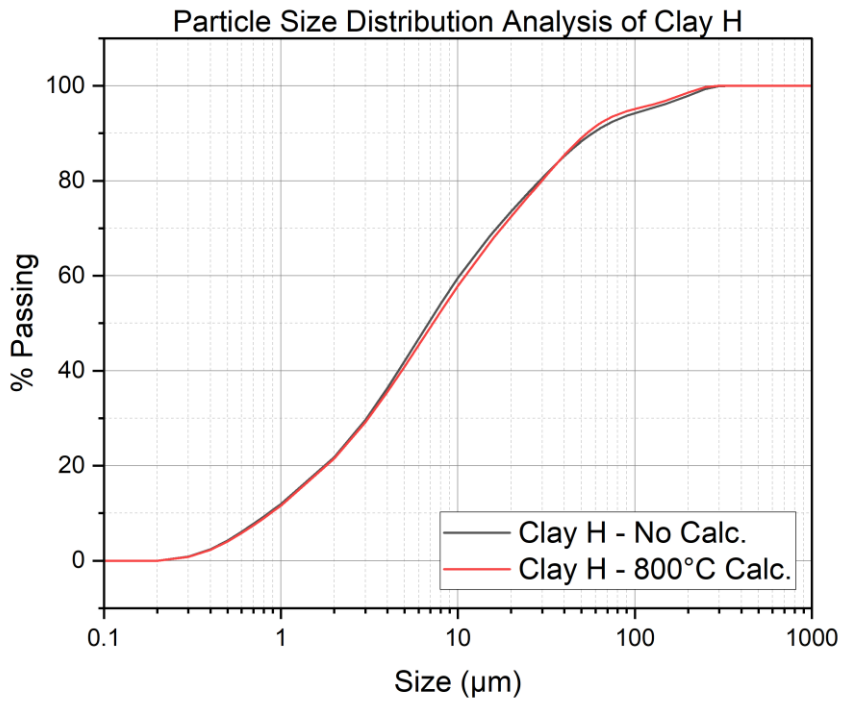


Figure 4.23. Particle Size Distribution (PSD) analysis of Clay H.

Information obtained from the XRD analysis results of Clay H (Figure 4.24) is as follows: Peak at 2θ=6.3°, montmorillonite, and clinochlore peak disappear. The peak at 2θ=12.5°, kaolinite, and clinochlore peak, disappears. Montmorillonite peak at 2θ=34.7° is still partially observed at 600 °C and 800 °C. Consequently, it is safe to say that clinochlore and kaolinite decomposed with the calcination, while there might be some intact (non-decomposed) montmorillonite minerals after the calcination. Similarly to Clay G, Clay H does not include any calcite, thus, no peaks are observed as expected. Similarly to Clay A and G, a peak at 2θ=19.7°, which indicates the potassium aluminum silicate formation is observed in Clay H after the calcination. Mechanisms behind the potassium aluminum silicate formation are detailed in section 4.2.1. About Clay Compositions.

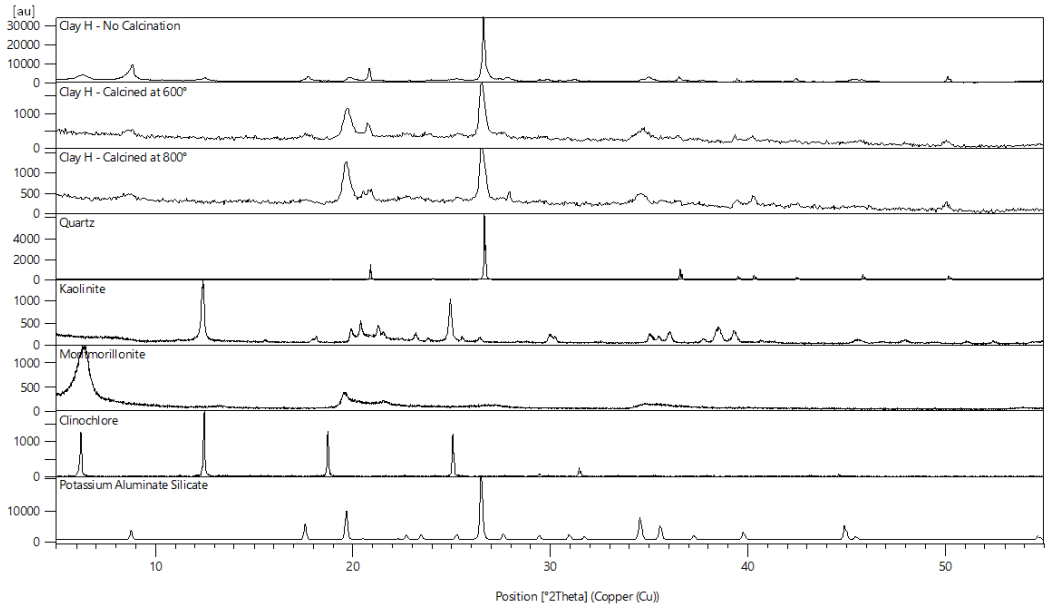


Figure 4.24. XRD patterns of raw and calcined Clay H.

Compressive strength and SAI results of Clay H are given in Table 4.16. Similar to Clay G, Clay H performs poorly even after the calcination. The strength development of 600 °C and 800 °C calcined samples is likely due to the aluminates of the

decomposed clay minerals reacting with the portlandite sources from the cement and this mechanism rapidly halts since no limestone is present within the blend. Furthermore, no SAI change at 28 and 90 days shows that the calcined clay mechanisms occur at the same pace as of control's, after the first 7 days. Flexure strength results of Clay H are given in Appendix B.

Table 4.16 Compressive Strength Test, Coefficient of Variation, and Strength Activity Index results of Clay H

| | *7-day* | | | *28-day* | | | *90-day* | | |
|---|---|---|---|---|---|---|---|---|---|
| Sample | *MPa* | *CoV (%)* | *SAI (%)* | *MPa* | *CoV (%)* | *SAI (%)* | *MPa* | *CoV (%)* | *SAI (%)* |
| Not Calcined | 22.4 | 3.1 | 55.9 | 30.0 | 1.7 | 58.0 | 33.3 | 1.5 | 57.2 |
| Calcined at 600 °C | 26.0 | 1.7 | 65.0 | 35.0 | 2.5 | 67.6 | 38.1 | 1.8 | 65.4 |
| Calcined at 800 °C | 27.7 | 2.2 | 69.2 | 35.0 | 1.3 | 67.7 | 39.7 | 2.2 | 68.2 |

## 4.2 Discussion of Results

### 4.2.1 About Clay Compositions

When the Rietveld Analyses of 8 clays were inspected, it can be seen that out of the 8 clays, only 2 (Clay B and C) included a single clay mineral, as the others included up to 4 different clay minerals. Illite or kaolinite exists in 7 clays (Clays A, G, H, C, D, E, F), making them the most common clay minerals. The kaolinite content of the kaolinite-containing clays (Clays A, D, F, G, H) ranged from 14-28.3%, making them low-grade. Illite content was similarly low-grade with 5-17.1% (Clays A, C, E, G, H). Montmorillonite content range of the montmorillonite-group clays (Clays A, B, D, F and H) was wider (8%, 34.7%, 33.5%, 27.9% and 16%, respectively). This indicates that the clays obtained from cement plants in Türkiye are low-grade, which

illite/kaolinite being the dominant clay minerals. Clays B, C, and E incorporated relatively high calcite content (>25%), while Clays D, F, A incorporated low, and Clays G and H incorporated no calcite. Clinochlore, a chlorite group clay mineral, was observed in Clay E and H. Apart from the quartz, another inert material, albite, was also common in the composition. Notably, anorthite, a rare mineral, is also observed in one of the clays (Clay D). The grouping of the clays based on their clay mineral composition is given in Table 4.17**.**

Table 4.17 Clays and Their Clay Mineral Groups

| Clay | *Dominant Clay Mineral* | *Group* |
|---|---|---|
| Clay A | Illite & kaolinite | Illite/kaolinite |
| Clay B | Nontronite | Smectite |
| Clay C | Illite | Illite |
| Clay D | Montmorillonite | Smectite |
| Clay E | Clinochlore | Chloride |
| Clay F | Kaolinite & Montmorillonite | Kaolinite/Smectite |
| Clay G | Illite & kaolinite | Illite/kaolinite |
| Clay H | Kaolinite | Kaolinite |

While the thermal analysis results show that each clay presented an endothermic peak between 700-750 °C (Figure 4.25), the weight change was relatively smaller at clays that incorporate little to no calcite within their composition (Clays A, G, and H). Additionally, XRD results presented the disappearance of calcite peaks between 600 °C and 800 °C in all clays with significant calcite content (Clays B, C, D, E, and F). Combining the two results, it is safe to assume that the calcite within the composition decarbonated between 700-750 °C and the weight loss might be due to the release of $CO_2$ sourced from the calcites. Possible mechanisms behind the lower-temperature decarbonation of the calcites are explained in detail in section 2.4.

Calcination Temperature for Optimum Reactivity. In addition to that, Rodriguez-Navarro et al. (2016)'s study about amorphous and crystalline calcite phases proves that between 550-800 °C, $CaCO_3$ decomposes into CaO and $CO_2$. The smaller peaks observed in little to no calcite-incorporating clays are due to the decomposition of the clay minerals, as mineralogical analysis results indicate.

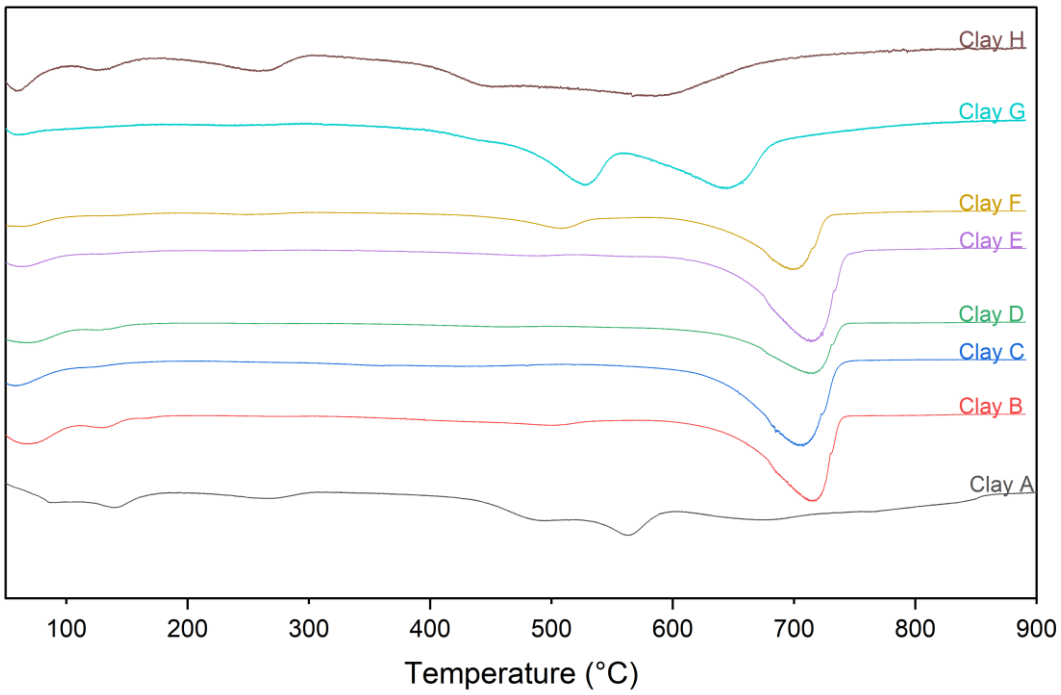


Figure 4.25. Y-Offset Stacked Temperature versus Derived Weight Curves of the Clays.

Interestingly, after calcination, the formation of a new crystalline phase, potassium aluminum silicate ($Al_3KO_{11}Si_3$), is observed in Clays A, G, and H, all of which incorporate very little to no calcite within their composition. While the study regarding the formation of potassium incorporating silicate spinel phases within the calcined clays is quite limited, the studies (Guihua et al., 1998; Nduka et al., 2021) indicate that the formation of such phases depends on the cation concentration within

the matrix. Considering that the potassium aluminum silicate formation is only observed when the calcite is absent in the composition, its formation might be related to the lack of $Ca^{+2}$ ion provided by the calcite, as the tendency of cation exchange where $Ca^{+2}$ replace $K^{+}$ increases with the available $Ca^{+2}$. Furthermore, the hypothesis of the release of $K^{+}$ from the phyllosilicate interlayers is known (Rahmatullah & Mengel, 2000), and the presence of illite, a clay mineral that has $K^{+}$ between the interlayers, in both clays further hints that the potassium ions might have sourced from the decomposed clays. This assumption coheres with the increased potassium aluminum silicate peak from 600 °C calcination to 800 °C calcination, where decomposition is enhanced.

### 4.2.2 About Strength Activity of Calcined Clays

As expected, in the raw state, clay incorporation reduced the strength by approximately 40% compared to the control OPC blend at all ages (Figure 4.26). With 600 °C calcination, all clays showed >70% SAI results at 7-days, except Clay H which only reached 65% SAI (Figure 4.27). This strength improvement is also observed in clays that contain no or very low calcite (Clays A, G, and H) and it may be due to the two mechanisms: With the calcination, aluminates, and silicates sourced from the clays react with the portlandite sourced from the cement, to form additional binding C-A-S-H phases, until a $Ca^{+2}$ balance between the pore solution and the phases is achieved. Due to the lack of any calcites in the clay composition, the reactions quickly came to a halt, which explains the lack of strength development at later ages. Secondly, Ferreiro et al., (2019) discuss that after calcination the clay minerals are known to form spherical shapes and improve their workability which may have reduced the water demand for the same flow, as observed in the flow table results (Table 3.3). Reduction of the water demand is likely to positively contribute to the SAI results of the calcined blends compared to the raw state. The same mechanisms are also possible for 800 °C calcination SAI results given in Figure 4.28 but enhanced since (i) with the increased temperature, decarbonation of the calcites

occurs, which is observed to benefit the strength development in the system. Decarbonation of the calcites allows for more reactant Ca-phases in the system, which can react with aluminates, silicates, and water to form binding C-A-S-H gel. Additionally, with the decarbonation of the calcite, quicklime present in the matrix can work as a mineral admixture that provides more nuclei for phase growth and increases pH. (ii) With elevated calcination temperatures both the decomposition of the clay mineral structure and the thermally-induced cracking is likely to enhance, and contribute to the strength development. For Clays A, B, E, F, G, and H, SAI results either decreased or remained the same between the 7 and 28-days, for at least one of the calcined states, which indicates that the reaction of aluminates occurs at similar or slightly lower speeds than the cement binding phase reactions. For 90-days, clays with very low or no calcite in their composition (Clay G, and H) showed a SAI decrease. This is likely due to binding phase reactions coming to the halt because of the available calcium oxide depletion. On the other hand, the clays with calcite showed an SAI improvement at 90-days, as such, all clays that showed lower SAI at 28-days were able to either catch or surpass their 7-day SAI results, with the only exception being the Clay G and H, which lack the calcite for later age reactions. Improved performance at 90-day was even more noticeable with 800 °C calcination, as all calcite-containing clays showed >~85% SAI. The effect of calcite presence is further noticed in the highest calcite incorporation clay, Clay C, which also showed overall the best SAI results. One of the main reasons for that might be as follows: In C-A-S-H phase formation, the C part (CaO), is usually the limiting component which creates a bottleneck effect, as $SiO_2$ and $Al_2O_3$ are abundantly supplied with the clay, assuming there is enough $H_2O$. With more calcite, there is more phase formation and Clay C having the highest calcite content might have helped with overcoming the bottleneck effect. This not only helped the 800 °C calcined Clay C sample to surpass control at 90-days, but also show a 90% SAI at 7-days, which is quite promising for future applications. In short, at all ages, 800 °C calcined clays performed the best, while raw clays performed the worst. All calcite-incorporating clays performed better at 90-days compared to the 28-days.

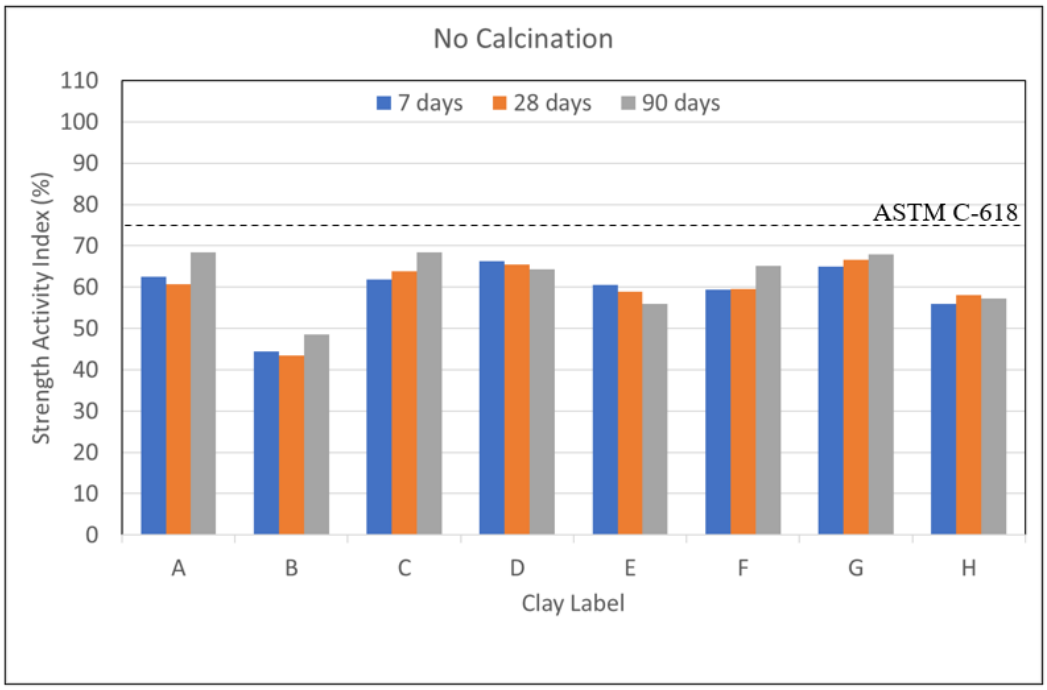


Figure 4.26. SAI Results of All Raw (Non-calcined) Clays.

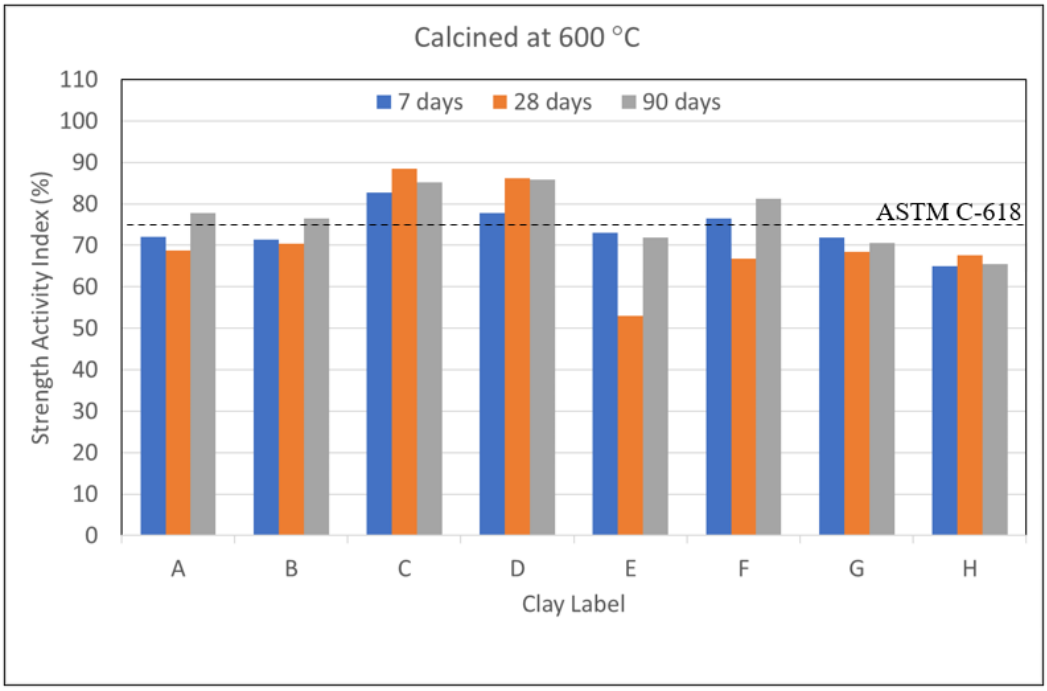


Figure 4.27. SAI Results of All Clays Calcined at 600 °C.

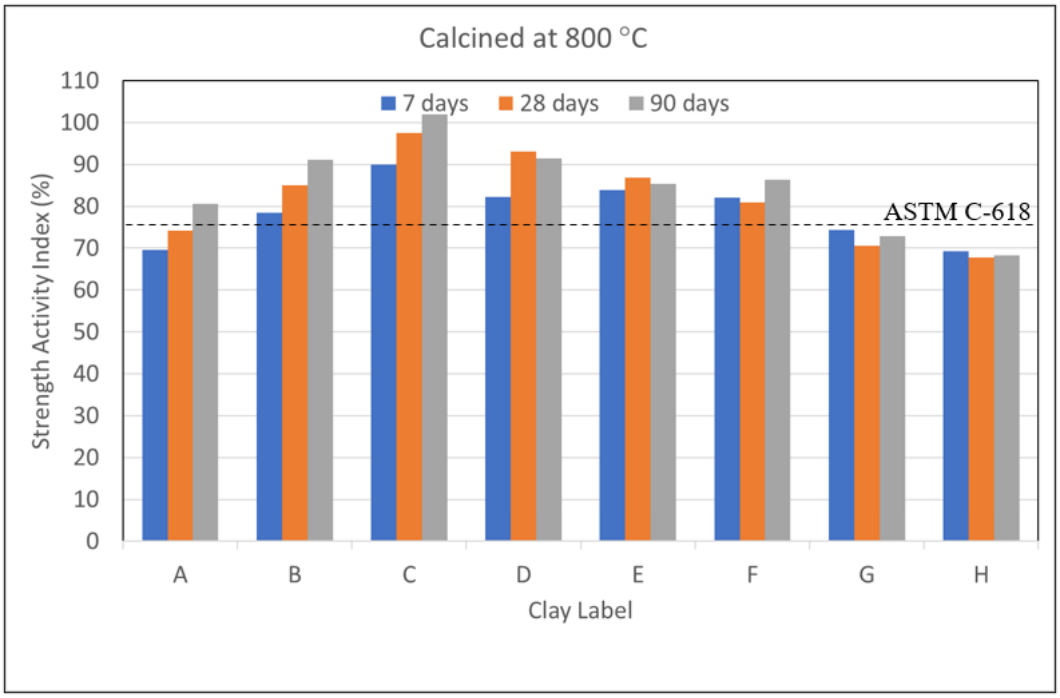


Figure 4.28. SAI Results of All Clays Calcined at 800 °C.

As standard and later age results versus the clay mineral content are presented in Figure 4.29, even the clays with lower clay mineral content were able to perform better than clays with high kaolinite contents. This indicates that the low-grade clays can also be used as a SCM when proper conditions are met. Adjunctly, when calcite content and SAI performance of the clays calcined at 800 °C compared (Figure 4.30) a direct correlation between the two factors is observed: 800 °C is selected for comparison because the effects of decomposed clays and decarbonized calcite were more impactful at the elevated temperatures, in terms of strength gain. Likewise, 28-day and 90-day are selected at standard and later ages, it is more convenient to differentiate the physical strength benefitting factors, such as filler effect, more nuclei for growth, etc, and the formation of the binding phases. It is clear that at 28-days, apart from Clay D, SAI performance is improved with the increasing calcite content. The main reason Clay D showed much better performance with relatively lower calcite content is the presence of 6.7% anorthite in its composition. As studies

(Harada & Hagiwara, 1984; Traore et al., 2003) show, anorthite decomposes into all three components (CaO, $SiO_2$, and $Al_2O_3$) of the ternary blend diagram given in Figure 2.1, thus its effect on the formation of binder phases is 3-fold, that is why Clay D was able to perform better than calcined clays with higher calcite contents.

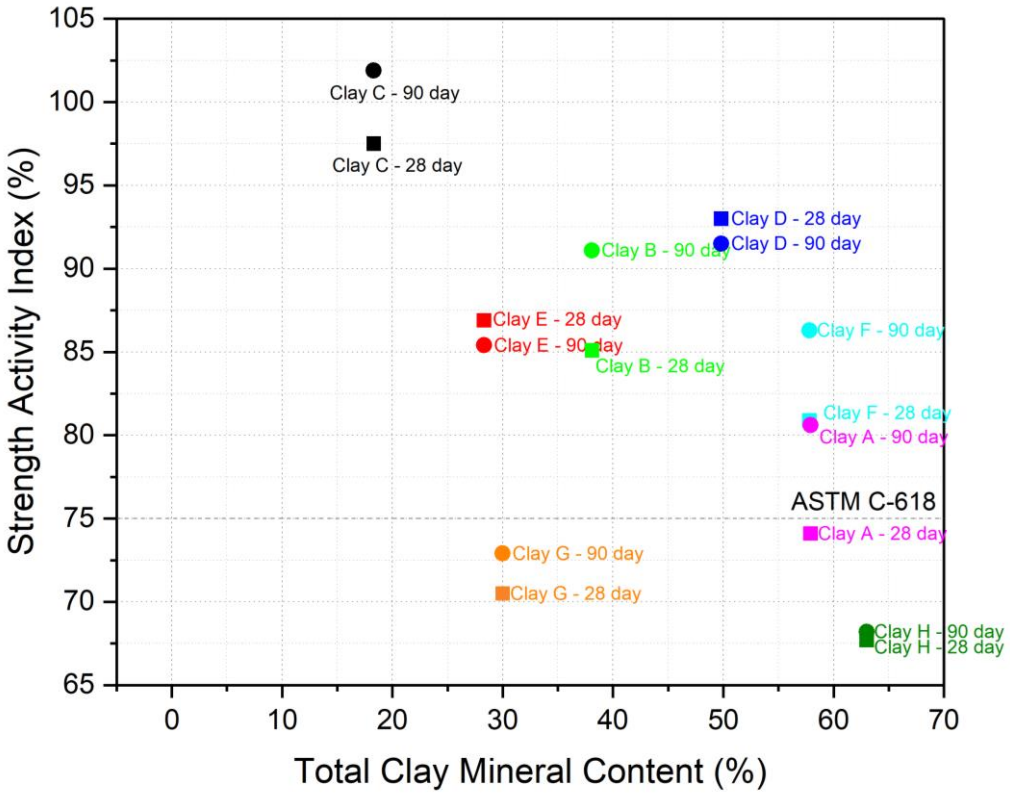


Figure 4.29. SAI vs Clay Mineral Content of Clays Calcined at 800 °C, for standard and late ages.

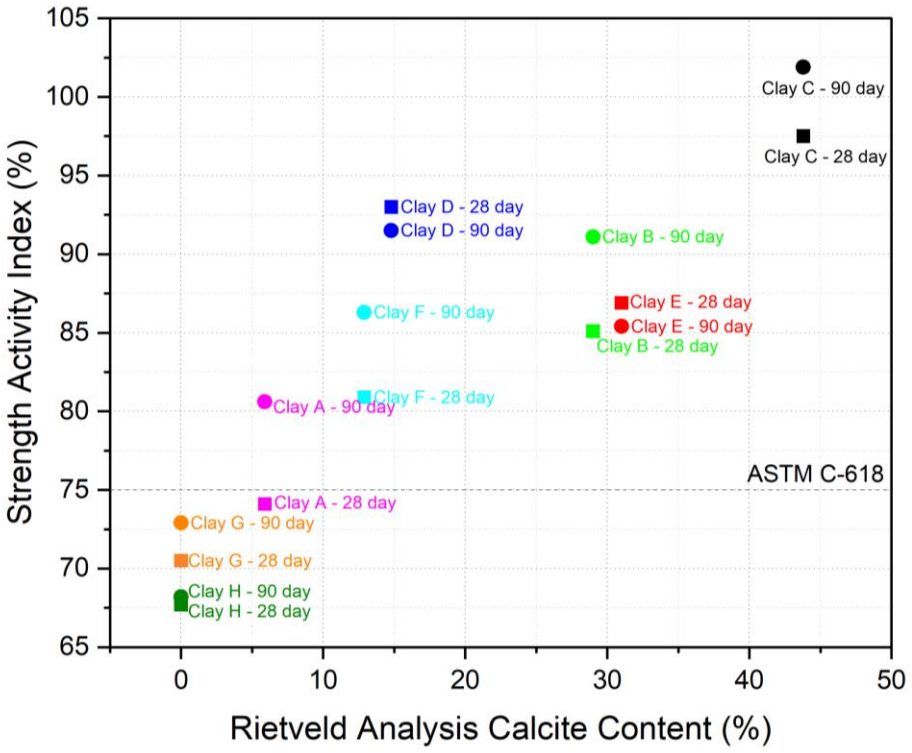


Figure 4.30. SAI vs Calcite Content of Clays Calcined at 800 °C, for standard and late ages.

Overall, at all ages, 800 °C calcined clays performed the best, while raw clays performed the worst, in terms of SAI. As expected none of the clays were able to satisfy the standard for calcined pozzolans, 75% SAI at 7 or 28 days, specified in ASTM C-618 (Figure 4.26), in the raw state. Out of the 8 clays calcined at 600 °C, 3 were able to satisfy the SAI standard: Clays C and D were able to surpass the 75% SAI at both 7 and 28 days, and Clay F only at 7 days (Figure 4.27). For the clays calcined at 800 °C, 5 clays (Clays B, C, D, E, and F) surpassed the 75% SAI threshold at both 7 and 28 ages (Figure 4.28). SAI of other clays ranges between 67.7% and 74.3%, which is arguably not too far from the requirement. While not specified in the standard (ASTM C-618), the 90-day SAI of the clays is also inspected: For 600 °C calcination, Clays B, C, D, and F surpassed the 75% SAI threshold at 90 days. For 800 °C calcination, Clays B, C, D, E, and F presented above 75% SAI. Out of all clay blends, only Clay C calcined at 800 °C surpassed the 100% SAI (101.9%) at 90-days, followed by Clay D (91.5%) with the same parameters.

# CHAPTER 5

# CONCLUSION AND RECOMMENDATIONS

## 5.1 Conclusions

In this study, 8 clays that are obtained from the cement plants of Türkiye are calcined at two temperatures and characterized by the utilization of various test methods. An endeavor to correlate the experimental findings with the clay compositions is taken, to form a basis for future studies investigating the clays of Türkiye, such as in ternary limestone-calcined clay cement (LC3) blends.

The raw clay materials and their compositions (Rietveld Analysis) are provided by TCMA. After the quartering, crushing, drying, grinding, and sieving procedures, the clays are calcined at 600 °C and 800 °C. TGA/DTA experiments are considered to determine the calcination temperatures. Flow table tests are conducted to ensure constant flow. XRD analyses for raw, 600 °C calcined, and 800 °C calcined clays are utilized to determine the decomposition of the clay minerals and other possible phase changes after the calcination. Compressive strength, flexural strength, and Strength Activity Index (SAI) of each raw, calcined at 600 °C and calcined at 800 °C clay incorporating mortar, with 20% substitution, is tested for 7, 28, and 90-days, according to ASTM C311 and ASTM C-618.

Based on the experimental results, the following conclusions can be drawn:

1. Out of the 8 clays studied, each of the kaolinite, illite, or montmorillonite minerals was present in 5 clay compositions, making these the equally and most common clay minerals. This is followed by clinochlore presence in 3 clay compositions. Nontronite presence was only observed in a single clay. This indicates that a wide range of clay minerals are present within the clays obtained from cement factories of Türkiye.

2. In TGA/DTA analysis results, an endothermic peak between 700-750 °C is observed, which was significantly more notable in clays with relatively higher calcite content. This possibly corresponds to the decarbonation of the calcite.
3. In all but one clay incorporating calcite, the disappearance of calcite peaks with 800 °C calcination is observed in XRD results. This is likely due to the decarbonation of the calcite, as the $CO_2$ pressure build-up may have caused relatively lower temperature calcite decomposition.
4. Formation of the Potassium Aluminum Silicate phase is observed in the clays which contain very low or no calcite (Clays A, G, and H). This indicates that the formation of this phase is related to the calcite content within the composition.
5. In all clays, a decrease in water demand for the constant flow is observed with the calcination. While raw clay blends required 10.8% to 38.2% more water relative to the control, for the same flow; this range dropped to 7.0% to 14.6% with 600 °C calcination and 7.6% to 12.1% with 800 °C calcination. This may be due to the workability improvement caused by the agglomeration and spherical shape formation of the clay minerals after the calcination.
6. Particle Size Distribution analyses conducted on raw and 800 °C calcined clays show that with the calcination fineness increased in 3 clays (Clays A, D, and G), decreased in 2 clays (Clays B and F), and did not change for one clay (Clay H). For the remaining clays (Clays C, E), fineness increased for coarser particles and decrease for finer particles. This may be due to the thermally-induced cracking, cold-sintering, where thermal expansion of the particles increases contact zones and create a physical sintering-like effect, or simply due to the refraction changes, as the color change with the calcination is observed. Fineness changes were, arguably, not significant enough to greatly impact the strength test results.

7. With calcination, it is observed that the clay samples changed color. This is likely due to the oxidizing conditions which shifted the material's color to reddish, or reducing conditions where the color became grayish.
8. As expected, none of the clays were able to satisfy the requirement of 75% SAI at 7 or 28 days stated in ASTM C-618. With 600 °C calcination, 3 clays, and with 800 °C calcination, 5 clays were able to satisfy the requirement. Only clays which incorporate more than 10% calcite within their composition were able to satisfy the requirement. This shows that most of the clays used in the study are suitable to use as a calcined natural pozzolan and a cement substitute upon calcination.
9. A direct correlation between the calcite content and the SAI results were found. This was potentially due to the reactions between the aluminates and silicates sourced from the calcined clays to react with the calcite and form binding C-A-S-H phases. In a calcined clay blend, assuming adequate water is used, there is an abundance of A, S, and H phases. This makes C phases the bottleneck of the binder products, which is likely the reason for the correlation. Additionally, only the highest calcite incorporating clay, Clay C, was able to surpass 100% SAI at 90-days.
10. Clay D showed the second-highest overall SAI results, despite having relatively lower calcite content (14.8%) and fineness. This is suspected to be caused by the presence of anorthite, a rare earth mineral, which is known to decompose into CaO, $SiO_2$, and $Al_2O_3$ phases. These phases are the main parameters of the ternary phase diagram given in Figure 2.1 and anorthite presence can greatly improve the strength development by creating a third-dimensional increase in the diagram.

## 5.2 Recommendations For Future Studies

1. While the calcined clays of the study are discussed in terms of their strength, composition, workability, etc. durability, and volume stability performance needs to be investigated for their potential usage as supplementary cementitious material.
2. It is proven that the calcite content within the clay composition plays an important role in the experimental results. This can be further investigated by presenting external limestone to the system. Optimal limestone incorporation can be determined for each clay to minimize $CO_2$ emissions and improve sustainability.
3. XRD analysis results indicate the formation of potassium aluminum silicate phase when calcite is not present. This is suspected to be caused by the substitution of $K^+$ ions, sourced from clay interlayers to come into play since the $Ca^{+2}$ ions within the matrix are insufficient. This can be further investigated with potassium aluminum silicate synthesis with and without calcite presence.
4. While the calcination process and hydration mechanisms behind the kaolinite, montmorillonite, and illite are well-studied, research on the less popular clay minerals, such as clinochlore and nontronite, are limited. The reactivity of these materials, clinochlore-vaterite conversion, and their effects, their grindability, their effect on workability, etc. can make for valuable and interesting research topics.
5. While this study investigated the calcined clay behavior on mortars, the behavior and effects of the calcined clay incorporation for the concrete can be investigated to further discuss the commercial usage of these clays as cement substitutes.
6. Anorthite presence in the clay composition is suspected to significantly increase the SAI results, despite the relatively lower calcite content. The utilization of anorthite as a ternary blend additive can be investigated.

## REFERENCES


Abdrakhimov, D. v, Abdrakhimova, E. S., & Abdrakhimov, V. Z. (1999). Sintering quality of clay materials. *Glass and Ceramics*, *56*(5), 190–193. https://doi.org/10.1007/BF02681334

Ahmaruzzaman, M. (2010). A review on the utilization of fly ash. *Progress in Energy and Combustion Science*, *36*(3), 327–363.

Akbar, R. A. (2013). *Cement replacement materials: properties, durability, sustainability*. Springer London Limited.

Aldred, J. M., Holland, T. C., Morgan, D. R., Roy, D. M., Bury, M. A., Hooton, R. D., Olek, J., Scali, M. J., Detwiler, R. J., & Jaber, T. M. (2006). Guide for the use of silica fume in concrete. *ACI–American Concrete Institute–Committee: Farmington Hills, MI, USA*, *234*.

Alujas, A., Fernández, R., Quintana, R., Scrivener, K. L., & Martirena, F. (2015). Pozzolanic reactivity of low grade kaolinitic clays: Influence of calcination temperature and impact of calcination products on OPC hydration. *Applied Clay Science*, *108*, 94–101. https://doi.org/https://doi.org/10.1016/j.clay.2015.01.028

Alujas, A., & Fernando Martirena, J. (2015). Influence of calcination temperature in the pozzolanic reactivity of a low grade kaolinitic clay. In *Calcined Clays for Sustainable Concrete* (pp. 331–338). Springer.

Ambroise, J., Martin-Calle, S., & Pera, J. (1992). Pozzolanic behavior of thermally activated kaolin. *Special Publication*, *132*, 731–748.

Ambroise, J., Maximilien, S., & Pera, J. (1994). Properties of Metakaolin blended cements. *Advanced Cement Based Materials*, *1*(4), 161–168. https://doi.org/https://doi.org/10.1016/1065-7355(94)90007-8

Ambroise, J., Murat, M., & Péra, J. (1985). Hydration reaction and hardening of calcined clays and related minerals V. Extension of the research and general conclusions. *Cement and Concrete Research*, *15*(2), 261–268. https://doi.org/https://doi.org/10.1016/0008-8846(85)90037-7

Ambroise, J., Murat, M., & Pera, J. (1986). Investigations on synthetic binders obtained by middle-temperature thermal dissociation of clay minerals. *Silicates Industriels*, *51*(7–8), 99–107.

American Coal Ash Association. (2003). *Fly ash facts for highway engineers*. US Department of Transportation, Federal Highway Administration.

Amin, N., Alam, S., & Gul, S. (2016). Effect of thermally activated clay on corrosion and chloride resistivity of cement mortar. *Journal of Cleaner Production*, *111*, 155–160. https://doi.org/https://doi.org/10.1016/j.jclepro.2015.06.097

Antoni, M. (2013). *Investigation of cement substitution by blends of calcined clays and limestone*. EPFL.

Antoni, M., Rossen, J., Martirena, F., & Scrivener, K. (2012). Cement substitution by a combination of metakaolin and limestone. *Cement and Concrete Research*, *42*(12), 1579–1589. https://doi.org/https://doi.org/10.1016/j.cemconres.2012.09.006

Assi, L., Carter, K., Deaver, E. E., Anay, R., & Ziehl, P. (2018). Sustainable concrete: Building a greener future. *Journal of Cleaner Production*, *198*, 1641–1651.

ASTM C109. (2008). Standard test method for compressive strength of hydraulic cement mortars. *ASTM International, West Conshohocken, PA*.

ASTM C117-17. (2018). *Standard test method for materials finer than 75-μm (no. 200) sieve in mineral aggregates by washing, Annual book of ASTM standards*. ASTM International West Conshohocken.

ASTM C125. (2003). Standard terminology relating to concrete and concrete aggregates. *Annual Book of ASTM Standards*, *4*, 23.

ASTM C136. (2006). Standard test method for sieve analysis of fine and coarse aggregates. *ASTM C136-06*.

ASTM C230. (2014). Standard specification for flow table for use in tests of hydraulic cement. *ASTM West Conshohocken*, 1–6.

ASTM C305. (2014). Standard practice for mechanical mixing of hydraulic cement pastes and mortars of plastic consistency. *ASTM West Conshohocken, PA*.

ASTM C308. (2018). *Standard Practice for Working, Initial Setting, and Service Strength Setting Times of Chemical-Resistant Resin Mortars*.

ASTM C311–16. (2013). *Standard Test Methods for Sampling and Testing Fly Ash or Natural Pozzolans for Use in Portland-Cement Concrete*.

ASTM C-618. (2002). *American Society for Testing and Materials, ASTM Specification for Fly Ash and Raw or Calcined Natural Pozzolan for use as a Mineral Admixture in Portland Cement Concrete, Designation C618*. ASTM international Philadelphia.

ASTM C702/C702M-18. (2018). *Standard practice for reducing samples of aggregate to testing size*. ASTM International West Conshohocken, PA, USA.

ASTM C1202. (2012). Standard test method for electrical indication of concrete's ability to resist chloride ion penetration. *American Social Test. Materials*, *4*(2), 1–8.

ASTM C1240. (2005). Standard specification for silica fume used in cementitious mixtures. *ASTM International: West Conshohocken, PA, USA*.

ASTM C1437. (2007). *Standard test method for flow of hydraulic cement mortar*.

Atiş, C. D., Sevim, U. K., Özcan, F., Bilim, C., Karahan, O., Tanrikulu, A. H., & Ekşi, A. (2004). Strength properties of roller compacted concrete containing a non-standard high calcium fly ash. *Materials Letters*, *58*(9), 1446–1450.

Atkins, M., Glasser, F. P., & Kindness, A. (1992). Cement hydrate phase: Solubility at 25°C. *Cement and Concrete Research*, *22*(2), 241–246. https://doi.org/https://doi.org/10.1016/0008-8846(92)90062-Z

Avet, F., Boehm-Courjault, E., & Scrivener, K. (2019). Investigation of C-A-S-H composition, morphology and density in Limestone Calcined Clay Cement (LC3). *Cement and Concrete Research*, *115*, 70–79. https://doi.org/https://doi.org/10.1016/j.cemconres.2018.10.011

Avet, F., & Scrivener, K. (2020). Effect of temperature on the water content of C-A-S-H in plain Portland and blended cements. *Cement and Concrete Research*, *136*, 106124. https://doi.org/https://doi.org/10.1016/j.cemconres.2020.106124

Avet, F., Snellings, R., Diaz, A. A., Haha, M. ben, & Scrivener, K. (2016). Development of a new rapid, relevant and reliable (R3) test method to evaluate the pozzolanic reactivity of calcined kaolinitic clays. *Cement and Concrete Research*, *85*, 1–11.

Badogiannis, E., Kakali, G., & Tsivilis, S. (2005). Metakaolin as supplementary cementitious material: optimization of kaolin to metakaolin conversion. *Journal of Thermal Analysis and Calorimetry*, *81*(2), 457–462.

Bahhou, A., Taha, Y., Khessaimi, Y. el, Hakkou, R., Tagnit-Hamou, A., & Benzaazoua, M. (2021). Using calcined marls as non-common supplementary cementitious materials—a critical review. *Minerals*, *11*(5), 517.

Bedard, C., & Sordyl, D. (2007). Concrete summit on sustainable development. *Concrete International*, *29*(7), 54–58.

Behim, M., Beddar, M., & Clastres, P. (2013). Reactivity of granulated blast furnace slag. *Slovak Journal of Civil Engineering*, *21*(2), 7.

Bentur, A., Goldman, A., & Cohen, M. D. (1987). The contribution of the transition zone to the strength of high quality silica fume concretes. *MRS Online Proceedings Library (OPL)*, *114*.

Bergaya, F., & Lagaly, G. (2006). General introduction: clays, clay minerals, and clay science. *Developments in Clay Science*, *1*, 1–18.

Berman, H. A., & Newman, E. S. (1963). Heat of formation of calcium aluminate monosulfate at 25 C. *Journal of Research of the National Bureau of Standards. Section A, Physics and Chemistry*, *67*(1), 1.

Bhattacharjee, U., & Kandpal, T. C. (2002). Potential of fly ash utilisation in India. *Energy*, *27*(2), 151–166.

Boakye, K., Khorami, M., Ganjian, E., & Saidani, M. (2021). A review of the Effect of Calcination Temperature on the Properties of Calcined Clay Concrete. *Int J. Eng Technol. Inf*, *2*, 72–74.

Bougara, A., Lynsdale, C., & Milestone, N. B. (2010). Reactivity and performance of blastfurnace slags of differing origin. *Cement and Concrete Composites*, *32*(4), 319–324.

Bratoev, B., Doykov, I., Ninov, J., & Lenchev, A. (2018). Pozzolanic activity assessment of calcined clays with complex minerals content. *Advances in Cement Research*, *30*(3), 103–112.

Brigatti, M. F., Galan, E., & Theng, B. K. G. (2006). Structures and mineralogy of clay minerals. *Developments in Clay Science*, *1*, 19–86.

Brindley, G. W., & Nakahira, M. (1959a). The KaoIinite-MuIIite Reaction Series: Ill, The High-Temperature Phases. *Journal of the American Ceramic Society*, *42*(7), 319–324.

Brindley, G. W., & Nakahira, M. (1959b). The kaoIinite-mullite reaction series: I, a survey of outstanding problems. *Journal of the American Ceramic Society*, *42*(7), 311–314.

Brindley, G. W., & Nakahira, M. (1959c). The kaolinite-mullite reaction series: II, metakaolin. *Journal of the American Ceramic Society*, *42*(7), 314–318.

Brough, A. R., Dobson, C. M., Richardson, I. G., & Groves, G. W. (1995). A study of the pozzolanic reaction by solid-state 29Si nuclear magnetic resonance using selective isotopic enrichment. *Journal of Materials Science*, *30*(7), 1671–1678.

Brown, G. (1982). *Crystal structures of clay minerals and their X-ray identification* (Vol. 5). The Mineralogical Society of Great Britain and Ireland.

Brown, I. W. M., MacKenzie, K. J. D., & Meinhold, R. H. (1987). The thermal reactions of montmorillonite studied by high-resolution solid-state29Si and27Al NMR. *Journal of Materials Science*, *22*(9), 3265–3275.

Bullard, J. W., Jennings, H. M., Livingston, R. A., Nonat, A., Scherer, G. W., Schweitzer, J. S., Scrivener, K. L., & Thomas, J. J. (2011). Mechanisms of cement hydration. *Cement and Concrete Research*, *41*(12), 1208–1223. https://doi.org/https://doi.org/10.1016/j.cemconres.2010.09.011

Cai, N., & Inoue, T. (2019). High-pressure and high-temperature stability of chlorite and 23-Å phase in the natural chlorite and synthetic MASH system. *Comptes Rendus Geoscience*, *351*(2), 104–112. https://doi.org/https://doi.org/10.1016/j.crte.2018.09.010

Canut, M., Miller, S., & Jolnæs, M. (2020). Calcined Clay: Process Impact on the Reactivity and Color. In *Calcined Clays for Sustainable Concrete* (pp. 163–167). Springer.

Carrillo García, A., Latifi, M., & Chaouki, J. (2021). Kinetic study of calcination of a rare earth ore. *Hydrometallurgy*, *200*, 105557. https://doi.org/https://doi.org/10.1016/j.hydromet.2021.105557

Celik, K., Meral, C., Petek Gursel, A., Mehta, P. K., Horvath, A., & Monteiro, P. J. M. (2015). Mechanical properties, durability, and life-cycle assessment of self-consolidating concrete mixtures made with blended portland cements containing fly ash and limestone powder. *Cement and Concrete Composites*, *56*, 59–72. https://doi.org/https://doi.org/10.1016/j.cemconcomp.2014.11.003

Chappex, T., & Scrivener, K. L. (2012). The influence of aluminium on the dissolution of amorphous silica and its relation to alkali silica reaction. *Cement and Concrete Research*, *42*(12), 1645–1649. https://doi.org/https://doi.org/10.1016/j.cemconres.2012.09.009

Chen, W., & Brouwers, H. J. H. (2006). The reaction of slag in cement: theory and computer modelling. *Proceedings 16th Ibausil, International Conference on Building Materials (Internationale Baustofftagung), Weimar*, 20–22.

Cheng, A., Huang, R., Wu, J.-K., & Chen, C.-H. (2005). Influence of GGBS on durability and corrosion behavior of reinforced concrete. *Materials Chemistry and Physics*, *93*(2–3), 404–411.

Chiotis, E., Dimou, E., Papadimitriou, G. D., & Tzoutzopoulos, S. (2001). The study of some ancient and prehistoric plasters and watertight coatings from Greece. *Archaeometry Issues in Greek Prehistory and Antiquity*, 327–342.

Chung, D. D. L. (2002). Improving cement-based materials by using silica fume. *Journal of Materials Science*, *37*(4), 673–682.

Claisse, P. A. (1988). *The properties and performance of high strength silica fume concrete (Doctoral dissertation, University of Leeds).*

Collins, F., & Sanjayan, J. G. (1999). Effects of ultra-fine materials on workability and strength of concrete containing alkali-activated slag as the binder. *Cement and Concrete Research*, *29*(3), 459–462.

Cwik, K., Broström, M., Backlund, K., Fjäder, K., Hiljanen, E., & Eriksson, M. (2022). Thermal Decrepitation and Thermally-Induced Cracking of Limestone Used in Quicklime Production. *Minerals*, *12*(10), 1197.

Dathe, F., Strelnikova, V., Werling, N., Emmerich, K., & Dehn, F. (2021). Influence of lime, calcium silicate and portlandite on alkali activation of calcined common clays. *Open Ceramics*, *7*, 100152.

David Kingery, W., Vandiver, P. B., & Prickett, M. (1988). The beginnings of pyrotechnology, part II: production and use of lime and gypsum plaster in the Pre-Pottery Neolithic Near East. *Journal of Field Archaeology*, *15*(2), 219–243.

de Belie, N., Soutsos, M., & Gruyaert, E. (2018). *Properties of fresh and hardened concrete containing supplementary cementitious materials* (Vol. 25). Springer.

de Silva, P. S., & Glasser, F. P. (1990). Hydration of cements based on metakaolin: thermochemistry. *Advances in Cement Research*, *3*(12), 167–177.

de Silva, P. S., & Glasser, F. P. (1992). Pozzolanic activation of metakaolin. *Advances in Cement Research*, *4*(16), 167–178.

Detwiler, R. J., & Mehta, P. K. (1989). Chemical and physical effects of silica fume on the mechanical behavior of concrete. *Materials Journal*, *86*(6), 609–614.

Dhandapani, Y., Sakthivel, T., Santhanam, M., Gettu, R., & Pillai, R. G. (2018). Mechanical properties and durability performance of concretes with Limestone Calcined Clay Cement (LC3). *Cement and Concrete Research*, *107*, 136–151. https://doi.org/https://doi.org/10.1016/j.cemconres.2018.02.005

Diamond, S. (1986). The microstructures of cement paste in concrete. *Proceedings of the 8th International Congress on the Chemistry of Cement*, *1*, 113–121.

Díaz, A. A., Almenares Reyes, R. S., Carratalá, F. A., & Martirena Hernández, J. F. (2018). Proposal of a methodology for the preliminary assessment of kaolinitic clay deposits as a source of SCMs. In *Calcined Clays for Sustainable Concrete* (pp. 29–34). Springer.

Dixon, J. B., & Schulze, D. G. (2002). *Soil mineralogy with environmental applications.* Soil Science Society of America Inc.

Dodson, V. H. (2013). *Concrete admixtures*. Springer Science & Business Media.

Donatello, S., Tyrer, M., & Cheeseman, C. R. (2010). Comparison of test methods to assess pozzolanic activity. *Cement and Concrete Composites*, *32*(2), 121–127. https://doi.org/https://doi.org/10.1016/j.cemconcomp.2009.10.008

Douglas, J. T., Goss, M. J., & Hill, D. (1980). Measurements of pore characteristics in a clay soil under ploughing and direct drilling, including use of a radioactive tracer (144Ce) technique. *Soil and Tillage Research*, *1*, 11–18.

Drdácký, M., Fratini, F., Frankeová, D., & Slížková, Z. (2013). The Roman mortars used in the construction of the Ponte di Augusto (Narni, Italy)–A comprehensive assessment. *Construction and Building Materials*, *38*, 1117–1128.

Duchesne, J. (2021). Alternative supplementary cementitious materials for sustainable concrete structures: a review on characterization and properties. *Waste and Biomass Valorization*, *12*(3), 1219–1236.

Dunster, A. M., Parsonage, J. R., & Thomas, M. J. K. (1993). The pozzolanic reaction of metakaolinite and its effects on Portland cement hydration. *Journal of Materials Science*, *28*(5), 1345–1350.

Eberl, D. D. (1984). Clay mineral formation and transformation in rocks and soils. *Philosophical Transactions of the Royal Society of London. Series A, Mathematical and Physical Sciences*, *311*(1517), 241–257.

El-Didamony, H., Amer, A., Heikal, M., & Shoaib, M. (1999). Effect of calcium acetate as accelerator and water reducer on the properties of silica fume blended cement. *CERAMICS SILIKATY*, *43*, 29–33.

EN 196-1. (2005). Methods of testing cement–Part 1: Determination of strength. *European Committee for Standardization*, *26*.

EN 12390-1. (2000). Testing hardened concrete–Part 1: Shape, dimensions and other requirements for specimens and moulds. *European Committee for Standardization*, *2*.

EN 13263-1+ A1: (2009). *Silica Fume for Concrete-Part. 1: Definitions, Requirements and Conformity Criteria*. European Committee for Standardization Brussels, Belgium.

Fahn, R. (1965). The mining and preparation of bentonite. *InterCeram*, *12*, 119–122.

Federal Highway Administration. (n.d.). *Blast Furnace Slag - Material Description - User Guidelines for Waste and Byproduct Materials in Pavement Construction - FHWA-RD-97-148*. Retrieved July 27, 2022, from https://www.fhwa.dot.gov/publications/research/infrastructure/structures/97148/bfs1.cfm

Feiz, R., Ammenberg, J., Baas, L., Eklund, M., Helgstrand, A., & Marshall, R. (2015). Improving the CO2 performance of cement, part I: Utilizing life-cycle assessment and key performance indicators to assess development within the cement industry. *Journal of Cleaner Production*, *98*, 272–281. https://doi.org/10.1016/J.JCLEPRO.2014.01.083

Fernandez, R., Martirena, F., & Scrivener, K. L. (2011). The origin of the pozzolanic activity of calcined clay minerals: A comparison between kaolinite, illite and montmorillonite. *Cement and Concrete Research*, *41*(1), 113–122.

Ferreiro, S., Canut, M. M. C., Lund, J., & Herfort, D. (2019). Influence of fineness of raw clay and calcination temperature on the performance of calcined clay-limestone blended cements. *Applied Clay Science*, *169*, 81–90. https://doi.org/https://doi.org/10.1016/j.clay.2018.12.021

François, M., Renaudin, G., & Evrard, O. (1998). A cementitious compound with composition 3CaO. Al2O3. CaCO3. 11H2O. *Acta Crystallographica Section C: Crystal Structure Communications*, *54*(9), 1214–1217.

Frías, M., Villar-Cociña, E., Sánchez de Rojas, M. I., & Valencia-Morales, E. (2005). The effect that different pozzolanic activity methods has on the kinetic constants of the pozzolanic reaction in sugar cane straw-clay ash/lime systems: Application of a kinetic–diffusive model. *Cement and Concrete Research*, *35*(11), 2137–2142. https://doi.org/https://doi.org/10.1016/j.cemconres.2005.07.005

Fujii, K., & Kondo, W. (1981). Heterogeneous equilibrium of calcium silicate hydrate in water at 30 C. *Journal of the Chemical Society, Dalton Transactions*, *2*, 645–651.

Garg, N., & Skibsted, J. (2014). Thermal Activation of a Pure Montmorillonite Clay and Its Reactivity in Cementitious Systems. *The Journal of Physical Chemistry C*, *118*(21), 11464–11477. https://doi.org/10.1021/jp502529d

Garg, N., & Skibsted, J. (2015). Heated montmorillonite: structure, reactivity, and dissolution. In *Calcined clays for sustainable concrete* (pp. 117–124). Springer.

Garg, N., & Skibsted, J. (2016). Pozzolanic reactivity of a calcined interstratified illite/smectite (70/30) clay. *Cement and Concrete Research*, *79*, 101–111.

Gartner, E. (2004). Industrially interesting approaches to “low-CO2” cements. *Cement and Concrete Research*, *34*(9), 1489–1498. https://doi.org/https://doi.org/10.1016/j.cemconres.2004.01.021

Gartner, E., & Hirao, H. (2015). A review of alternative approaches to the reduction of CO2 emissions associated with the manufacture of the binder phase in concrete. *Cement and Concrete Research*, *78*, 126–142.

Gasparini, E., Tarantino, S. C., Ghigna, P., Riccardi, M. P., Cedillo-González, E. I., Siligardi, C., & Zema, M. (2013). Thermal dehydroxylation of kaolinite under isothermal conditions. *Applied Clay Science*, *80*, 417–425.

Gettu, R., Patel, A., Rathi, V., Prakasan, S., Basavaraj, A. S., Palaniappan, S., & Maity, S. (2019). Influence of supplementary cementitious materials on the sustainability parameters of cements and concretes in the Indian context. *Materials and Structures*, *52*(1), 1–11.

Giaccio, G. M., & Malhotra, V. M. (1988). Concrete incorporating high volumes of ASTM Class F fly ash. *Cement, Concrete and Aggregates*, *10*(2), 88–95.

Gieseking, J. E. (2012). *Soil Components: Vol. 2: Inorganic Components*. Springer Science & Business Media.

Gourdin, W. H., & Kingery, W. D. (1975). The beginnings of pyrotechnology: Neolithic and Egyptian lime plaster. *Journal of Field Archaeology*, *2*(1–2), 133–150.

Grim, R. E. (1952). Objectives of the first national conference on clays and clay technology and definitions of terms used in the industry. In *Clays and Clay Minerals* (Vol. 1, Issue 1, pp. 13–15). Springer International Publishing.

Grim, R. E. (1953). *Clay mineralogy* (Vol. 76, Issue 4). LWW.

Grim, R. E., Bray, R. H., & Bradley, W. F. (1937). The mica in argillaceous sediments. *American Mineralogist: Journal of Earth and Planetary Materials*, *22*(7), 813–829.

Grim, R. E., & Guven, N. (2011). *Bentonites: geology, mineralogy, properties and uses*. Elsevier.

Guggenheim, S., Chang, Y.-H., & Koster van Groos, A. F. (1987). Muscovite dehydroxylation; high-temperature studies. *American Mineralogist*, *72*(5–6), 537–550.

Guggenheim, S., & Martin, R. T. (1995). Definition of clay and clay mineral: joint report of the AIPEA nomenclature and CMS nomenclature committees. *Clays and Clay Minerals*, *43*(2), 255–256.

Guihua, L., Xiaobin, L., Chuanfu, Z., & Zhihong, P. (1998). Formation and solubility of potassium aluminosilicate. *Transactions of Nonferrous Metals Society of China*, *8*, 120–122.

Guillerme, A. (1986). From lime to cement: the industrial revolution in French civil engineering (1770–1850). *History and Technology, an International Journal*, *3*(1), 25–85.

Güneyisi, E., Özturan, T., & Gesoğlu, M. (2005). A study on reinforcement corrosion and related properties of plain and blended cement concretes under different curing conditions. *Cement and Concrete Composites*, *27*(4), 449–461. https://doi.org/https://doi.org/10.1016/j.cemconcomp.2004.05.006

Gupta, V. K., & Sharma, S. (2003). Removal of zinc from aqueous solutions using bagasse fly ash− a low cost adsorbent. *Industrial & Engineering Chemistry Research*, *42*(25), 6619–6624.

Gutteridge, W. A., & Dalziel, J. A. (1990). Filler cement: the effect of the secondary component on the hydration of Portland cement: part I. A fine non-hydraulic filler. *Cement and Concrete Research*, *20*(5), 778–782.

Hanein, T., Simoni, M., Woo, C. L., Provis, J. L., & Kinoshita, H. (2021). Decarbonisation of calcium carbonate at atmospheric temperatures and

pressures, with simultaneous CO 2 capture, through production of sodium carbonate. *Energy & Environmental Science*, *14*(12), 6595–6604.

Hanein, T., Thienel, K.-C., Zunino, F., Marsh, A., Maier, M., Wang, B., Canut, M., Juenger, M. C. G., ben Haha, M., & Avet, F. (2022). Clay calcination technology: state-of-the-art review by the RILEM TC 282-CCL. *Materials and Structures*, *55*(1), 1–29.

Harada, M., & Hagiwara, Y. (1984). Experimental study on the reactivity of aggregate in concrete. *Bulletin of the International Association of Engineering Geology-Bulletin De L'association Internationale De Géologie De L'ingénieur*, *30*(1), 235–239.

He, C., Makovicky, E., & Øsbæck, B. (1995). Thermal stability and pozzolanic activity of calcined illite. *Applied Clay Science*, *9*(5), 337–354. https://doi.org/https://doi.org/10.1016/0169-1317(94)00033-M

He, C., Osbaeck, B., & Makovicky, E. (1995). Pozzolanic reactions of six principal clay minerals: activation, reactivity assessments and technological effects. *Cement and Concrete Research*, *25*(8), 1691–1702.

Hillier, S. (1978). *Clay mineralogy* (pp. 223–228). https://doi.org/10.1007/3-540-31079-7_47

Hjorth, J., Skibsted, J., & Jakobsen, H. J. (1988). 29Si MAS NMR studies of Portland cement components and effects of microsilica on the hydration reaction. *Cement and Concrete Research*, *18*(5), 789–798.

Hogan, F., Meusel, J., & Wedding, P. (1981). Evaluation for durability and strength development of a ground granulated blast furnace slag. *Cement, Concrete and Aggregates*, *3*(1), 40–52.

Hollanders, S., Adriaens, R., Skibsted, J., Cizer, Ö., & Elsen, J. (2016). Pozzolanic reactivity of pure calcined clays. *Applied Clay Science*, *132–133*, 552–560. https://doi.org/https://doi.org/10.1016/j.clay.2016.08.003

Irassar, E. F., Bonavetti, V. L., Castellano, C. C., Trezza, M. A., Rahhal, V. F., Cordoba, G., & Lemma, R. (2019). Calcined illite-chlorite shale as supplementary cementing material: Thermal treatment, grinding, color and pozzolanic activity. *Applied Clay Science*, *179*, 105143.

Ishak, S. A., & Hashim, H. (2015). Low carbon measures for cement plant–a review. *Journal of Cleaner Production*, *103*, 260–274.

Ito, A., & Wagai, R. (2017). Global distribution of clay-size minerals on land surface for biogeochemical and climatological studies. *Scientific Data*, *4*(1), 1–11.

Jaskulski, R., Jóźwiak-Niedźwiedzka, D., & Yakymechko, Y. (2020). Calcined clay as supplementary cementitious material. *Materials*, *13*(21), 4734.

Joshi, R. C., & Lohita, R. P. (1997). *Fly ash in concrete: production, properties and uses* (Vol. 2). CRC Press.

Juenger, M. C. G., & Siddique, R. (2015). Recent advances in understanding the role of supplementary cementitious materials in concrete. *Cement and Concrete Research*, *78*, 71–80. https://doi.org/https://doi.org/10.1016/j.cemconres.2015.03.018

Juenger, M. C. G., Snellings, R., & Bernal, S. A. (2019). Supplementary cementitious materials: New sources, characterization, and performance insights. *Cement and Concrete Research*, *122*, 257–273.

Kajaste, R., & Hurme, M. (2016). Cement industry greenhouse gas emissions – management options and abatement cost. *Journal of Cleaner Production*, *112*, 4041–4052. https://doi.org/https://doi.org/10.1016/j.jclepro.2015.07.055

Katsioti, M., Tsakiridis, P. E., Giannatos, P., Tsibouki, Z., & Marinos, J. (2009). Characterization of various cement grinding aids and their impact on grindability and cement performance. *Construction and Building Materials*,

*23*(5), 1954–1959. https://doi.org/https://doi.org/10.1016/j.conbuildmat.2008.09.003

Kim, T., & Olek, J. (2012). Effects of sample preparation and interpretation of thermogravimetric curves on calcium hydroxide in hydrated pastes and mortars. *Transportation Research Record*, *2290*(1), 10–18.

Kishar, E. A., Ahmed, D. A., & Mohammed, M. R. (2010). Hydration of Portland cement in presence of silica fume. *Advances in Cement Research*, *22*(3), 143–148.

Kitsopoulos, K. P., & Dunham, A. C. (1996). Heulandite and mordenite-rich tuffs from Greece: a potential source for pozzolanic materials. *Mineralium Deposita*, *31*(6), 576–583.

Knechtel, M. M., & Patterson, S. H. (1962). *Bentonite deposits of the northern Black Hills district, Wyoming, Montana, and South Dakota*. US Government Printing Office.

Kohno, M. (2020). Effects of hydraulic gradient and clay type on permeability of clay mineral materials. *Minerals*, *10*(12), 1064.

Kosmatka, S. H., Panarese, W. C., & Kerkhoff, B. (2002). *Design and control of concrete mixtures* (Vol. 5420). Portland Cement Association Skokie, IL.

Kostuch, J. A., Walters, G. v, & Jones, T. R. (2000). High performance concretes incorporating metakaolin: a review. *Concrete*, *2*(1993), 1799–1811.

Krishnan, S., Emmanuel, A. C., & Bishnoi, S. (2019). Hydration and phase assemblage of ternary cements with calcined clay and limestone. *Construction and Building Materials*, *222*, 64–72. https://doi.org/https://doi.org/10.1016/j.conbuildmat.2019.06.123

Krishnan, S., Emmanuel, A. C., Shah, V., Parashar, A., Mishra, G., Maity, S., & Bishnoi, S. (2018). Industrial production of limestone calcined clay cement: experience and insights. *Green Materials*, *7*(1), 15–27.

Krishnan, S., Gopala Rao, D., & Bishnoi, S. (2020). Why Low-Grade Calcined Clays Are the Ideal for the Production of Limestone Calcined Clay Cement (LC 3). In *Calcined Clays for Sustainable Concrete* (pp. 125–130). Springer.

Kumar, A., & Roy, D. M. (1984). A Study of Silica-Fume-Modified Cements of Varied Fineness. *Journal of the American Ceramic Society*, *67*(1), 61–64.

Ledley, T. S., Sundquist, E. T., Schwartz, S. E., Hall, D. K., Fellows, J. D., & Killeen, T. L. (1999). Climate change and greenhouse gases. *Eos, Transactions American Geophysical Union*, *80*(39), 453–458. https://doi.org/https://doi.org/10.1029/99EO00325

Lemma, R., Irassar, E. F., & Rahhal, V. (2015). Calcined illitic clays as portland cement replacements. In *Calcined Clays for Sustainable Concrete* (pp. 269–276). Springer.

Lewis, R. C. (2018). Silica fume. In *Properties of Fresh and Hardened Concrete Containing Supplementary Cementitious Materials* (pp. 99–121). Springer.

Loginova, E., Proskurnin, M., & Brouwers, H. J. H. (2019). Municipal solid waste incineration (MSWI) fly ash composition analysis: a case study of combined chelatant-based washing treatment efficiency. *Journal of Environmental Management*, *235*, 480–488.

Lothenbach, B., & Nonat, A. (2015). Calcium silicate hydrates: Solid and liquid phase composition. *Cement and Concrete Research*, *78*, 57–70. https://doi.org/https://doi.org/10.1016/j.cemconres.2015.03.019

Lothenbach, B., Scrivener, K., & Hooton, R. D. (2011). Supplementary cementitious materials. *Cement and Concrete Research*, *41*(12), 1244–1256. https://doi.org/https://doi.org/10.1016/j.cemconres.2010.12.001

Lovecchio, N., Shaikh, F., Rosano, M., Ceravolo, R., & Biswas, W. (2020). Environmental assessment of supplementary cementitious materials and

engineered nanomaterials concrete. *AIMS Environmental Science*, *7*(1), 13–30.

Malhotra, V. M. (1990). Durability of concrete incorporating high-volume of low-calcium (ASTM Class F) fly ash. *Cement and Concrete Composites*, *12*(4), 271–277.

Malhotra, V. M., & Mehta, P. K. (2004). *Pozzolanic and cementitious materials*. Crc Press.

Malinowski, R., & Garfinkel, Y. (1991). Prehistory of concrete. *Concrete International*, *13*(3).

Marchetti, G., Rahhal, V., Pavlík, Z., Pavlíková, M., & Irassar, E. F. (2020). Assessment of packing, flowability, hydration kinetics, and strength of blended cements with illitic calcined shale. *Construction and Building Materials*, *254*, 119042.

Massazza, F. (1976). Chemistry of pozzolanic additions and mixed cements. *Il Cemento*, *1*, 3–38.

Massazza, F. (1993). Pozzolanic cements. *Cement and Concrete Composites*, *15*(4), 185–214. https://doi.org/https://doi.org/10.1016/0958-9465(93)90023-3

Matschei, T., Lothenbach, B., & Glasser, F. P. (2007). The role of calcium carbonate in cement hydration. *Cement and Concrete Research*, *37*(4), 551–558.

McCarter, W. J., & Tran, D. (1996). Monitoring pozzolanic activity by direct activation with calcium hydroxide. *Construction and Building Materials*, *10*(3), 179–184. https://doi.org/https://doi.org/10.1016/0950-0618(95)00089-5

Mehta, P. K. (1987). Natural pozzolans: Supplementary cementing materials. *Proc., Int. Symp. on Advances in Concrete Technology*, 407–430.

Mellaart, J. (1967). *Çatal Hüyük: a neolithic town in Anatolia*.

Meunier, A. (2005). *Clays*. Springer Science & Business Media.

Meyer, C. (2009). The greening of the concrete industry. *Cement and Concrete Composites*, *31*(8), 601–605.

Miller, S. A. (2018). Supplementary cementitious materials to mitigate greenhouse gas emissions from concrete: can there be too much of a good thing? *Journal of Cleaner Production*, *178*, 587–598. https://doi.org/https://doi.org/10.1016/j.jclepro.2018.01.008

Mishra, G., Emmanuel, A., & Bishnoi, S. (2019). Influence of temperature on hydration and microstructure properties of limestone-calcined clay blended cement. *Materials and Structures*, *52*. https://doi.org/10.1617/s11527-019-1390-5

Mitchell, D. R. G., Hinczak, I., & Day, R. A. (1998). Interaction of silica fume with calcium hydroxide solutions and hydrated cement pastes. *Cement and Concrete Research*, *28*(11), 1571–1584.

Monteiro, P. J. M., Miller, S. A., & Horvath, A. (2017). Towards sustainable concrete. *Nature Materials 2017 16:7*, *16*(7), 698–699. https://doi.org/10.1038/nmat4930

Morgan, A. B., & Gilman, J. W. (2003). Characterization of polymer-layered silicate (clay) nanocomposites by transmission electron microscopy and X-ray diffraction: A comparative study. *Journal of Applied Polymer Science*, *87*(8), 1329–1338.

Mostafa, N. Y., El-Hemaly, S. A. S., Al-Wakeel, E. I., El-Korashy, S. A., & Brown, P. W. (2001). Hydraulic activity of water-cooled slag and air-cooled slag at different temperatures. *Cement and Concrete Research*, *31*(3), 475–484.

Msinjili, N. S., Gluth, G. J. G., Sturm, P., Vogler, N., & Kühne, H.-C. (2019). Comparison of calcined illitic clays (brick clays) and low-grade kaolinitic

clays as supplementary cementitious materials. *Materials and Structures*, *52*(5), 1–14.

Mukherjee, S. (2013). The science of clays. *Netherlands: Springer Science and Business Media*.

Müller, N., & Harnisch, J. (2008). How to turn around the trend of cement related emissions in the developing world. *WWF—Lafarge Conservation Partnership: Gland, Switzerland*.

Muñoz, J. F., Tejedor, M. I., Anderson, M. A., & Cramer, S. M. (2010). Detection of aggregate clay coatings and impacts on concrete. *ACI Materials Journal*, *107*(4), 387.

Murray, H. H. (1991). Overview — clay mineral applications. *Applied Clay Science*, *5*(5), 379–395. https://doi.org/https://doi.org/10.1016/0169-1317(91)90014-Z

Murray, H. H. (1999). Applied clay mineralogy today and tomorrow. *Clay Minerals*, *34*(1), 39–49.

Murray, H. H. (2000). Clays. *Ullmann's Encyclopedia of Industrial Chemistry*.

Murray, H. H., & Staff, U. by. (2000). Clays, Survey. *Kirk-Othmer Encyclopedia of Chemical Technology*, 1–29.

Naik, T. R., Sivasundaram, V., & Singh, S. S. (1991). Use of high-volume class F fly ash for structural-grade concrete. *Transportation Research Record*, *1301*.

Nduka, D. O., Olawuyi, B. J., Fagbenle, O. I., & Fonteboa, B. G. (2021). Effect of KyAl4 (Si8-y) O20 (OH) 4 Calcined Based-Clay on the Microstructure and Mechanical Performances of High-Performance Concrete. *Crystals*, *11*(10), 1152.

Neisser-Deiters, A., Scherb, S., Beuntner, N., & Thienel, K.-C. (2019). Influence of the calcination temperature on the properties of a mica mineral as a suitability study for the use as SCM. *Applied Clay Science*, *179*, 105168.

Nguyen, Q. D., Afroz, S., & Castel, A. (2020). Influence of calcined clay reactivity on the mechanical properties and chloride diffusion resistance of limestone calcined clay cement (LC3) concrete. *Journal of Marine Science and Engineering*, *8*, 301. https://doi.org/10.3390/jmse8050301

Nguyen, Q. D., & Castel, A. (2020). Reinforcement corrosion in limestone flash calcined clay cement-based concrete. *Cement and Concrete Research*, *132*, 106051. https://doi.org/https://doi.org/10.1016/j.cemconres.2020.106051

Norrish, K. (1954). The swelling of montmorillonite. *Discussions of the Faraday Society*, *18*, 120–134.

Odler, I., & Skalny, J. (1973). Hydration of tricalcium silicate at elevated temperatures. *Journal of Applied Chemistry and Biotechnology*, *23*(9), 661–667.

Ogawa, K., Uchikawa, H., Takemoto, K., & Yasui, I. (1980). The mechanism of the hydration in the system C3S-pozzolana. *Cement and Concrete Research*, *10*(5), 683–696. https://doi.org/https://doi.org/10.1016/0008-8846(80)90032-0

Ollivier, J. P., Maso, J. C., & Bourdette, B. (1995). Interfacial transition zone in concrete. *Advanced Cement Based Materials*, *2*(1), 30–38.

Oriol, M., & Pera, J. (1995). Pozzolanic activity of metakaolin under microwave treatment. *Cement and Concrete Research*, *25*(2), 265–270. https://doi.org/https://doi.org/10.1016/0008-8846(95)00007-0

Ortega, A., Macías, M., & Gotor, F. J. (2010). The multistep nature of the kaolinite dehydroxylation: kinetics and mechanism. *Journal of the American Ceramic Society*, *93*(1), 197–203.

Pacheco Torgal, F., Miraldo, S., Labrincha, J. A., & de Brito, J. (2012). An overview on concrete carbonation in the context of eco-efficient construction: Evaluation, use of SCMs and/or RAC. *Construction and Building Materials*, *36*, 141–150. https://doi.org/https://doi.org/10.1016/j.conbuildmat.2012.04.066

Padhye, R. D., & Deo, N. S. (2016). Cement Replacement by Fly Ash in Concrete. *International Journal of Engineering Research*, *5*(1), 60–62.

Pal, S. C., Mukherjee, A., & Pathak, S. R. (2003). Investigation of hydraulic activity of ground granulated blast furnace slag in concrete. *Cement and Concrete Research*, *33*(9), 1481–1486.

Panesar, D. K. (2019). 3 - Supplementary cementing materials. In S. Mindess (Ed.), *Developments in the Formulation and Reinforcement of Concrete (Second Edition)* (pp. 55–85). Woodhead Publishing. https://doi.org/https://doi.org/10.1016/B978-0-08-102616-8.00003-4

Payá, J., Borrachero, M. v, Monzó, J., Peris-Mora, E., & Amahjour, F. (2001). Enhanced conductivity measurement techniques for evaluation of fly ash pozzolanic activity. *Cement and Concrete Research*, *31*(1), 41–49. https://doi.org/https://doi.org/10.1016/S0008-8846(00)00434-8

Pei-Wei, G., Xiao-Lin, L., Hui, L., Xiaoyan, L., & Jie, H. (2007). Effects of fly ash on the properties of environmentally friendly dam concrete. *Fuel*, *86*(7–8), 1208–1211.

Perederij, V. I. (2001). Clay mineral composition and palaeoclimatic interpretation of the Pleistocene deposits of Ukraine. *Quaternary International*, *76*, 113–121.

Pérez, A., Favier, A., Scrivener, K., & Martirena, F. (2018). Influence grinding procedure, limestone content and PSD of components on properties of clinker-calcined clay-limestone cements produced by intergrinding. In *Calcined Clays for Sustainable Concrete* (pp. 358–365). Springer.

Pinho, L. F. de, Rainer Fabiani, L. F. von, & Celeghini, N. B. G. (2020). A Flexible Technology to Produce Gray Calcined Clays. In *Calcined Clays for Sustainable Concrete* (pp. 169–178). Springer.

Pöllmann, H. (2006). Syntheses, properties and solid solution of ternary lamellar calcium aluminate hydroxi salts (AFm-phases) containing SO42, CO32 and OH. *Neues Jahrbuch Für Mineralogie-Abhandlungen*, 173–181.

Poon, C. S., Kou, S. C., & Lam, L. (2006). Compressive strength, chloride diffusivity and pore structure of high performance metakaolin and silica fume concrete. *Construction and Building Materials*, *20*(10), 858–865. https://doi.org/https://doi.org/10.1016/j.conbuildmat.2005.07.001

Prakasan, S., Palaniappan, S., & Gettu, R. (2020). Study of Energy Use and CO2 Emissions in the Manufacturing of Clinker and Cement. *Journal of The Institution of Engineers (India): Series A*, *101*(1), 221–232. https://doi.org/10.1007/s40030-019-00409-4

Punkki, J., Golaszewski, J., & Gjørv, O. E. (1996). Workability loss of high-strength concrete. *ACI Materials Journal*, *93*, 427–431.

Qian, X., & Li, Z. (2001). The relationships between stress and strain for high-performance concrete with metakaolin. *Cement and Concrete Research*, *31*(11), 1607–1611. https://doi.org/https://doi.org/10.1016/S0008-8846(01)00612-3

Rahmatullah, & Mengel, K. (2000). Potassium release from mineral structures by H+ ion resin. *Geoderma*, *96*(4), 291–305. https://doi.org/https://doi.org/10.1016/S0016-7061(00)00014-8

Rakhimova, N., & Rakhimov, R. (2020). Advances in development of calcined clays as supplementary cementitious materials. *IOP Conference Series: Materials Science and Engineering*, *890*(1), 012085.

Rao, U. S., & Babu, M. S. (2017). Study of strength parameters on concrete with partial replacement of cement by sodium polyacrylate and fly ash. *International Journal of Civil Engineering*, *8*(3).

Ravina, D., & Mehta, P. K. (1986). Properties of fresh concrete containing large amounts of fly ash. *Cement and Concrete Research*, *16*(2), 227–238.

Regourd, M. (1984). Microstructure of high strength cement paste systems. *MRS Online Proceedings Library (OPL)*, *42*.

Richardson, D. N. (2006). *Strength and durability characteristics of a 70% ground granulated blast furnace slag (GGBFS) concrete mix*.

Richardson, I. G. (1999). The nature of CSH in hardened cements. *Cement and Concrete Research*, *29*(8), 1131–1147.

Richardson, I. G. (2008). The calcium silicate hydrates. *Cement and Concrete Research*, *38*(2), 137–158. https://doi.org/https://doi.org/10.1016/j.cemconres.2007.11.005

Richardson, I. G., & Groves, G. W. (1997). The structure of the calcium silicate hydrate phases present in hardened pastes of white Portland cement/blast-furnace slag blends. *Journal of Materials Science*, *32*(18), 4793–4802.

Rodriguez-Navarro, C., Elert, K., & Ševčík, R. (2016). Amorphous and crystalline calcium carbonate phases during carbonation of nanolimes: implications in heritage conservation. *CrystEngComm*, *18*(35), 6594–6607.

Roller, P. S., & Ervin Jr, G. (1940). The system calcium oxide-silica-water at 30. The association of silicate* ion in dilute alkaline solution. *Journal of the American Chemical Society*, *62*(3), 461–471.

Ross, C. S., & Kerr, P. F. (1930). The kaolin minerals 1. *Journal of the American Ceramic Society*, *13*(3), 151–160.

Sabir, B. B., Wild, S., & Bai, J. (2001). Metakaolin and calcined clays as pozzolans for concrete: a review. *Cement and Concrete Composites*, *23*(6), 441–454.

Samson, E., Marchand, J., & Snyder, K. A. (2003). Calculation of ionic diffusion coefficients on the basis of migration test results. *Materials and Structures*, *36*(3), 156–165.

Sayanam, R. A., Kalsotra, A. K., Mehta, S. K., Singh, R. S., & Mandal, G. (1989). Studies on thermal transformations and pozzolanic activities of clay from Jammu region (India). *Journal of Thermal Analysis and Calorimetry*, *35*(1), 99–106.

Scrivener, K. L., John, V. M., & Gartner, E. M. (2018). Eco-efficient cements: Potential economically viable solutions for a low-CO2 cement-based materials industry. *Cement and Concrete Research*, *114*, 2–26. https://doi.org/https://doi.org/10.1016/j.cemconres.2018.03.015

Scrivener, K. L., & Kirkpatrick, R. J. (2008). Innovation in use and research on cementitious material. *Cement and Concrete Research*, *38*(2), 128–136.

Scrivener, K., Martirena, F., Bishnoi, S., & Maity, S. (2018). Calcined clay limestone cements (LC3). *Cement and Concrete Research*, *114*, 49–56.

Sellevold, E. J., & Radjy, F. F. (1983). Condensed silica fume (microsilica) in concrete: water demand and strength development. *Special Publication*, *79*, 677–694.

Serry, M. A., Taha, A. S., El-Hemaly, S. A. S., & El-Didamony, H. (1984). Metakaolin—lime hydration products. *Thermochimica Acta*, *79*, 103–110. https://doi.org/https://doi.org/10.1016/0040-6031(84)87097-5

Shah, V., & Bishnoi, S. (2018). Carbonation resistance of cements containing supplementary cementitious materials and its relation to various parameters of concrete. *Construction and Building Materials*, *178*, 219–232. https://doi.org/https://doi.org/10.1016/j.conbuildmat.2018.05.162

Shaw, J. W. (2009). *Minoan architecture: materials and techniques*. Bottega d'Erasmo.

Shi, C., & Day, R. L. (1993). Acceleration of strength gain of lime-pozzolan cements by thermal activation. *Cement and Concrete Research*, *23*(4), 824–832.

Shi, C., & Day, R. L. (2000). Pozzolanic reaction in the presence of chemical activators: Part II — Reaction products and mechanism. *Cement and Concrete Research*, *30*(4), 607–613. https://doi.org/https://doi.org/10.1016/S0008-8846(00)00214-3

Shirkhanloo, S., Najafi, M., Kaushal, V., & Rajabi, M. (2021). A Comparative Study on the Effect of Class C and Class F Fly Ashes on Geotechnical Properties of High-Plasticity Clay. *CivilEng*, *2*(4), 1009–1018.

Siddique, R. (2004). Performance characteristics of high-volume Class F fly ash concrete. *Cement and Concrete Research*, *34*(3), 487–493.

Siddiquie, H. N., & Bahl, D. P. (1965). *Geology of the bentonite deposits of Barmer district, Rajasthan*. Government of India, Manager of Publ.

Singh, G., & Siddique, R. (2016). Effect of iron slag as partial replacement of fine aggregates on the durability characteristics of self-compacting concrete. *Construction and Building Materials*, *128*, 88–95.

Smothers, W. J., & Chiang, Y. (1966). *Handbook of differential thermal analysis*. Chemical Pub. Co.,.

Snellings, R. (2016). Assessing, understanding and unlocking supplementary cementitious materials. *RILEM Technical Letters*, *1*, 50–55.

Snellings, R., Mertens, G., & Elsen, J. (2012). Supplementary cementitious materials. *Reviews in Mineralogy and Geochemistry*, *74*(1), 211–278.

Souza, P. S. L., & Dal Molin, D. C. C. (2005). Viability of using calcined clays, from industrial by-products, as pozzolans of high reactivity. *Cement and Concrete Research*, *35*(10), 1993–1998. https://doi.org/https://doi.org/10.1016/j.cemconres.2005.04.012

Sperinck, S., Raiteri, P., Marks, N., & Wright, K. (2011). Dehydroxylation of Kaolinite to Metakaolin - A Molecular Dynamics Study. *Journal of Materials Chemistry*, *21*. https://doi.org/10.1039/C0JM01748E

Staudigel, H., & Schreyer, W. (1977). The upper thermal stability of clinochlore, Mg5Al [AlSi3O10](OH) 8, at 10–35 kb PH2O. *Contributions to Mineralogy and Petrology*, *61*(2), 187–198.

Steudel, A., Kleeberg, R., Koch, C. B., Friedrich, F., & Emmerich, K. (2016). Thermal behavior of chlorites of the clinochlore-chamosite solid solution series: Oxidation of structural iron, hydrogen release and dehydroxylation. *Applied Clay Science*, *132–133*, 626–634. https://doi.org/https://doi.org/10.1016/j.clay.2016.08.013

Suresh, D., & Nagaraju, K. (2015). Ground granulated blast slag (GGBS) in concrete–a review. *IOSR Journal of Mechanical and Civil Engineering*, *12*(4), 76–82.

Swamy, R. N. (1993). Fly ash and slag: standards and specifications—help or hindrance? *Materials and Structures*, *26*(10), 600–613.

Tardy, Y., Bocquier, G., Paquet, H., & Millot, G. (1973). Formation of clay from granite and its distribution in relation to climate and topography. *Geoderma*, *10*(4), 271–284.

Taylor, H. F. W. (1997). *Cement chemistry* (Vol. 2). Thomas Telford London.

Thomas, M. D. A. (2007). *Optimizing the use of fly ash in concrete* (Vol. 5420). Portland Cement Association Skokie, IL, USA.

Thomas, M. D. A., Shehata, M. H., Shashiprakash, S. G., Hopkins, D. S., & Cail, K. (1999). Use of ternary cementitious systems containing silica fume and fly ash in concrete. *Cement and Concrete Research*, *29*(8), 1207–1214.

Tironi, A., Trezza, M. A., Irassar, E. F., & Scian, A. N. (2012). Thermal treatment of kaolin: effect on the pozzolanic activity. *Procedia Materials Science*, *1*, 343–350.

Tironi, A., Trezza, M. A., Scian, A. N., & Irassar, E. F. (2013). Assessment of pozzolanic activity of different calcined clays. *Cement and Concrete Composites*, *37*, 319–327. https://doi.org/https://doi.org/10.1016/j.cemconcomp.2013.01.002

Todd, I. A. (1968). The Dating of Aşikli Hüyük in Central Anatolia. *American Journal of Archaeology*, *72*(2), 157–158.

Traore, K., Kabre, T. S., & Blanchart, P. (2003). Gehlenite and anorthite crystallisation from kaolinite and calcite mix. *Ceramics International*, *29*(4), 377–383.

Trümer, A., & Ludwig, H.-M. (2018). Assessment of calcined clays according to the main criterions of concrete durability. In *Calcined Clays for Sustainable Concrete* (pp. 475–481). Springer.

Turrizani, R. (1964). The chemistry of cement, vol. 2. *HFW Taylor*, *1964*, P69-86.

United Nations. (2015). Paris Agreement. *Report of the Conference of the Parties to the United Nations Framework Convention on Climate Change (21st Session, 2015: Paris). Retrived December*, *4*, 2017.

van Gerven, T., van Keer, E., Arickx, S., Jaspers, M., Wauters, G., & Vandecasteele, C. (2005). Carbonation of MSWI-bottom ash to decrease heavy metal leaching, in view of recycling. *Waste Management*, *25*(3), 291–300.

van Oss, H. G., & Padovani, A. C. (2003). Cement Manufacture and the Environment Part II: Environmental Challenges and Opportunities. *Journal of Industrial Ecology*, *7*(1), 93–126. https://doi.org/https://doi.org/10.1162/108819803766729212

Velde, B. (2013). *Origin and mineralogy of clays: clays and the environment*. Springer Science & Business Media.

Vizcaino Andres, L. M., Antoni, M. G., Alujas Diaz, A., Martirena Hernandez, J. F., & Scrivener, K. L. (2015). Effect of fineness in clinker-calcined clays-limestone cements. *Advances in Cement Research*, *27*(9), 546–556.

Walker, C. S., Savage, D., Tyrer, M., & Ragnarsdottir, K. V. (2007). Non-ideal solid solution aqueous solution modeling of synthetic calcium silicate hydrate. *Cement and Concrete Research*, *37*(4), 502–511. https://doi.org/https://doi.org/10.1016/j.cemconres.2006.12.002

Walters, G. V., & Jones, T. R. (1991). Effect of metakaolin on alkali-silica reaction (asr) in concrete manufactured with reactive aggregate. *Special Publication*, *126*, 941–954.

Wang, Q., Zhu, C., Yun, J., & Yang, G. (2017). Isomorphic substitutions in clay materials and adsorption of metal ions onto external surfaces: A DFT investigation. *The Journal of Physical Chemistry C*, *121*(48), 26722–26732.

Wardhono, A. (2018). Comparison study of class F and class C fly ashes as cement replacement material on strength development of non-cement mortar. *IOP Conference Series: Materials Science and Engineering*, *288*(1), 012019.

WBCSD. (2014). *The Cement Sustainability Initiative, Getting the Numbers Right, Project Emissions Report*.

Weaver, C. E. (1989). *Clays, muds, and shales*. Elsevier.

Wentworth, C. K. (1922). A scale of grade and class terms for clastic sediments. *The Journal of Geology*, *30*(5), 377–392.

Wesley, L. R. (2014). *Clays and clay minerals: geological origin, mechanical properties and industrial applications*. Nova Science Publishers, Incorporated.

Wild, S., Khatib, J. M., & Jones, A. (1996). Relative strength, pozzolanic activity and cement hydration in superplasticised metakaolin concrete. *Cement and Concrete Research*, *26*(10), 1537–1544.

Wilson, I. R. (2004). Kaolin and halloysite deposits of China. *Clay Minerals*, *39*(1), 1–15.

Wilson, I. R., de Souza Santos, H., & de Souza Santos, P. (2006). Kaolin and halloysite deposits of Brazil. *Clay Minerals*, *41*(3), 697–716.

Wright, P. C. (1968). *The meandu creek bentonite—a reply*.

Xing, X., Pang, Z., Mo, C., Wang, S., & Ju, J. (2020). Effect of MgO and BaO on viscosity and structure of blast furnace slag. *Journal of Non-Crystalline Solids*, *530*, 119801. https://doi.org/https://doi.org/10.1016/j.jnoncrysol.2019.119801

Yamei, Z., Wei, S., & Lianfei, S. (1997). Mechanical properties of high performance concrete made with high calcium high sulfate fly ash. *Cement and Concrete Research*, *27*(7), 1093–1098.

Yariv, S. (1992). The effect of tetrahedral substitution of Si by Al on the surface acidity of the oxygen plane of clay minerals. *International Reviews in Physical Chemistry*, *11*(2), 345–375.

Yi, Y., Gu, L., Liu, S., & Jin, F. (2016). Magnesia reactivity on activating efficacy for ground granulated blastfurnace slag for soft clay stabilisation. *Applied Clay Science*, *126*, 57–62.

Yuksel, I. (2018). Blast-furnace slag. In *Waste and supplementary cementitious materials in concrete* (pp. 361–415). Elsevier.

Žemlička, M., Kuzielová, E., Kuliffayova, M., Tkacz, J., & Palou, M. T. (2015). Study of hydration products in the model systems metakaolin–lime and metakaolin–lime–gypsum. *Ceram Silik*, *59*(4), 283–291.

Zhang, M.-H., Bilodeau, A., Malhotra, V. M., Kim, K.-S., & Kim, J.-C. (1999). Concrete incorporating supplementary cementing materials: effect on compressive strength and resistance to chloride-ion penetration. *ACI Materials Journal*, *96*, 181–189.

Zhou, H. M., Qiao, X. C., & Yu, J. G. (2013). Influences of quartz and muscovite on the formation of mullite from kaolinite. *Applied Clay Science*, *80–81*, 176–181. https://doi.org/https://doi.org/10.1016/j.clay.2013.04.004

Zunino, F., Boehm-Courjault, E., & Scrivener, K. (2020). The impact of calcite impurities in clays containing kaolinite on their reactivity in cement after calcination. *Materials and Structures*, *53*(2), 44. https://doi.org/10.1617/s11527-020-01478-9

# APPENDICES

## A. Strength Activity Index Calculation

$$Strength\ Activity\ Index\ (SAI) = \frac{A}{B} * 100$$

where:

$$A = \ average\ compressive\ strength\ of\ test\ mixture\ cubes, MPa$$

$$B = \ average\ compressive\ strength\ of\ control\ mix\ cubes, MPa$$

## B. Flexural Strength Results

Table B.1 Flexural Strength Results of the Clay Mortars

| | *Flexural Strength (MPa)* | | |
|---|---|---|---|
| Sample | *7-day* | *28-day* | *90-day* |
| Clay A – No Calc. | 6.20 | 6.27 | 6.90 |
| Clay A - 600 °C Calc. | 6.90 | 7.33 | 8.10 |
| Clay A - 800 °C Calc. | 6.17 | 7.33 | 8.23 |
| Clay B - No Calc. | 4.60 | 5.27 | 5.33 |
| Clay B - 600 °C Calc. | 6.20 | 8.07 | 7.40 |
| Clay B - 800 °C Calc. | 7.00 | 9.40 | 8.57 |
| Clay C – No Calc. | 5.20 | 6.07 | 7.63 |
| Clay C - 600 °C Calc. | 5.80 | 8.53 | 9.63 |
| Clay C - 800 °C Calc. | 7.10 | 9.50 | 8.27 |
| Clay D - No Calc. | 6.03 | 7.17 | 9.40 |
| Clay D - 600 °C Calc. | 5.90 | 8.60 | 9.10 |
| Clay D - 800 °C Calc. | 6.07 | 8.97 | 9.30 |
| Clay E – No Calc. | 5.27 | 6.40 | 7.33 |
| Clay E - 600 °C Calc. | 5.90 | 6.43 | 8.40 |
| Clay E - 800 °C Calc. | 6.70 | 9.17 | 7.63 |
| Clay F - No Calc. | 5.60 | 6.80 | 7.13 |
| Clay F - 600 °C Calc. | 6.77 | 8.13 | 8.37 |
| Clay F - 800 °C Calc. | 7.17 | 9.47 | 8.87 |
| Clay G – No Calc. | 5.93 | 7.57 | 7.37 |
| Clay G - 600 °C Calc. | 6.70 | 8.67 | 7.77 |
| Clay G - 800 °C Calc. | 6.43 | 8.40 | 7.40 |
| Clay H - No Calc. | 5.17 | 6.30 | 8.03 |
| Clay H - 600 °C Calc. | 5.53 | 7.57 | 8.80 |
| Clay H - 800 °C Calc. | 5.93 | 7.37 | 8.50 |